The Meteoritical Society

Meteoritics & Planetary Science 56, Nr 5, 1024–1070 (2021)
doi: 10.1111/maps.13657

The terrestrial impact crater record: A statistical analysis of morphologies, structures, ages, lithologies, and more

Thomas KENKMANN*

Institute of Earth and Environmental Sciences, Geology, Albert-Ludwigs-Universität Freiburg, Albertstraße 23b, Freiburg im Breisgau 79104, Germany
*Corresponding author. E-mail: thomas.kenkmann@geologie.uni-freiburg.de

(Received 07 December 2020; revision accepted 30 March 2021)

Abstract–The number of newly discovered and confirmed impact structures on earth is growing continuously. In this review paper, the main attributes of 198 confirmed impact structures and 10 further structures, for which final confirmation based on the identification of shock features is not yet entirely satisfying, are presented. The impact craters are compared statistically, with regard to their morphology, structure, and status of erosion or burial. The size– and age–frequency distributions of terrestrial impact structures are presented. Additional aspects concern target petrography and shock effects found in the craters. Based on the discovery statistics of presently known crater structures, an estimate can be made of the number of craters that await discovery. The paper is complementary to the recently published atlas of terrestrial impact structures by Gottwald et al. (2020).

IMPACT CRATER STUDIES ON EARTH: A DYNAMICALLY EVOLVING FIELD OF RESEARCH

"Impact of solid bodies is the most fundamental process that has taken place on the terrestrial planets" (Shoemaker 1977). This statement marked a paradigm shift in understanding the Earth as a planetary body that interacts with space and emphasized the collision history of the Earth that was recognized to be similar to that of the Moon. In comparison to the Moon, Mars, Mercury, Venus, and all the smaller, mostly icy bodies in the solar system, the Earth's surface undergoes a much faster resurfacing by erosion, sedimentation, mountain building, volcanism, and plate subduction, which significantly reduces the number of recognizable impact structures. For example, the oceanic lithosphere that accounts for two-thirds of the Earth's surface has a mean age of only 56–62 Myr (Cognéa et al. 2006). Apart from its coverage by kilometers of water, this young age makes it unlikely that the ocean floor contains many impact structures. Regions on Earth that have been facing cosmic bombardment over extended periods of the Earth history—the Archean and Proterozoic cratons—are the sites where the density of impact craters is the highest (Grieve 1982; Johnson and Bowling 2014).

Almost every year ancient impact structures are discovered or confirmed. These newly recognized crater structures are often heavily eroded and have no or only a subdued morphological expression. Others are buried and our information entirely relies on bore hole sampling and geophysical surveying. Each new crater adds important aspects to the general comprehension of the fundamental process of impact cratering and is worth being thoroughly studied.

However, our current understanding of the morphology and structure of impact craters is strongly influenced by planetary impact craters that are often pristine. Impact cratering is by far the most widespread process shaping the surfaces of planetary bodies such as Mars or the Moon. The large number of impact craters allowed us to precisely analyze crater morphologies including depth, rim height, central peak height and diameter, terrace zone width, ejecta blanket extent, block size as a function of the crater size (e.g., Pike 1977). Our understanding of the process of impact crater formation relies heavily on explosion and impact experiments (e.g., Oberbeck 1968; Gault et al. 1974; Kenkmann et al. 2018a) and numerical simulation of impact craters (e.g., Melosh 1989; Ivanov and Artemieva 2002; Collins et al. 2004).

Today, more than a century after the impact of an extraterrestrial projectile was first proposed for Meteor

Crater, 198 geological structures of confirmed impact origin are known (Gottwald et al. 2020). Their impact origin is based on the established criteria of (1) shock-metamorphic evidence such as macroscopic shatter cones or microscopic shock deformation features (e.g., Stöffler and Langenhorst 1994; French 1998; Stöffler et al. 2017), and (2) relics of the meteoritic projectile or chemical traces of it left in impact melt rock (e.g., French and Koeberl 2010). Ten additional craters, where final proof is not yet entirely unequivocal, are included in this study.

The rapid increase of our knowledge on impact craters requires from time to time a renewed summary of the vast amount of available data. Comprehensive summaries of the terrestrial impact crater record were given by Grieve (1991), Grieve and Pesonen (1992), Pilkington and Grieve (1992), and McCall (2009). These summaries dealt with 130–190 impact structures and require updates. A widely appreciated and accepted database of terrestrial impact structures has been the Earth Impact Database (EID 2020). It goes back to the Dominion Observatory's meteorite crater research program (Innes 1964), a Canadian effort to identify impact structures on the Canadian Shield, and was later developed to a global database under the auspices of the Geological Survey of Canada. Since 2001, it has been hosted and maintained by John Spray of the Planetary and Space Science Center (PASSC) of the University of New Brunswick, Canada (http://www.passc.net/EarthImpactDatabase/Newwebsite_05-2018/Index.html). It is a frequently used platform for experts and the lay public to acquire fast information and references on specific impact structures. However, it requires updates. Other databases are curated on a more informal base and are currently less accessible. The recently published atlas on terrestrial impact structures (Gottwald et al. 2020) presents novel remote sensing images and geological information of each impact structure. This is complemented by review papers and books that summarize the impact crater record of single continents, for example, for South America (Crósta et al. 2019a, 2019b), Africa (Reimold and Koeberl 2014), and Australia (Haines 2005), or large terrains such as Arabia (Chabou 2019), Canada (Grieve 2006), and northeastern Eurasia (Masaitis et al. 1980; Masaitis 1999). Apart from this, the physics behind the impact cratering process and its planetary dimension are summarized in the benchmark book by Melosh (1989). More recently, various aspects of impact cratering have been reviewed in the book *Impact Cratering: Processes and Products*, edited by Osinski and Pierazzo (2012).

The aim of this paper is to provide an update of the terrestrial impact crater record from a statistical standpoint. Why do we need a statistical analysis and summary of the current impact structure record? In general, statistical approaches enable correlations between parameters. In the field of impact cratering, it allows us, for example, to systematically compare crater morphologies, structures, lithologies, and other parameters for a given crater size. Moreover, comparisons with craters on other planetary bodies become possible. Systematic impact crater catalogs are available, for example, for Mercury, Moon, and Mars (e.g., Fassett et al. 2011; Wang et al. 2015). Terrestrial and planetary craters provide complementary sets of information. While the latter are commonly better preserved morphologically, the former give insights into the deep subsurface of impact structures and allow detailed inspections of target rocks and impactite lithologies. The comparative approach provides a solid base to elucidate fundamental processes and mechanisms of cratering. The comprehensive summary of the currently known craters is a prerequisite to assess the significance of impact cratering throughout the Earth's history. It may help to answer the questions of whether impact bombardment has been a constant process over the past three billion years or whether there have been periods of enhanced or missing impact activity. The history of crater discoveries may also give an indication of craters still awaiting discovery or confirmation. The statistical analysis of terrestrial craters may have some unexpected spin-off for other geosciences disciplines: For example, it can help to disentangle average erosion and sedimentation rates on Earth (Hergarten and Kenkmann 2019).

PARAMETERS AND METHODS

The basis of this paper is a database, in which up to 75 parameters have been gathered for each impact structure. Table 1 summarizes the major categories and parameters that were investigated. Note that for some craters only a fraction of these parameters could be collected. The structure of the database (Table 1) also provides a frame for this paper. Figure 1 and Table 2 define the structural and morphometric parameters used throughout this paper. The parameters are adapted from Melosh (1989) and Turtle et al. (2005), and some parameters are new. Table 3 shows that part of the database that is used in this article. The full interactive database will be made available through the author's website at https://www.geology.uni-freiburg.de/en?set_language=en.

Crater structures labeled in Table 3 with an [a] are not listed in the EID (2020). For 10 of the craters listed in the table (indicated with a [b]), more documentation efforts are desired. These are Quarkziz, Yilan, Crawford, Flaxman, Hickman, Piccaninny, Hiawatha,

Table 1. Parameters analyzed in the impact crater database and in this article.

Category	Parameter
Location	Latitude, longitude
Discovery	First proposal, year of confirmation
Age	Age including error, method
Surface expression	
Outline	Apparent diameter, circularity, polygonality
Exposure	Exposed, buried, submerged, boreholes
Visibility	Subdued, invisible, ring
Hydrology	Concentric, radial, unspecific, combined, glacial
Structure	
Type	Simple, complex, transitional
Central uplift	Width, diameter, depth, peak ring, central pit
Moat	Width, diameter, depth
Rim	Overturned flap, height, width rim, fault
Depth	Crater floor, top breccia infill, geophysical depth
Shock effects	Shatter cones, planar deformation features (PDFs), planar fracture (PFs), feather features (FFs), diaplectic glasses, fused melt, high-pressure (HP) phases
Target lithologies	Crystalline, sedimentary, mixed, lithologies
Impact lithologies	Impact melt rock, lithic monomict breccia, lithic polymict breccia, pseudotachylites, dikes
Projectile	Presence of meteorites, bolide type, trajectory, number of impacts, strewn field
Ejecta	Allochthonous crater fill, proximal ejecta, distal ejecta, tektite, ramparts
Impact into water	Water depth, resurge deposits
Postimpact history	Hydrothermal alteration, erosion, burial, deformation
Geophysics	Seismics, gravity, magnetics, electromagnetics
Economic use	Type of resource

Pantasma, Colonia, and Rio Cuarto. Concerning the vast amount of literature published on the various craters, a citation restriction to those publications that led to the confirmation of the crater structure was inevitable for this paper. For additional publications, the reader is explicitly referred to the references given in the complementary atlas (Gottwald et al. 2020) and in the EID (2020).

Some of the parameters derived are not explicitly mentioned in published papers, but could be inferred from published data and from satellite imagery (Gottwald et al. 2020). For example, the diameter of the ring syncline axis has rarely been given in the literature, but often it has been possible to measure this feature from published geological maps or seismic sections. Three categories are distinguished: pristine craters, buried craters, and eroded craters (Fig. 1). In eroded craters, the morphometric and structural parameters are modified with respect to the pristine crater state and are, therefore, denoted as "apparent." The measurable apparent dimensions can be roughly converted into pristine crater dimensions, if the amount of erosion is known and other assumptions are made. Such conversions of the apparent crater diameter and other structural parameters have not been done in the database, because such reconstructions have a number of uncertainties and assumptions. Estimates of the amount of erosion are commonly vague. Guidelines to obtain rough estimates of the amount of erosion are the presence/absence of allochthonous breccia deposits in the moat, the remains/absence of ejecta deposits, shock pressure isobars, and the critical depth down to which a crater of a given size is detectable (Hergarten and Kenkmann 2015) (Fig. 1). To compare the measured morphometric data with a sort of standard, the frequently used web-based computer program by Collins et al. (2005) was used as a reference. The calculation of crater dimensions is based on a number of scaling relationships (Grieve and Garvin 1984; McKinnon and Schenk 1985; Schmidt and Housen 1987; Herrick et al. 1997).

The listed crater ages are based on either relative or absolute dating methods and are of variable quality (Table 3). To use crater ages and their uncertainties in a statistical overall analysis, it was necessary to convert stratigraphic ages to absolute ages. If the crater age is constrained by an upper stratigraphic age Ts_{max} and a lower stratigraphic age Ts_{min} this age is converted into a mean stratigraphic age Ts_{mean}, and a stratigraphic uncertainty Es:

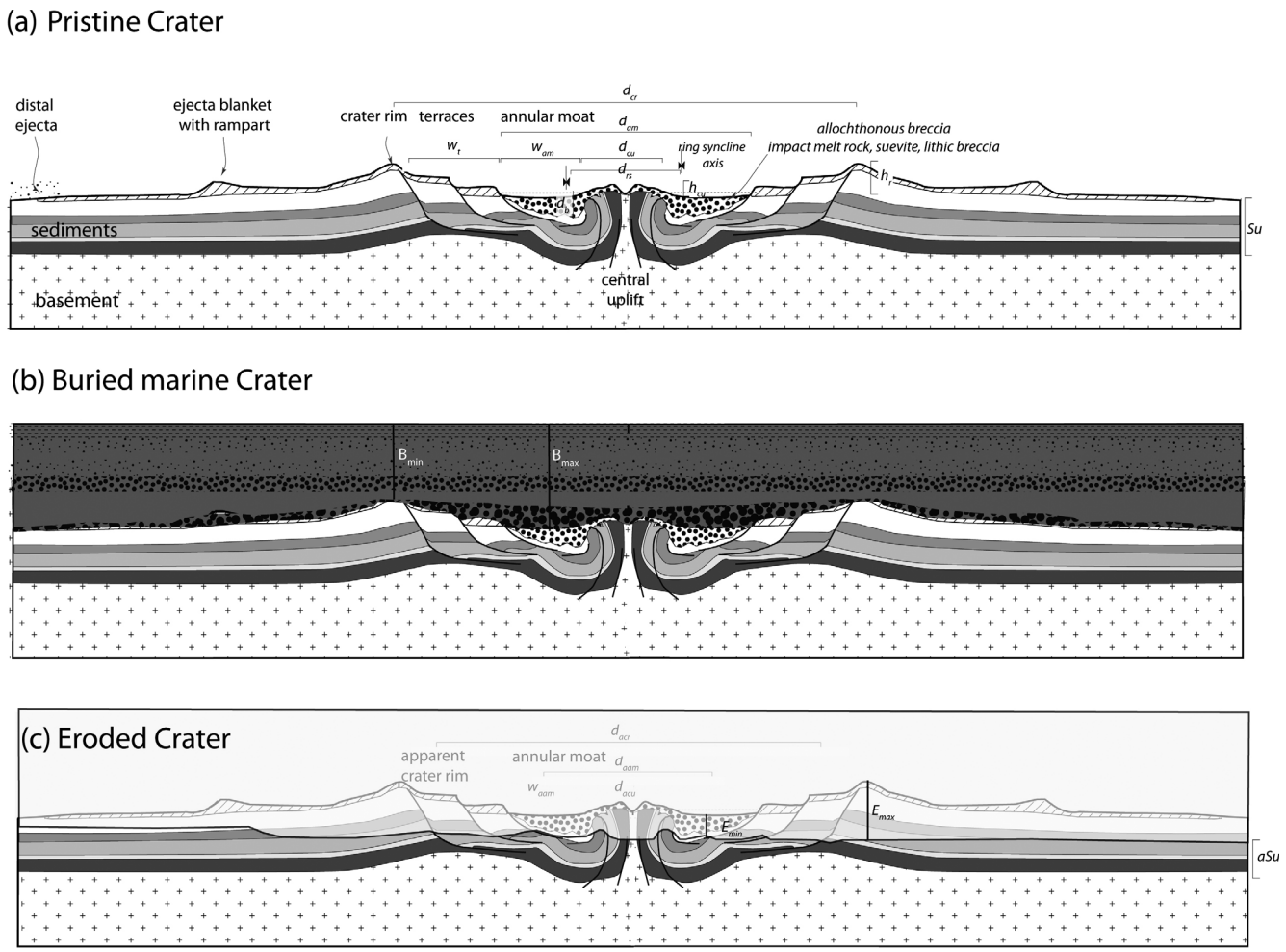

Fig. 1. Schematic cross section through a complex impact crater in (a) pristine state, (b) buried beneath postimpact sediments, and (c) after selective erosion. Morphometric parameters are displayed. Note that the postimpact history allows combinations of (b) and (c).

$$Ts_{\text{mean}} = \frac{Ts_{\max} + Ts_{\min}}{2} \tag{1}$$

and

$$Es = \frac{Ts_{\max} - Ts_{\min}}{2} \tag{2}$$

I used the 2020 updated IUGS International chronostratigraphic chart (Cohen et al. 2013) for the conversion of stratigraphic names into absolute ages. Normalized triangular probability density functions were calculated for each stratigraphic age that give the probability density, *Ps*, as a function of time *x*:

$$Ps(x) = \frac{1}{Es^2} * (x - Ts_{\text{mean}}) + \frac{1}{Es_{\text{mean}}}, \text{for } Ts_{\min} < x < Ts_{\text{mean}} \tag{3a}$$

and

$$Ps(x) = -\frac{1}{Es^2} * (Ts_{\text{mean}} - x) + \frac{1}{Es_{\text{mean}}}, \text{for } Ts_{\max} > x > Ts_{\text{mean}} \tag{3b}$$

For radiometric ages, *Tr*, with a standard deviation, σ the density function of the Gaussian normal distribution was calculated, that gives the probability density, *Pr*, at a time *x*:

Table 2. Abbreviations of measured parameters; for explanation, see Fig. 1.

Abbr.	Meaning	Crater type S: simple C: complex
Pristine crater		
D_{cr}	Crater diameter	S,C
D_{rs}	Ring syncline diameter	C
D_{cu}	Central uplift diameter	C
SU	Stratigraphic uplift	C
W_t	Terrace width	C
W_{am}	Width of the annular moat	C
D_{am}	Diameter of the annular moat	C
d_b	Depth to breccia lens base	S, C
d_f	Depth to crater floor (top breccia)	S, C
h_r	Rim height to target surface	S, C
hcu	Central uplift elevation	C
Buried crater		
B_{max}	Maximum depth of burial (moat)	S, C
B_{min}	Minimum depth of burial (rim)	S, C
Eroded crater		
E_{max}	Maximum erosion (rim)	S, C
E_{min}	Minimum erosion (moat)	S, C
D_{acr}	Apparent crater diameter	S, C
D_{ars}	Apparent ring syncline diameter	C
D_{acu}	Apparent central uplift diameter	C
aSU	Apparent stratigraphic uplift	C
d_{ab}	Depth to breccia lens base	S, C
d_{af}	Depth to crater floor (top breccia)	S, C

$$Pr(x) = \frac{1}{\sigma\sqrt{2\pi}} * \exp\left(-\frac{1}{2} * \left[\frac{x - Tr}{\sigma}\right]^2\right) \quad (4)$$

To calculate the frequency probability density, $Pt(x)$, of impacts based on the recorded craters in the Earth history at a time x, $Pr(x)$ and $Ps(x)$ were combined:

$$Pt(x) = \Sigma_1^{208} Ps(x) + \mathrm{Pr}(x) \quad (5)$$

LOCATION OF TERRESTRIAL IMPACT CRATERS

The most fundamental parameter of an impact structure is its location. The location of impact structures showing a topographic imprint, often with circular morphology, can be determined with high precision in geographic latitude and longitude. The required positional accuracy is a function of impact crater diameter and latitude. For small impact craters, an accuracy of seconds is required to prevent that the quoted location being several crater radii from the true position (Table 3). However, even when a topographic imprint is visible, locations listed in literature may not provide an exactly true location, for example, Beyenchime-Salaatin (Masaitis 1999) or Sobolov (Khryanina 1981) only give vague hints as to location. Positioning of buried structures can require particular effort, where the location can only be inferred from geophysical studies. Particularly challenging are those buried impact structures that can be found on the territories of the former Soviet Union. Often they are only quoted in sparse Russian literature, where they are displayed on crude maps and/or with contradicting positions, for example, Boltysh (Gurov et al. 2006). The position data presented in Table 3 coincide with the positions given in Gottwald et al. (2020).

DISTRIBUTION OF TERRESTRIAL IMPACT CRATERS

The probability of impact events is independent of longitude and nearly independent of latitude (Le Feuvre and Wieczorek 2008). In contrast, the currently known distribution of impact structures is highly uneven. For allocation of craters to continents, their current geographic position is used. Note that the position of the craters at the time of their formation deviates from the indicated ones due to plate tectonic processes. The two-thirds of the Earth that is covered by oceans is almost devoid impact structures. The impact-induced deep sea disturbance of Eltanin (Gersonde et al. 1997) is the only known deep sea impact. It is not further considered here, as it led only to a disturbance of mostly unconsolidated sediments on the sea floor and not a crater form. On land, crustal ages positively correlate with crater density, so that the old shield and cratons such as the Canadian or Baltic shield contain the majority of impact structures (Johnson and Bowling 2014; Hergarten and Kenkmann 2015) (Fig. 2). In contrast, a deficit of craters exists in young orogens with high relief (Hergarten and Kenkmann 2019). Intracontinental basins and marine shelves' environments also have crater densities below average. They, however, likely contain yet undetected buried structures.

The majority of impact structures are found in North America (65), Europe (54), and Australia (31). Many fewer have been identified in Asia (23), Africa (21), and South America (14; Gottwald et al. 2020). One reason for this is that on continents with a high number of impact structures, countries have pursued intense geological surveying in the past. For instance, almost all of the buried crater structures that required drilling and geophysical surveying have been identified in North America or Europe. In large regions with an

obvious impact structure deficiency and dense vegetation, studies have been hindered by the lack of infrastructure and accessibility, for example, the vast areas of rainforest in South America or Central Africa. Areas with enduring civil strife also lack exploration for impact structures.

DISCOVERY OF TERRESTRIAL IMPACT CRATERS

Figure 3 displays the history of impact crater discoveries on Earth from 1900 until today (Table 3). The discovery year is considered as the year when the structure has been confirmed as an impact crater by written documentation of unequivocal shock features or associated meteoritic materials that are described in detail, for example, Grieve et al. (1996), French (1998), French and Koeberl (2010), and Stöffler et al. (2017).

The discovery history of terrestrial impact structures started with the widely disputed hypothesis that Meteor crater, Arizona, USA, was of impact origin (Barringer 1910). The rate of discoveries, however, was low in the first half of the 20th century. Discoveries concentrated on morphologically visible simple craters and crater strewn fields that were associated with meteorites. The cumulative plot (Fig. 3) shows that the rate of crater discoveries increased relatively abruptly in the early 1960s. In the context of the emerging space exploration and lunar missions, it was realized that impact processes may have played an important role in shaping planetary surfaces. This also inspired more intense investigations on Earth. Structures that had formerly been interpreted as being of cryptovolcanic or crytpoexplosion origin (Bucher 1936) were reinterpreted as impact craters. The discovery of high-pressure polymorphs of quartz in rocks of these structures (Chao et al. 1960; Shoemaker and Chao 1961) and the recognition that shatter cones are associated with impact (Dietz 1960) were key for the onset of modern impact crater research. Likewise, the discovery of planar microstructures, now known as planar deformation features (PDFs) (McIntyre 1962) and basal PDFs (Carter 1965) were crucial discoveries for the start of this new era. The discovery rate suddenly increased and was highest in the late 1970s, when up to 12 new craters were confirmed per year. The overall discovery rate slightly decreased since about 1990. In recent times, more than two craters per year are discovered on average; although, in 2018 and 2019, five and six craters were discovered, respectively. The curve is relatively smooth. It is surprising that technical advancements important for the discovery of craters such as the public availability of high-resolution remote sensing resources like Google Earth© in 2005 did not lead to an enhanced discovery rate and consequently a kink in the cumulative plot. A good mathematical fit to the discovery curve was found by using the sigmoid-shaped logistic function. The initial stage of this function of growth is approximately exponential; then, as saturation begins, the growth slows to linear, and at maturity, growth stops. The function is given by:

$$N_{\text{cum}} = \frac{N_{\max}}{1 + e^{-k(y-y_0)}} \tag{6}$$

where N_{cum} is the cumulative number of discovered terrestrial craters at a year y, $N_{\max}$ is the maximum of the curve, k is the logistic growth rate or steepness of the curve, and y_0 is the midpoint or inflection point of the curve. A best fit to the discovery statistics is given for: $k = 0.065$, $y_0 = 1990$, and $N_{\max} = 235$ (Fig. 3, green dotted curve). From this, the diagram also provides a projection of the discovery rate into the future. The logistic function fit means that a totality of only 235 impact craters or so might be expected. In other words, the prognosis is that only 27 craters would remain to be discovered. The logistic function was successfully applied to a range of fields, including ecology, demography, economics, pandemics, and also for the assessment of georesources. For example, a logistic function was used to characterize peak and ultimate production of global crude oil and petroleum-derived liquid fuels (Gallagher 2011). However, the application of the logistic function is problematic in the context of impact crater discoveries as the tools to prove craters were not developed before 1960.

A good fit to the data since 1960 is provided by a simple exponential saturation curve.

$$N_{\text{cum}} = N_{\max} * (1 - e^{-b(y-y_0)}), \tag{7}$$

where b is the growth rate with a best fit of 0.015, y the year of discovery, and y_0 the year at $N = 0$ (year 1960). A projection toward future would result in a total number of craters of $N_{\max} \approx 350$ or 142 structures that remain to be discovered.

The estimate based on Equation 7 derived from the projection of the discovery rate is somewhat lower but of the same order of magnitude as recent estimates by Hergarten and Kenkmann (2015). They calculated the crater population exposed at the Earth's surface on the basis of the size–frequency distribution of lunar craters (Bland and Artemieva 2006). They adopted the size–frequency distribution to the Earth and took into account the permanent removal of craters by a mean erosion rate of 59 m Ma^{-1}. The result of this calculation is that about 90 craters in the diameter range from 1 to 6 km await discovery. About 250 are lacking between 0.25 and 1 km diameter. The

Table 3 Data of the known terrestrial impact structures.

		Location			D_{acr}			Age (Myr)		Type	D_{acu}	aSU	D_{ars}	d_{af}
Name	Country	Latitude	Longitude	Confirmation	(km)	Exposure	Hydrology	Age (yr)	Method		(km)	[m]	(km)	(m)
AFRICA														
Agoudal	Morocco	31°59′12″ N	05°30′57″ W	El Kerni et al. (2019)	2.8	ex	u	> 0.3	strat	c	0.6	?	?	?
Amguid	Algeria	26°05′15″ N	04°23′42″ E	Lambert et al (1980)	0.45	ex,pc,mor	r	< 0.1	strat	s				20
Aorounga	Chad	19°05′31″ N	19°14′37″ E	Becq-Giraudon et al. (1992)	16	ex,mor	c	< 355	strat	c	8.0	?	12.6	?
Aouelloul	Mauritania	20°14′28″ N	12°40′28″ W	Koeberl et al. (1998)	0.39	ex,pc,mor	r	3.1 ± 0.3	rad	s				30
Bosumtwi	Ghana	06°30′09″ N	01°24′27″ W	Littler et al. (1962)	10.5	ex,mor,sub	r+c+l	1.07	rad	c	2.0	800	6.0	550
B.P. Structure	Libya	25°19′08″ N	24°18′37″ E	French et al. (1974)	3.4	ex,mor	c	< 120	strat	c	0.7	?	1.3	?
Gweni-Fada	Chad	17°25′07″ N	21°45′17″ E	Vincent and Beauvilain (1996)	22	ex,pc,mor	r+c	< 355	strat	c	8.0	?	11.0	?
Kalkkop	South Africa	32°42′31″ S	24°25′56″ E	Koeberl et al. (1994a)	0.64	ex,pc,smor	u	0.25 ± 0.05	rad	s				89
Kamil	Egypt	22°01′06″ N	26°05′15″ E	Folco et al. (2010)	0.045	ex,mor	r	0.00302 ± 0.0006	rad	s				10
Kgagodi	Botswana	22°28′28″ S	27°34′48″ E	Brandt et al. (2002)	3.4	b	u	< 180	strat	t				156
Libyan desert glass[a]	Egypt	25°25′ N	25°30′ E	Koeberl and Ferrière (2019)	?	ex, ?	u	29 ± 1	rad	?				?
Luizi	DR Congo	10°10′09″ S	28°00′21″ E	Ferrière et al. (2011)	17	ex,mor	r+c	< 573	strat	c	6.0	?	10.0	?
Morokweng	South Africa	26°28′ S	23°32′ E	Andreoli et al. (1995)	70	b	u	145 ± 2	rad	c	30.0	?	50.0	100
Oasis	Libya	24°34′33″ N	24°24′43″ E	French et al. (1974)	18	ex,mor,pc	r+c	< 120	strat	c	5.5	?	10.0	?
Ouarkziz[b]	Algeria	29°00′38″ N	07°33′02″ W	Fabre et al. (1970)	3.5	ex,pc,mor	r	> 66	strat	t				?
Roter Kamm	Namibia	27°45′58″ S	16°17′21″ E	Reimold and Miller (1989)	2.5	ex,pc,mor	r	< 5	rad	s				800
Talemzane	Algeria	33°18′52″ N	04°02′05″ E	Lambert et al. (1980)	1.75	ex,pc,mor	r+c	0.5 - 3	strat	s				?
Tenoumer	Mauritania	22°55′07″ N	10°24′20″ W	French et al. (1970)	1.9	ex,pc,mor	r+c	1.52 ± 0.14	rad	s				250
Tin Bider	Algeria	27°36′07″ N	05°06′44″ E	Lambert et al. (1981)	6	ex,pc,mor	c	50 - 66	strat	c	2.0	500	3.8	?
Tswaing	South Africa	25°24′31″ S	28°04′57″ E	Reimold et al. (1991)	1.13	ex,mor,sub	r+l	0.220 ± 0.052	rad	s				150
Vredefort	South Africa	27°00′ S	27°30′ E	Hargraves (1961)	275	ex,pc,mor	r+c	2023 ± 4	rad	c	40.0	8000	55.0	?
ASIA														
Beyenchime-Salaatin	Russia	71°03′29″ N	121°41′23″ E	Mikhailov et al. (1979)	8	ex,pc,mor	r+c	< 66	strat	c				50
Bigach	Kazakhstan	48°34′33″ N	82°02′11″ E	Kiselev and Korotushenko (1986)	8	ex,pc,mor	r	5 ± 3	strat	c				?
Chiyli	Kazakhstan	49°10′32″ N	57°50′01″ E	Vishnevsky and Korobkov (1989)	5.5	ex,pc,mor	c	46 ± 7	strat	c	1.2	120	1.6	?
Chukcha	Russia	75°42′22″ N	97°50′46″ E	Vishnevsky (1995)	6	ex,pc,smor	r	< 70	strat	c	1.0	?	0.0	210
Dhala	India	25°17′55″ N	78°08′33″ E	Pati (2005)	12	ex,pc,smor	c	1700 – 2500	both	c	3.0	?	0.0	?
El'ygytgyn	Russia	67°29′31″ N	172°03′37″ E	Gurov et al. (1978)	18	ex,sub,mor	r+l	3.58 ± 0.04	rad	c	3.0	350	12.0	500
Jebel Waqf as Suwwan	Jordan	31°02′54″ N	36°48′24″ E	Salameh et al. (2008)	6.1	ex,pc,mor	r+c	< 37	strat	c	1.0	350	5.5	?
Kara-Kul[b]	Tajikistan	39°04′ N	73°26′ E	Gurov et al. (1993)	52	ex,sub,smor	r+l	> 5-50	strat	c	8.0	?	30.0	1200
Logancha	Russia	65°29′54″ N	95°57′15″ E	Masaitis et al. (1971)	14	ex,mor	r	23 - 66	strat	c	4.0	?	14.0	400
Lonar	India	19°58′36″ N	76°30′32″ E	Nayak (1972)	1.88	ex,sub,mor	r+l	0.570 ± 0.047	rad	s				?
Macha	Russia	60°05′07″ N	117°39′08″ E	Gurov et al. (1987)	0.3	ex,sub,smor	r+l	0.007315 ± 0.00008	rad	s				57

Shock features	Target	Target lithologies	Impact in water	Hydrothermal alteration	Crater fill breccia	Ejecta (prox. or distal)	Erosion		Burial		Geophysics	Drilled	Resources
							Min	Max	Min	Max			
SC	S	l					400	600			e		
PDF, PF	S	s				x	0	50	0	50			
PDF, PF	S	s							0	100			
glass, PF	S	s, qutz			x	x	0	50	0	23	g		
coes, bad, PDF, PF, FF, bal, glass	M	sch, mgray, mvolc		x	x	x	0	100	0	300	s, g, e	x	
PDF, PF, FF	S	s, l, congl					300	500	0	20			
PDF, PF, FF	S	s, l, congl					200	400	0	100			
PDF, glass, SC	S	s, m			x	x	0	0	0	89		x	
met, PDF, glass, coes, bad, stish	S	s, soil			x	x	0	1	0	1	e		
PDF (qtz/fsp), mask, diapl, glass	M	gr, doler			x		0	0	0	158	g	x	
PDF, FF, glass	S	s					0	0	0	0			
PDF (qtz/fsp), SC, glass	S	s					400	800	0	0			
PDF (qtz/fsp), PF, FF, glass	C	gr, bif, mvolc			x		0	100	25	100	s, g, e	x	Ni
PDF, PF, FF, glass	S	s, si, m, congl		x	x		300	500	0	100			
PDF, PF	S	l, m			x		0	100	0	200			
glass, PDF (qtz/fsp)	M	s, gn, mar, sch		x	x	x	0	50	0	800	g, e		
PDF, glass	S	l			x	x	0	100	0	200	g, e	x	
PDF, ballen, glass, diapl.	M	gn, gr, amph, gab			x	x	0	100	0	250	g		
PDF	S	l, m, s					300	500	0	50			
PDF (qtz/fsp) diapl, glass	M	gr, s, gray			x	x	0	50	0	90	g, e	x	trona, salt
PDF, PF, FF, coes, stish, red, glass, SC, pst	M	msed., gn, mvolc.		x			5000	10000	0	1000	s, g, e	x	Au, U
SC	S	l, s		x	x	x	0	50	0	100			Ore
SC	M	s, bas, and, rhy			x	x	0	50	0	300	g, e	x	
PDF	S	mud, sand, s	x				100	150	0	50	s	x	
PF, PDF	M	s, l, gr					300	400	0	100		x	
PDF (qtz/fsp), FF, bal, glass, coes	C	gr		x	x		1000	2000	0	100			
PF, PDF, FF, glass, diapl, pst, SC	C	rhy, dac, and.		x	x	x	0	100	0	400	s, g, e	x	
SC, PDF, PF, FF	S	chert, l, marl					300	420	0	30	s, g, e	x	
PDF, SC?	M	sch, l, gr		x			0	0	0	0			
PDF, SC, mask	M	bas, si, s, m			x		0	0	0	0	g, e		
SC, mask, lec, spherules	C	bas, si, s, m		x	x	x	0	30	0	100		x	Salt
PDF, PF, stish	S	bas			x	x	0	10	0	15			

Table 3 *Continued*. Data of the known terrestrial impact structures.

		Location			D_{acr}			Age (Myr)		Type	D_{acu}	aSU	D_{ars}	d_{af}
Name	Country	Latitude	Longitude	Confirmation	(km)	Exposure	Hydrology	Age (yr)	Method		(km)	[m]	(km)	(m)
Popigai	Russia	71°38′ N	111°11′ E	Masaitis et al. (1976)	100	ex,mor	r+c	35.7 ± 0.2	rad	c	45.0	?	60.0	?
Ragozinka	Russia	58°42′17″ N	61°47′50″ E	Vishnevsky and Lagutenko (1986)	9	acb,pb,smor	r+c	50	strat	c	1.2	?	0.0	300
Ramgarh[a]	India	25°20′03″ N	76°37′28″ E	Kenkmann et al. (2019)	10.20	ex,pc,mor	r	164.8 ± 1.3	strat	c	3.5	900	7.5	?
Saqqar	Saudi Arabia	29°35′ N	38°42′ E	Kenkmann et al. (2015)	34	acb,smor	u	70 - 410	strat	c	10.0	2900	25.0	?
Shunak	Kazakhstan	47°12′35″ N	72°45′41″ E	Fel'dman et al. (1978)	2.8	ex,pc,mor	r	< 34	strat	s				180
Sikhote Alin	Russia	46°09′36″ N	134°39′12″ E	impact 1947; Krinov (2017)	0.026	ex,mor	r	0.000072	observed	s				6
Sobolev	Russia	46°18′22″ N	137°52′24″ E	Yarmolyuk (1951)	0.053	ex,mor	u	0.000175 ± 0.000025	strat	s				10
Tabun-Khara-Obo	Mongolia	44°07′52″ N	109°39′17″ E	Amgaa and Koeberl (2009)	1.3	ex,pc,mor	r	145 - 163	strat	s				?
Wabar	Saudi Arabia	21°30′12″ N	50°28′20″ E	Philby (1933)	0.116	ex,pc,mor	r	0.000290 ± 0.000038	rad	s				?
Xiuyan	China	40°21′52″ N	123°27′39″ E	Chen et al. (2010)	1.8	ex,pc,mor	r	0.050 ± 0.005	rad	s				107
Yilan[a,b]		46°23′03″ N	129°18′40″ E	Chen et al. (2019)	1.85	ex,pc,mor	r	> 0.01	strat	s				55
Zhamanshin	Kazakhstan	48°21′38″ N	60°56′12″ E	Florenskiy et al. (1977)	14	ex,pc,smor	r	0.75 - 1.10	rad	c	0.8	200	5.5	?
AUSTRALIA														
Acraman	South Australia	32°01′ S	135°27′ E	Williams (1986)	90	ex,sub,mor	r+l	580	both	c	20.0		35.0	?
Amelia Creek	Northern Territory	20°51′ S	134°53′ E	MacDonald and Mitchel (2003)	20	ex	u	600 - 1,660	strat	c				?
Boxhole	Northern Territory	22°36′45″ S	135°11′43″ E	Madigan (1973)	0.17	ex,mor	r	0.0177 ± 0.0123	rad	s				?
Cleanskin[a]	Northern Territory	18°10′00″ S	137°56′30″ E	Haines et al. (2012)	15	ex,pc,mor	r+c	540 - 1,400	strat	c	6.0	?	8.0	?
Connolly Basin	Western Australia	23°32′03″ S	124°45′38″ E	Shoemaker and Shoemaker (1985)	9	ex,pc,mor	r	55 - 75	strat	c	2.0	?	3.8	?
Crawford[b]	South Australia	34°43′ S	139°02′ E	Haines et al. (1999)	8.5	ex	u	32 - 38	strat	c				?
Dalgaranga	Western Australia	27°38′06″ S	117°17′20″ E	Nininger and Huss (1960)	0.024	ex,pc,mor	r	0. 27	rad	s				4
Flaxman[b]	South Australia	34°37′ S	139°04′ E	Haines et al. (1999)	10	ex	u	32 - 38	strat	c				?
Foelsche	Northern Territory	16°40′15″ S	136°47′02″ E	Haines and Rawlings (2002)	6	ex,pc,smor	c	541 - 981	strat	c	2.0	?	4.0	?
Glikson	Western Australia	23°58′40″ S	121°33′22″ E	Shoemaker and Shoemaker (1997)	19	ex,pc	u	< 508 ± 5	rad	c	10.0	?	?	?
Goat Paddock	Western Australia	18°20′02″ S	126°40′36″ E	Harms et al. (1980)	5	ex,pc,mor	r	56 - 64	strat	t				320
Gosses Bluff	Northern Territory	23°49′10″ S	132°18′27″ E	Dietz (1967)	22	ex,pc,mor	r+c	142.5 ± 0.8	rad	c	4.5	800	10.0	?
Goyder	Northern Territory	13°28′31″ S	135°02′24″ E	Haines (1996)	3	ex,smor	c	150 - 1400	strat	c	1.6	?	2.7	?
Henbury	Northern Territory	24°34′18″ S	133°08′52″ E	Alderman (1931)	0.18	ex,pc,mor	r	0.0042 ± 0.0019	rad	s				15
Hickman[a,b]	Western Australia	23°02′13″ S	119°41′00″ E	Haines (2017)	0.26	ex,pc,mor	r	0.02 - 0.10	strat	s				10
Kelly West	Northern Territory	19°55′42″ S	133°57′12″ E	Tonkin (1973)	14	ex,pc,smor	u	> 541	strat	c	2.0	?	?	?
Lake Raeside[a]	Western Australia	28°44′54″ S	120°56′55″ E	Glikson et al. (2016)	11	b,sub	u	< 295	strat	c				?
Lawn Hill	Queensland	18°41′19″ S	138°39′06″ E	Stewart and Mitchell (1987)	20	ex,pc,smor	r+c	472 ± 8	strat	c	7.5	?	11.5	?
Liverpool	Northern Territory	12°23′45″ S	134°02′50″ E	Brett et al. (1970)	2	ex,pc,mor	r	540 - 1000	strat	s				190

Shock features	Target	Target lithologies	Impact in water	Hydrothermal alteration	Crater fill breccia	Ejecta (prox. or distal)	Erosion		Burial		Geophysics	Drilled	Resources
							Min	Max	Min	Max			
PDF (qtz/fsp), diapl, PF, glass, dia, SC	M	gn, sch, l, doler		x	x	x	0	200	0	50	s, g, e	x	Diamond
SC, PDF	M	volc, l, s	x		x	x	0	100	50	300		x	Diatomite
PDF, PF, FF	S	s, m	x	x	x		0	200	0	20	s, g, e	x	
PDF, PF, FF	S	s					1000	1500	300	400	s, q, e	x	
PDF, SC	C	rhy			x	x	0	100	0	190		x	
met	C	soil			x	x	0	0.5	0	1	e		
met, SC	C	volc			x	x	0	1	0	1	e		
PDF, PF	C	gn, sch, amph			x		0	50	0	171		x	
PDF, coes, stish, met	S	sand			x	x	0	5	0	30			
PDF, coes, red, glass	C	gn, amph, mar			x	x	0	50	0	107	s, g, e	x	
PDF?	C	gr			x		0	150	0	100			
coes, PDF, diapl, glass, SC	M	s, sch, m			x	x	0	100	0	120	s, g, e	x	Bauxite, glass
SC, PF, glass	C	dac					2500	5000	0	0	e		
SC, PF, FF	M	volc., sed.						0			e		
met	C	sch, gn			x	x	0	2	0	1			
SC, PDF, PF, FF	S	s,m					1000	2000	0	100			
?	S	si, s			x		200	350	0	3	s, g		
PDF, mask, pst	C	metam., ign.					0	0	0	0			
met	C	gr			x	x	0	2	0	0			
PDF, mask, pst, SC?	C	metam., ign.					0	0	0	0			
PDF, PF, FF	M	doler, s,m, dolo			x		0	150	0	125	e		
SC, PF, FF	M	doler, s, si, congl					1000	1500	0	10	e		
SC, PDF, PF	S	s			x		0	100	0	200		x	
SC, PDF, PF, FF, diapl, glass, pst	S	s, si, l		x	x		100	600	0	200	s, g, e	x	
PDF, PF, FF, SC	S	s, si, m				x	400	700	0	20	e		
met	S	s, gray, m			x	x	0	3	0	5			
PF	C	ryh			x	x	0	50	0	100	s	x	
SC, PF, FF	S	s, m, congl					400	800	0	200	g		
PDF, diapl, mask	C	gr, amph, gn			x		0	0	108	0	s, g, e	x	
SC, PDF, glass, dia, pst	S	s, si, m, tuff	x	x			0	0	0	100	s, g		Zn, Pb, Ag
?	S	s			x		0	150	0	200			

Table 3 *Continued*. Data of the known terrestrial impact structures.

		Location			D_{acr}			Age (Myr)		Type	D_{acu}	aSU	D_{ars}	d_{af}
Name	Country	Latitude	Longitude	Confirmation	(km)	Exposure	Hydrology	Age (yr)	Method		(km)	[m]	(km)	(m)
Matt Wilson	Northern Territory	15°30′00″ S	131°10′51″ E	Kenkmann and Poelchau (2009)	7.5	ex,mor	r+c	1400 - 1500	strat	c	2.5	200	4.5	?
Mount Toondina	South Australia	27°56′41″ S	135°21′31″ E	Youles (1976)	4	ex,smor	u	66 - 144	strat	c	1.5	250	2.2	?
Piccaninny[b]	Western Australia	17°25′31″ S	128°26′18″ E	Shoemaker and Shoemaker (1985)	7	ex,smor	r+c	< 360	strat	c	4.0	70	6.5	?
Shoemaker	Western Australia	25°52′ S	120°53′ E	Bunting et al. (1980)	30	ex,pc,smor	r+l	1630 ± 5	rad	c	12.0	?	17.0	?
Spider	Western Australia	16°44′27″ S	126°05′21″ E	Shoemaker and Shoemaker (1985)	13	ex,smor	c	600 - 900	strat	c	4.0	300	10.0	?
Strangways	Northern Territory	15°12′ S	133°34′ E	Guppy et al. (1971)	40	ex,pc,smor	c	646 ± 42	rad	c	20.0	2500	?	?
Tookoonooka	Queensland	27°07′ S	142°50′ E	Gostin and Therriault (1997)	66	b	u	128 ± 5	rad	c	15.0	?	22.0	?
Veevers	Western Australia	22°58′12″ S	125°22′20″ E	Yeates et al. (1976)	0.07	ex,pc,mor	r	0.012 ± 0.008	rad	s				10
Wolfe Creek	Western Australia	19°10′18″ S	127°47′43″ E	Reeves and Chalmers (1949)	0.88	ex,pc,mor	r	0.120 ± 0.009	rad	s				50
Woodleigh	Western Australia	26°03′ S	114°40′ E	Mory et al. (2000)	60	b	u	265 - 318	rad	c	8.0	1600	20.0	?
Yallalie[a]	Western Australia	30°26′40″ S	115°46′16″ E	Cox et al. (2019)	12	acb,smor	r	83.6 - 89.8	strat	c	3.5	?	6.0	?
Yarrabubba	Western Australia	27°11′ S	118°50′ E	Macdonald et al. (2003)	30	ex	u	2246 ± 17	rad	c				?
EUROPE														
Boltysh	Ukraine	48°57′30″ N	32°14′23″ E	Masaitis (1974)	24	b	u	65.17 ± 0.64	rad	c	6.0	500	12.0	500
Dellen	Sweden	61°50′49″ N	16°40′38″ E	Svensson (1968)	20	ex,sub,smor	gl+l	140.82 ± 0.51	rad	c	4.5	?	11.0	300
Dobele	Latvia	56°34′12″ N	23°17′24″ E	Masaitis (1999)	4.5	b	u	260 - 340	strat	c	2.5	500	3.0	240
Gardnos	Norway	60°38′29″ N	09°00′39″ E	Dons and Naterstad (1992)	5	ex,pc,smor	gl	546 ± 5	rad	c	0.5	400	3.0	?
Granby	Sweden	58°25′34″ N	14°55′53″ E	Alwmark (2009)	2	b	u	470	strat	s				180
Gusev	Russia	48°29′ N	40°32′ E	Movshoviceh and Milayvskay (1975)	3	b	u	50.36 ± 0.33	both	s				240
Hummeln	Sweden	57°22′05″ N	16°15′10″ E	Alwmark et al. (2015)	1.2	pc,sub	r+l	463 ± 7	strat	s				?
Ilumetsä	Estonia	57°57′36″ N	27°24′10″ E	Aaloe (1963)	0.08	ex,pc,mor	r	0.0066	rad	s				13
Ilyinets	Ukraine	49°07′ N	29°06′ E	Masaitis (1974)	8.5	acb,ex,pc	u	445 ± 10	both	c	0.8	300	2.2	?
Iso-Naakkima	Finland	62°11′46″ N	27°07′48″ E	Elo et al. (1993)	3	b	u	900 - 1,200	strat	s				100
Jänisjärvi	Russia	61°58′44″ N	30°56′40″ E	Masaitis and Orlova (1986)	16	ex,sub,smor	gl+l	682 ± 4	rad	c				50
Kaalijärv	Estonia	58°22′22″ N	22°40′10″ E	Reinwald (1928)	0.11	ex,sub,mor	r	0.00351 ± 0.00004	rad	s				10
Kärdla	Estonia	58°58′26″ N	22°46′51″ E	Masaitis et al. (1971)	4	acb	u	455	strat	c	0.3	100	3.0	200
Kaluga	Russia	54°30′ N	36°12′ E	Masaitis (1974)	15	b	u	395 ± 4	strat	c	2.0	?	7.0	200
Kamenetsk[a]	Ukraine	47°46′ N	32°21′ E	Gurov et al. (2017)	1.1	b	u	250 - 540	strat	s				70
Kamensk	Russia	48°21′ N	40°30′ E	Masaitis (1974)	25	b	u	50.36 ± 0.33	rad	c	5.8	3000	0.0	?
Kara	Russia	69°05′ N	64°20′ E	Masaitis (1974)	65	ex,pc,mor	r	70.3 ± 2.2	rad	c	10.0	5000	30.0	220
Karikkoselkä	Finland	62°13′17″ N	25°14′55″ E	Lehtinen et al. (1996)	1.4	sub,mor	sub	230 - 260	strat	s				120
Karla	Russia	54°57′23″ N	47°57′04″ E	Masaitis et al. (1976)	10	acb	u	< 5	strat	c	0.9	?	0.0	200
Keurusselkä	Finland	62°08′ N	24°37′ E	Hietala and Moilanen (2004)	30	ex, sub	gl+l	1,151 ± 10	rad	c	14.0	?	0.0	?
Kursk	Russia	51°42′ N	36°00′ E	Masaitis et al. (1976)	6	b	u	250 ± 80	strat	c	0.8	?	2.0	?
Lappajärvi	Finland	63°08′26″ N	23°41′04″ E	Lehtinen (1976)	23	ex,sub,smor	gl+l	77.80 ± 0.78	rad	c	5.0	?	11.0	?
Lockne	Sweden	63°00′01″ N	14°49′11″ E	Lindström et al. (1991)	7	ex,sub	gl+l	461 ± 5	strat	c	1.0	?	7.0	150
Logoisk	Belarus	54°15′46″ N	27°47′10″ E	Veretennikov et al. (1979)	17	b	u	29.71 ± 0.48	rad	c	1.5	200	4.5	280
Lumparn	Finland	60°08′17″ N	20°07′59″ E	Svensson (1993)	7	sub,smor	sub	450 - 1250	strat	t				100

Shock features	Target	Target lithologies	Impact in water	Hydrothermal alteration	Crater fill breccia	Ejecta (prox. or distal)	Erosion		Burial		Geophysics	Drilled	Resources
							Min	Max	Min	Max			
PDF, PF, FF	S	s, si, qutz					700	950	0	10			
?	S	m					500	700	0	200	s, g, e		
?	S	s, congl					1000	2500	0	0			
SC, PDF, pst	M	gr, sye, bif, s		x			1000	1500	0	50	g, e		
SC, PDF, PF (Zir/Xeno), FF	S	s, si					400	700	0	50			
SC, PDF, melt	M	gr, s, qutz			x	x	100	300	0	50	e		
PDF, glass	M	qutz, phyl, sch	x		x	x	3000	5000	900	900	s, g, e	x	Oil
met	S	lat			x	x	0	2	0	5	e		
met, SC	S	s, lat			x	x	0	6	0	50	e		
PDF, diapl	M	gr		x	x		1000	2000	60	520	s, g, e	x	
PF (qtz/zir), bal, PDF	S	s, si, m, chalk			x	x	0	100	100	300	s, g, e	x	
PDF, SC, pst	C	gr		x			2000	3000	0	100	e		
SC, PDF (qtz/fsp), PF, glass, mask	C	gr, migm, gn		x	x	x	0	20	180	580	s, g, e	x	Oil shale
PDF (qtz/fsp), diapl, glass, coes	C	gr		x	x		0	70	0	100	g, e		
SC	S	l, s			x		0	50	50	70	s	x	
PDF, PF, FF, glass	C	gr, gn, amph	x	x	x		0	700	0	0		x	
PDF	M	l,s,m,gn	x		x	x	0	20	20	280	g, e	x	
PDF, PF	S	s, m, l, coal	x		x	x	0	100	50	250	s, g, e	x	Coal
PDF	M	gr, dio, s, l, m	x		x	x	0	70	0	150		x	
glass spherule	S	s, si			x		0	1	0	3	e	x	
PDF, SC, coes, diapl, glass, mask	M	gr, gn,sedi		x	x		200	400	0	75	s, g	x	Agate
PDF, PF, FF	M	sch, amph, s, congl					300	600	25	150	s, g, e	x	
SC, coes, PDF (qtz/fsp), diapl	M	sch, gn, s		x	x	x			0	100	s, g, e		
met	S	dolo, till			x	x	0	1	0	2	e	x	
PDF	M	l, s, m, gr, gn, amph	x	x	x	x	0	50	50	200	s, g, e	x	Oil, ore
PDF, PF, glass, diapl	M	gn,gr,sch, s, si, m	x	x	x	x	0	100	600	850	s, g	x	Water
PDF, PF	C	gn			x	x	0	100	30	70	g		
coes, PDF, PF, diapl, SC	S	s, si, l, coal	x	x	x	x	0	100	50	350	s, g, e	x	Coal
PDF, PF, coes, dia, diapl, glass, SC	S	m, l, bas		x	x	x	0	200	0	220	s, g	x	Diamond, Zn
SC, PDF, PF, FF	C	gr			x	x	0	0	0	0	g, e		
SC	S	dolo, l, s, m			x	x	0	100	0	100		x	
SC, PDF(qtz/fsp), PF, FF, pst	C	gr, grano, mvolc, sch					1000	1500	0	50	g, e		
PDF, PF, mask, diap, glass	M	gr, gn, amph, m, l, s			x		0	150	100	150	s, g, e	x	
PDF, PF, mask, diap, glass, SC	M	gn, sch, gr, grano, amph, s		x	x	x	300	500	0	100	s, g, e	x	
PDF, PF, Lin	M	gr, l, m	x	x	x	x	0	150	0	100	s, g	x	
PDF, PF, diapl, mask, glass, SC	M	gn, s, si, m		x	x		0	100	190	480	s, g	x	Amber, phosphate
diapl, SC, PDF, PF, glass	C	gr			x		0	0	0	0	s, g	x	

Table 3 *Continued*. Data of the known terrestrial impact structures.

		Location			D_{acr}			Age (Myr)		Type	D_{acu}	aSU	D_{ars}	d_{af}
Name	Country	Latitude	Longitude	Confirmation	(km)	Exposure	Hydrology	Age (yr)	Method		(km)	[m]	(km)	(m)
Målingen	Sweden	62°55′01″ N	14°33′59″ E	Ormö et al. (2014)	0.85	ex,sub,smor	gl+l	461 ± 5	strat	s				100
Mien	Sweden	56°25′05″ N	14°51′23″ E	Svensson and Wickman (1965)	9	ex,sub,mor	gl+l	118.7 ± 2.3	rad	c	1.0	?	?	?
Mishina Gora	Russia	58°34′57″ N	28°05′27″ E	Masaitis (1974)	2.5	ex,pc	u	< 359	strat	s				200
Mizarai	Lithuania	54°01′ N	23°54′ E	Motuza and Gailius (1978)	5	b	u	520 - 560	strat	c				152
Mjølnir	Norway	73°48′ N	29°40′ E	Dypvik et al. (1996)	40	sub,b	sub	142.0 ± 2.6	strat	c	8.0	1750	16.0	70
Morasko	Poland	52°29′25″ N	16°53′47″ E	Karaszewski 1974)	0.096	ex,sub,mor	r+l	0.0057 ± 0.0007	rad	s				12
Neugrund	Estonia	59°20′00″ N	23°31′30″ E	Suuroja and Suuroja (2000)	8	sub,b	sub	535	strat	c	?	?	5.5	?
Obolon	Ukraine	49°35′48″ N	32°54′33″ E	Masaitis et al. (1976)	18	b	u	169	rad	c	2.5	?	5.0	400
Paasselkä	Finland	62°08′55″ N	29°24′46″ E	Pesonen et al. (1999)	10	ex,sub,smor	sub	228.7 ± 3.0	rad	t				?
Puchezh-Katunki	Russia	56°58′ N	43°43′ E	Firsov and Kieffer (1973)	40	acb	u	192 - (196	rad	c	10.0	1800	22.0	400
Ries	Germany	48°52′09″ N	10°34′41″ E	Shoemaker and Chao (1961)	26	ex,pc,mor	r	14.8	rad	c	8.0	?	15.0	200
Ritland	Norway	59°14′08″ N	06°25′18″ E	Riis et al. (2011)	2.7	ex,pc	gl	500 - 540	strat	s				140
Rochechouart	France	45°49′27″ N	00°46′54″ E	Lambert (1977)	23	ex	u	201 ± 2	rad	c				?
Rotmistrovka	Ukraine	49°08′00″ N	31°44′52″ E	Val'ter and Ryabenko (1977)	2.7	b	u	95 - 145	strat	s				150
Sääksjärvi	Finland	61°24′40″ N	22°22′45″ E	Papunen (1969)	6	ex,sub	gl+l	< 520-600	rad	c	0.5	?	?	?
Saarijärvi	Finland	65°17′37″ N	28°23′31″ E	Pesonen (1998)	1.5	ex,sub,smor	gl+l	560 ± 12	strat	s				?
Siljan	Sweden	61°01′ N	14°56′ E	Svennson (1971)	65	ex,sub,mor	r+c	380.9 ± 4.6	rad	c	30.0	?	45.0	?
Söderfjärden	Finland	63°00′19″ N	21°34′37″ E	Lehtovaara (1985)	6.6	ex,pc,mor	r	520 - 600	both	c	1.2	?	2.5	?
Steinheim	Germany	48°41′12″ N	10°04′02″ E	Dietz (1959)	3.8	ex,pc,mor	r+c	14.8	strat	c	1.0	400	1.5	130
Sterlitamak	Russia	53°36′12″ N	55°35′12″ E	Petaev et al. (1991)	0.0094	destroyed	r+l	0.000029	observed	s				?
Suavjärvi	Russia	63°07′21″ N	33°22′24″ E	Mashchak and Orlova (1986)	16	ex,sub	gl+l	2090 - 2700	rad	c				?
Summanen[a]	Finland	62°39′00″ N	25°22′30″ E	Plado et al. (2004)	2.6	sub	sub	< 1880	strat	s				?
Suvasvesi N	Finland	62°39′35″ N	28°10′22″ E	Pesonen et al. (1996)	4	sub	sub	85	rad	s				90
Suvasvesi S	Finland	62°35′36″ N	28°13′38″ E	Lehtinen et al. (2002)	3.8	sub	sub	> 710	rad	s				?
Ternovka	Ukraine	48°07′48″ N	33°31′12″ E	Masaitis et al. (1971)	11	b	u	280 ± 10	strat	c	2.5	?	?	?
Tvären	Sweden	58°46′30″ N	17°25′33″ E	Lindstrom et al. (1994)	3.2	sub,smor	sub	462 ± 5	strat	s				200
Vepriai	Lithuania	55°05′ N	24°35′ E	Motuza and Gailius (1978)	7.5	b	u	162 - 174	rad	c				125
Zapadnaya	Ukraine	49°44′00″ N	29°03′15″ E	Val'ter and Ryabenko (1977)	3.2	b	u	165 ± 5	rad	c	0.6	200	?	?
Zeleny Gai	Ukraine	48°53′17″ N	32°47′55″ E	Val'ter et al. (1976)	3.5	b	u	80	strat	c				165
NORTH & MIDDLE AMERICA														
Ames	Oklahoma, U.S.A.	36°15′ N	98°12′ W	Koeberl et al. (1994b)	15	b	u	470	strat	c	5.0	?	7.0	?
Avak	Alaska, U.S.A.	71°15′ N	156°30′ W	Kirschner et al. (1992)	12	b	u	90 - 94	strat	c	4.0	500	5.6	?
Beaverhead	Montana, U.S.A.	44°36′ N	112°58′ W	Hargraves et al. (1990)	75	ex,pc	u	< 900	rad	c				?
Bloody Creek[a,b]	Nova Scotia, Canada	44°45′ N	65°14′35″ W	Spooner et al. (2009)	0.4	sub	sub	unknown	strat	s				5
Brent	Ontario, Canada	46°04′30″ N	78°28′55″ W	Millman et al. (1960)		ex,pc,mor	l	453	both	s				260
Calvin	Michigan, USA	41°49′48″ N	85°57′00″ W	Milstein (1994)	8.5	b	u	450	strat	c	1.8	415	3.5	?
Carswell	Saskatchewan, Canada	58°25′ N	109°31′ W	Currie (1969)	39	ex,smor	gl	481.5 ± 0.8	rad	c	19.0	?	27.0	?
Charlevoix	Quebec, Canada	47°32′ N	70°21′ W	Rondot (1966)	55	ex,sub,mor	r+c	450 ± (20	both	c	12.0	6000	25.0	?
Chesapeake Bay	Virginia, U.S.A.	37°14′ N	76°01′ W	Koeberl et al. (1994b)	85	b,sub	u	35.2 ± 0.3	both	c	11.0	?	38.0	?

Shock features	Target	Target lithologies	Impact in water	Hydrothermal alteration	Crater fill breccia	Ejecta (prox. or distal)	Erosion		Burial		Geophysics	Drilled	Resources
							Min	Max	Min	Max			
PDF	M	gr, m, l	x		x		0	50	0	100		x	
coes, PDF, bal, diapl	C	gr, gn, amph		x	x		100	300	0	10	s, g, e	x	
PDF (qtz/fsp) , diapl, SC	M	gr,gn, s, si, m, l		x	x		0	150	0	50		x	
SC, glass, diapl	C	amph, gab, gn, gr		x	x	x	0	200	315	530	s, g	x	
PF, Ir, Ni spinel, spherules, glass	S	m, carb, si	x	x	x	x	0	2500	2000	2500	s, g, e	x	
met	S	till, sand, gravel			x	x	0	4	10	0	s		
PF	S	m, l, s	x		x	x	0	70	20	120	s, e		
PDF, PF, coes, glass, diapl, SC	M	gn, gr, m, si, s, l	x		x	x	0	200	300	750	s, g	x	Oil shale
PDF, PF, SC, diapl, glass	C	sch, gab				x	500	1000	0	40	g, e	x	
PDF, PF, SC, diapl, mask, glass, dia	M	gn, amph, l, dolo, m		x	x	x	0	100	100	600	s, g, e	x	Diamond
coes, stish, red, dia, PDF, PF, FF, SC, masc, glass	M	gr, gn, amph, s, l, m		x	x	x	0	100	0	300	s, g, e	x	Cement, gravel
PDF, glass, SC	M	gn, m, s	x		x		0	100	0	100			
SC, PDF, PF, FF, diapl, mask, glass, pst	C	gn, gr, grano		x	x		50	400	0	20	g, e	x	
pst	C	gr			x		0	0	0	0		x	Oil shale
PDF, PF, diapl, glass	M	grano, dio, ton, gn, mig, sch					0	0	0	0	g	x	
PDF, PF, FF, SC	C	ton, gn, diab			x		0	150	0	150	g, e	x	
SC, PDF (qtz/fsp), PF, FF, pst	M	gr, mvolc, s, l		x			400	600	1500	2500	s, g, e	x	Cement, oil, Pb, Zn
PDF, PF, FF	M	gr, s, m	x				50	200	0	80	g, e	x	
SC, PDF	S	s, si, m, l			x	x	0	100	0	50	s, g, e	x	
met	S	soil				x	0	4	0	4		x	
PDF(qtz/fsp), PF	C	gr, gn, sch		x	x		?		0		g, e		Ore
SC, PDF, PF, FF	C	gr		x			0	0	0	0	e		
PDF (qtz/zir), PF, bal	C	gr, mig, sch			x		0	150	0	0	g, e	x	
SC, masc, PDF	C	grano, sch					100	250	0	0	e		
SC, coes, stish, dia, masc, diapl, PDF	C	sch, qutz, amph, sye, gr, ore			x		0	0	0	0	s, g, e	x	Iron ore
?	M	gn, s, si, l	x		x		250	350	50	200	s, g, e	x	
SC, diapl, PDF	S	s, si, m, l			x		0	100	140	260	s, g, e	x	
dia, PDF, PF, coes, bal	C	gr, mig, gn			x		0	100	40	40	s, g	x	Diamond
SC, PDF, diapl	C	gr, mig, gn			x		0	100	50	160	s, g, e	x	
PDF (qtz/fsp), PF, glass	M	l, dolo	x	x	x		0	50	2700	2800	s, g, e	x	Oil, gas
SC, PDF, PF, coes	M	sch, s, m	x	x	x		0	0	30	100	s, g, e	x	Gas
SC, pst	M	gn, s		x			0	0	0	0			
PDF? (qtz/fsp)	C	gr			x		0	50	0	3.5	e	x	
PDF, PF, glass, glass	C	grano, gn, amph	x	x	x		0	400	0	260	s, g, e	x	
PDF, PF	S	s, m, l, dolo		x			0	100	300	600	s, g, e	x	Oil
SC, PDF, PF, FF, masc, diapl, glass, pst	M	gn, s, dolo		x			500	800	0	100	s, g, e	x	U
PDF, PF, FF, SC, pst	M	mig, anor, charn		x	x	x	400	700	0	100	s, g, e	x	Ilmenite
PDF, PF, glass, diapl, tek	M	gn, s, si, sand	x	x	x	x	0	0	444	444	s, g, e	x	Groundwater

Table 3 *Continued*. Data of the known terrestrial impact structures.

		Location			D_{acr}			Age (Myr)		Type	D_{acu}	aSU	D_{ars}	d_{af}
Name	Country	Latitude	Longitude	Confirmation	(km)	Exposure	Hydrology	Age (yr)	Method		(km)	[m]	(km)	(m)
Chicxulub	Yucatan, Mexico	21°20′ N	89°30′ W	Hildebrand et al. (1991)	180	b,sub,smor	u	66	both	c	45.0	3000	90.0	?
Clearwater East	Quebec, Canada	56°03′ N	74°05′ W	Dence (1964)	24	ex,sub,mor	sub	460 - 470	rad	c	2.0	?	0.0	170
Clearwater West	Quebec, Canada	56°12′ N	74°30′ W	Dence (1964)	32	ex,sub,mor	gl+l	290 - 300	rad	c	8.5	?	22.0	350
Cloud Creek	Wyoming, USA	43°10′36″ N	106°42′30″ W	Stone and Therriault (2003)	7	b	u	190 ± (20	strat	c	1.4	520	6.0	?
Couture	Quebec, Canada	60°07′47″ N	75°17′56″ W	Robertson (1968)	8	sub,mor	sub	425 ± 25	rad	c	1.0	?	5.0	120
Crooked Creek	Missouri, U.S.A.	37°50′05″ N	91°23′44″ W	Dietz and Lambert (1980)	7	ex	u	323 - 348	strat	c	2.0	300	3.6	?
Decaturville	Missouri, U.S.A.	37°53′33″ N	92°43′11″ W	Offield and Pohn (1979)	6	ex,mor	r+c	< 300	strat	c	2.4	540	5.6	?
Decorah[a]	Iowa, U.S.A.	43°18′50″ N	91°46′20″ W	French et al. (2018)	5.6	acb	u	460 - 483	strat	t				?
Deep Bay	Saskatchewan, Canada	56°24′ N	102°59′ W	Innes (1957)	13	sub,mor	gl+l	95 - 102	strat	c	2.0	?	6.0	400
Des Plaines	Illinois, U.S.A.	42°02′42″ N	87°52′24″ W	McHone et al. (1986)	8.8	b	u	< 280	strat	c	1.0	350	6.0	?
Douglas[a]	Wyoming, USA	42°40′ N	105°28′ W	Kenkmann et al. (2018)	0.1	ex,pc,mor	u	280	strat	s				?
Eagle Butte	Alberta, Canada	49°42′ N	110°30′ W	Ezeji-Okoye (1985)	1	ex,pc,smor	u	< 66	strat	c	5.5	300	8.0	?
Elbow	Saskatchewan, Canada	50°58′ N	106°45′ W	Grieve et al. (1998)	8	b	u	201 - 358	strat	c	3.0	300	3.5	?
Flynn Creek	Tennessee, U.S.A.	36°17′ N	85°40′ W	Roddy (1977)	3.8	ex,pc	u	382	strat	c	0.8	450	2.1	90
Glasford	Illinois, U.S.A.	40°36′06″ N	89°47′06″ W	McHone et al. (1986)	10	b	u	455 ± 2	strat	c	4.0	300	?	?
Glover Bluff	Wisconsin, U.S.A.	43°58′12″ N	89°32′18″ W	Read (1983)	10	ex,pc	u	455 - 459	strat	c	1.0	?	?	?
Gow	Saskatchewan, Canada	56°27′23″ N	104°28′56″ W	Thomas and Innes (1977)	5	ex,sub,mor	gl+l	250	rad	c	1.5	?	3.5	?
Haughton	Nunavut, Canada	75°23′ N	89°39′ W	Robertson and Mason (1975)	23	ex,pc,mor	r+c	39	rad	c	2.0	1450	16.0	?
Haviland	Kansas, U.S.A.	37°34′57″ N	99°09′49″ W	Niniger and Figgins (1933)	0.017	destroyed	u	0.020 ± 0.002	strat	s				?
Hiawatha[a,b]	Greenland	78°45′ N	66°15′ W	Kjær et al. (2018)	31	b	r	< 2.6	strat	c	8.0	?	20.0	2
Holleford	Ontario, Canada	44°27′34″ N	76°37′57″ W	Beals (1960)	2.35	b,smor	r	> 485	strat	s				260
Ile Rouleau	Quebec, Canada	50°40′53″ N	73°52′49″ W	Caty et al. (1976)	4	ex,sub	gl+l	< 300	strat	c	1.0	?	?	?
Kentland	Indiana, U.S.A.	40°45′ N	87°24′ W	Dietz (1947)	12.5	ex,pc	u	< 107	strat	c	4.0	600	6.4	?
La Moinerie	Quebec, Canada	57°26′10″ N	66°35′09″ W	Gold et al. (1978)	8	ex,sub,smor	gl+l	400 ± 50	rad	c				?
Manicouagan	Quebec, Canada	51°23′ N	68°41′ W	Bunch and Cohen (1967)	100	ex,sub,mor	gl+l	214	rad	c	25.0	?	55.0	?
Manson	Iowa, U.S.A.	42°35′ N	94°33′ W	Short (1996)	35	b	u	74.1 ± 0.1	rad	c	8.0	2800	11.0	?
Maple Creek	Saskatchewan, Canada	49°48′00″ N	109°06′30″ W	Grieve et al. (1998)	6	b,smor	u	< 75	strat	c	3.0	600	4.0	?
Marquez	Texas, U.S.A.	31°17′00″ N	96°17′30″ W	Sharpton and Gibson (1990)	15	ex,pc	u	58.3 ± 3.1	both	c	2.5	1120	5.0	50
Meteor Crater	Arizona, U.S.A.	35°01′39″ N	111°01′20″ W	Barringer (1910)	1.2	ex,pc,mor	r	0.049	rad	s				180
Middlesboro	Kentucky, U.S.A.	36°37′03″ N	83°43′39″ W	Dietz (1966)	6	ex,mor	r	290 - 300	strat	c	0.5	245	?	?
Mistastin	Newfoundland, Canada	55°53′ N	63°18′40″ W	Taylor and Dence (1969)	28	ex,sub,mor	gl+l	36.6 ± 2	rad	c	3.5	?	10.0	200
Montagnais	Nova Scotia, Canada	42°53′ N	64°13′ W	Jansa and Pe-Piper (1987)	45	sub, b	sub	50.5 ± 0.8	both	c	11.5	1800	18.0	500
Newporte	North Dakota, U.S.A.	48°58′ N	101°58′ W	Gerlach et al. (1994)	3	b	u	500	strat	s				100
Nicholson	NWT, Canada	62°40′ N	102°42′ W	Dence et al. (1968)	12.5	ex,sub,smor	gl+l	389.0 ± 6.7	rad	c	5.0	?	12.0	?
Odessa	Texas, U.S.A.	31°45′21″ N	102°28′43″ W	Bibbins (1926)	0.17	ex,pc,mor	r	0.0635 ± 0.0045	both	s				?
Pantasma[a,b]	Nicaragua	13°21′49″ N	85°57′14″ W	Rochette et al. (2019)	14	ex,mor	r	0.815 ± 0.011	rad	c				?
Pilot	NWT, Canada	60°17′06″ N	110°59′54″ W	Dence et al. (1968)	6	sub,smor	gl+l	445 ± 2	rad	c				130
Pingualuit (New Quebec)	Quebec, Canada	61°16′40″ N	73°39′36″ W	Currie and Dence (1963)	3.4	ex,sub,mor	r+l	1.4 ± 0.1	rad	s				250
Presqu′ile	Quebec, Canada	49°43′ N	74°50′ W	Higgins and Tait (1990)	22	ex,sub	gl+l	< 500	strat	c				?

Shock features	Target	Target lithologies	Impact in water	Hydrothermal alteration	Crater fill breccia	Ejecta (prox. or distal)	Erosion		Burial		Geophysics	Drilled	Resources
							Min	Max	Min	Max			
PDF (qtz/fsp), PF, FF, SC, lec, diapl, red, pst	M	gr, l, anh	x	x	x	x	0	0	400	800	s, g, e	x	
PDF, PF, glass, mask	M	gr, grano, gn		x	x		1300	2400	0	150	s, g, e	x	
PDF, FF, SC, glass, mask,	M	gr, grano, gn, amph, monz			x		1800	2200	0	50	s, g, e	x	
PDF	S	s, l					0	0	900	1200	s, g, e	x	Oil
melt, PDF (qtz/fsp)	C	gn, diab		x	x		100	500	0	50	g, e		
SC, PDF, PF, FF	S	s, l, dolo		x			100	400	0	50	g, e		Pb, Zn, Ba, Fe
SC, PDF, PF, FF	S	dolo		x	x		0	0	0	0	g, e	x	Pb
PDF, PF, FF	S	s, m, carb			x		0	100	0	111	e	x	
PDF (qtz/fsp), bal, glass	C	gn		x	x		0	200	0	300	s, g, e	x	
SC	S	s, dolo		x			0	0	25	60	g	x	
PDF, PF	S	s, sand	x			x	0	30	0	10			
SC, PF	S	s,si, m, coal					0	200	300	700	s, g, e	x	Oil
PDF	S	carb					0	200	850	1100	s, g, e	x	oil
SC, PDF	S	l, dolo	x		x	x	50	100	0	100	g, e	x	
SC	S	s, m, dolo,			x			0	500	800	s	x	Gas storage
SC	S	s, dolo	x				0	0	0	0	g, e	x	Gravel, mortar
PDF, bal, glass	C	gr, gn			x		150	350	0	50	g		
SC, PDF, PF, FF, coes, glass	S	gn, doler, l, dolo		x		x	200	200	0	0	g, e		
met	S	soil			x	x	0	1	0	2			
PDF, diapl	C	gr, gn, sch		x	x		0	200	900	1000	e		
PDF, coes	C	gn, mar		x	x		0	150	0	262	s, g, e	x	
SC, PDF	S	dolo, m					300	400	0	0	e		
SC, PDF, PF, FF	S	l, s, si, m		x			300	1900	0	70	s, g	x	Limestone, gravel
PDF, glass, diapl, pst	C	gn			x	x	100	200	0	50	g		
mask, diapl, PDF (qtz/fsp), PF, glass, pst, SC	M	gr, gn, gab, anor, char, l, dolo, m		x	x	x	50	150	0	50	s, g, e	x	
PDF, PF (qtz/fsp/apa), glass	M	gr, gn, s, m, carb		x	x		0	100	30	100	s, g, e	x	Groundwater
PDF	S	si, m			x				200	300	s, g	x	
SC, PDF, PF	S	s, ma, m	x		x		0	50	0	900	s, g, e	x	Gas
Met, Coes, Stish, PDF, PF, FF	S	s, l, m			x	x	0	20	0	60	s, g, e	x	
SC, PDF, PF, FF, pst	S	s, congl, si, coal			x				3000	4000		x	
SC, PDF, PF, diapl, mask	C	anor, grano		x	x		20	100	0	20	g, e		
PDF, PF, FF, melt rock	M	gr, qutz, grey, si	x		x		0	0	500	1000	s, g, e	x	Oil
PDF, PF, melt rock	M	gr, s	?		x		0	0	2880	3000	s, g, e	x	Oil sand
SC, PDF, PF, melt rock	M	gr, gn, l		x	x		300	600	0	0	g, e		
met.	S	s, l			x	x	0	0.002	0	0.027		x	
coes, FRIGN, glass	C	and, ryh, dac					0	250	0	0			
PDF, glass	C	gn					300	500	0	0	g, e		
PDF(qtz/fsp), PF, bal, glass	C	gn, grano		x	x		0	100	0	50	s, g, e		
SC	C	ton, green					500	1000	0	0	g, e		

Table 3 *Continued*. Data of the known terrestrial impact structures.

		Location			D_{acr}			Age (Myr)		Type	D_{acu}	aSU	D_{ars}	d_{af}
Name	Country	Latitude	Longitude	Confirmation	(km)	Exposure	Hydrology	Age (yr)	Method		(km)	[m]	(km)	(m)
Red Wing	North Dakota, U.S.A.	47°36′ N	103°33′ W	Brenan et al. (1975)	9	b	u	200 - 220	strat	c	6.0	1000	10.0	?
Rock Elm	Wisconsin, U.S.A.	44°43′25″ N	92°13′41″ W	French et al. (2004)	6.5	ex,smor	r+c	410 - 460	strat	c	1.5	300	4.5	48
Saint Martin	Manitoba, Canada	51°47′ N	98°32′ W	McCabe and Bannatyne (1970)	40	ex,sub	gl+l	227.4 ± 0.8	both	c	5.0	?	22.0	?
Santa Fe	New Mexico , U.S.A.	35°43′54″ N	105°51′04″ W	Fackelman et al. (2007)	9.5	ex	u	350 – 1,200	strat	c				?
Serpent Mound	Ohio, U.S.A.	39°01′56″ N	83°24′10″ W	Carlton et al. (1998)	8	ex,smor	r+c	256 - 290	strat	c	2.2	122	7.0	?
Sierra Madera	Texas, U.S.A.	30°35′44″ N	102°54′42″ W	Eggelton and Shoemaker (1961)	12	ex,pc,mor	r+c	< 100	strat	c	8.0	1200	11.0	?
Slate Islands	Ontario, Canada	48°39′ N	87°01′ W	Halls and Grieve (1976)	30	ex,sub	gl+l	436 ± 3	rad	c	12.0	1100	15.5	150
Steen River	Alberta, Canada	59°30′ N	117°38′ W	Carrigy and Short (1968)	22	b	u	108	both	c	6.0	1000	20.0	150
Sudbury	Ontario, Canada	46°36′ N	81°11′ W	Dietz and Butler (1964)	200	ex,pc,smor	gl+l	1849.3 ± 0.3	rad	c	90.0	?	?	?
Tunnunik	Arctic, Canada	72°28′ N	113°55′ W	Dewing et al. (2013)	25	ex,mor	gl+c	430 - 450	strat	c	20.0	?	?	?
Upheaval Dome	Utah, U.S.A.	38°26′09″ N	109°55′40″ W	Buchner and Kenkmann (2008)	6	ex,mor	c	66 - 100	strat	c	2.5	250	5.5	?
Viewfield	Saskatchewan, Canada	49°35′ N	103°04′ W	Grieve et al. (1998)	2.5	b	u	190	strat	s				180
Wanapitei	Ontario, Canada	46°44′44″ N	80°44′43″ W	Dence and Popelar (1972)	7.5	sub	sub	37 ± 2	rad	c				50
Wells Creek	Tennessee, U.S.A.	36°22′34″ N	87°39′33″ W	Dietz (1959)	12	ex,smor	r+c	70 - 325	strat	c	2.5	1000	5.0	?
West Hawk	Manitoba, Canada	49°45′41″ N	95°11′12″ W	Halliday and Griffi (1963)	2.4	sub	sub	351 ± 20	rad	s				260
Wetumpka	Alabama, U.S.A.	32°31′24″ N	86°10′32″ W	King et al. (1999)	7	ex,mor	r+c	84.4 ± 1.4	both	c	1.0	100	3.5	?
Whitecourt	Alberta, Canada	53°59′57″ N	115°35′50″ W	Herd et al. (2008)	0.036	ex,mor	r	< 0.0011	rad	s				6
SOUTH AMERICA														
Araguainha	Brazil	16°47′ S	52°59′ W	Dietz and French (1973)	40	ex,mor	r+c	252 - 259	rad	c	5.0	1200	7.0	?
Campo Del Cielo	Argentina	27°38′ S	61°42′ W	Spencer (1933)	0.08	ex,mor	u	0.004	rad	s				6
Carancas	Peru	16°39′52″ S	69°02′38″ W	Macedo and Macharé (2007)	0.014	ex,sub,mor	r+l	0.000012	observed	s				3
Cerro do Jarao[a]	Brazil	30°12′28″ S	56°32′21″ W	Reimold et al. (2018)	13	ex,smor	r+c	< 137	strat	c	5.5	?	?	?
Colônia[b]	Brazil	23°52′10″ S	46°42′22″ W	Crósta et al. (2019a)	3.6	ex,pc,mor	r	5 - 36	strat	t				350
Monturaqui	Chile	23°55′40″ S	68°15′42″ W	Sanchez and Cassidy (1966)	0.36	ex,mor	r	0.663 ± 0.090	rad	s				34
Novas Colinas[a]	Brazil	07°09′33″ S	46°06′30″ W	Reimold et al. (2020)	5	ex,smor	r+c	< 300	strat	c	0.8	0	3.0	?
Riachão Ring	Brazil	07°43′00″ S	46°38′36″ W	Maziviero et al. (2013)	4.1	ex,mor	r+c	< 300	strat	c	1.4	570	2.4	?
Rio Cuarto[b]	Argentina	32°52′ S	64°11′ W	Schultz and Lianza (1992)	4.5	ex,mor	u	< 0.114	rad	s				?
Santa Marta	Brazil	10°10′19″ S	45°13′58″ W	De Oliveira et al. (2014)	10	ex,pc,mor	r+c	< 93	strat	c	4.0	1000	6.0	?
Sao Miguel do Tapuio[a]	Brazil	05°37′36″ S	41°23′18″ W	Crósta et al. (2019c)	21	ex,mor	c	< 300	strat	c	5.0	?	10.0	?
Serra da Cangalha	Brazil	08°04′45″ S	46°51′24″ W	Kenkmann et al. (2011)	13.7	ex,mor	r+c	< 300	strat	c	5.8	750	8.0	?
Vargeão Dome	Brazil	26°48′53″ S	52°09′49″ W	Crósta et al. (2012)	12.4	ex,mor	c	< 137	rad	c	3.0	1150	5.5	200
Vista Alegre	Brazil	25°57′12″ S	52°41′23″ W	Crósta et al. (2010)	9.5	ex,mor	u	111 - 134	rad	c	2.2	800	3.2	150

ex = exposed; b = buried; acb = almost completely buried; pc = partly covered; sub = submerged; mor = morphologically visible; smor = subdued morphological expression; c = concentric; r = radial; r+c = radial and concentric; r+l = radial and lake; gl+l = glacial and lake; u = unrelated; sub = submerged; s = simple; c = complex; t = transitional; SC = shatter cone; PDF = planar deformation feature; PF = planar fracture; FF = feather feature; mask = maskelynite; diapl = diaplectic quartz glass; bad = baddelyite; glass = melt glass; pst = pseudotachylite; bal = ballen quartz; coes = coesite; stish = stishovite; red = redeite; S = sedimentary; C = crystalline; M = mixed; s = sandstone; si = siltstone; m -mudstone/shale; congl = conglomerate; l = limestone; dolo = dolomite; gr = granite; gn = gneiss; sch = schist; gab = gabbro; anor = anorthosite; char = charnockite; mig = migmatite; qutz = quartzite; qtzdio = quart diorite; dio = diorite; grano = granodiorite; doler = dolerite; dia = diabase; bas = basalt; ryh = ryholite; dac = dacite; mvolc = metavolcanics; mgrey = metagreywacke; s = seismic; g = gravity; e = electromagnetic, magnetic, radar.

[a]Not listed in EID.

[b]Needs further proof.

Shock features	Target	Target lithologies	Impact in water	Hydrothermal alteration	Crater fill breccia	Ejecta (prox. or distal)	Erosion		Burial		Geophysics	Drilled	Resources
							Min	Max	Min	Max			
SC, PDF, PF	S	s, m, carb			x		0	0	2000	2500	s, g, e	x	Oil, gas
PDF, PF, FF, red	S	s, m, dolo					250	350	0	15	g, e		
PDF, glass, pst	M	gr, carb		x	x		100	200	0	100	g, e	x	Gypsum
SC, PDF, PF (qtz/apa/zir), glass	M	gr, sch, qutz, l		x	x		500	1000					
SC, PDF, glass	S	s, m, l, dolo		x			300	400			g	x	Pb, Zn
SC, PDF, PF	S	l, dolo, s, m	?				300	600	0	50	g, e	x	Gas
SC, PDF (qtz/fsp), pst	C	rhy, bas, gr					200	500	0	50	s, g, e		Gold
PDF, glass, mask, diapl	M	gr, gn, congl, s, m		x	x	x	100	200	180	200	s, g, e	x	Oil, gas
SC, PDF (qtz/fsp), PF, FF, masc, diapl, glass, pst	C	gr, gab, gn, sch		x	x		0	4000	0	5000	s, g, e	x	Cu, Ni, Co, Pt
SC	S	dolo, l, s, m					700	5000	700	5000	g, e		
PDF	S	s, si, m					1000	1800	1400	1800	s, g	x	
PDF, PF	S	l	x		x	x	0	0	1250	1430	s, e	x	Oil, gas
PDF, diapl, glass, bal	C	gr, gn, dia, mgrey			x	x	0	50	0	50	g, e		
SC	S	l, dolo, m, s					0	0	0	0	s, g, e	x	
PDFs, PF, FF, diapl, glass	C	gn, mbas, mand		x	x	x	50	100	0	90	g, e	x	
PDF, PF, FF	M	gr, gn, sand, gravel, clay	x		x	x	0	100	0	0	g, e	x	
met	S	sand, gravel, soil			x	x	0	0	0	0			
SC, PDF, PF, FF, mask, diapl, melt, pst	M	gr, sch, qutz, s, congl		x		x	800	2000	0	20	g, e		
met	S	loess, soil			x	x	0	3	0	4	e	x	
met	S	sand, gravel, soil			x	x	0	1	0	4		x	
SC, PF, PDF, FF	S	s, bas					300	800	0	50	g, e		
PDF?	M	gn, mig, qtzdio, qutz, sch, m				x	0	0	0	0	s, g, e	x	
PDFs, PF, diapl, melt, coes, stish	C	gr, rhy			x	x	0	5	0	0	g		
PDF, PF, FF	S	s, si, m			x		200	500	0	20	g, e		
PDF, PF, FF	S	s, m					200	500	0	20	g, e		
met, glass, bad	S	loess, soil					0	30	0	0			
SC, PDF, PF, FF	S	s, m, congl					500	800	0	50	g		
PDF, PF, FF	S	s					500	1000	0	50	g, e		
SC, PDF, PF, FF	S	s, si, m, chert					500	700	0	50	s, g, e	x	
SC, PDF, PF, FF, mask	M	s, bas, dac			x		300	500	0	50	s, g, e	x	
SC, PDF, FF, PF	M	bas, s					200	400	0	20	g		

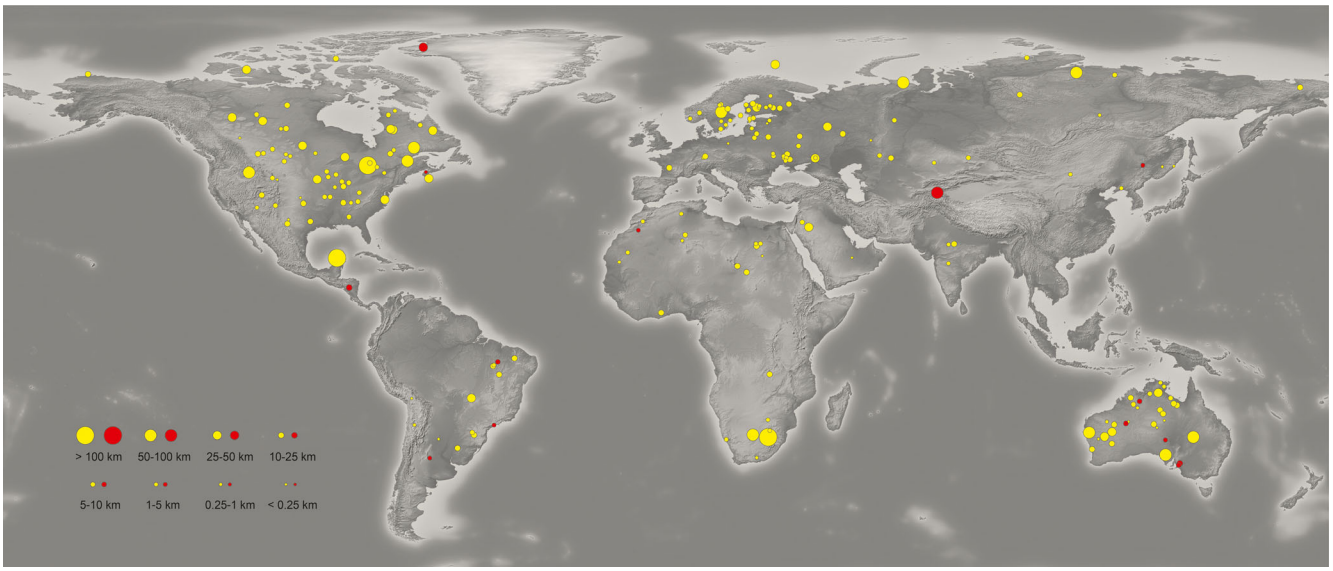

Fig. 2. The distribution of terrestrial impact structures. The size of a symbol is a measure for the structure's diameter. Yellow symbols show confirmed impact structures, whereas red symbols indicate those, where an unambiguous confirmation is still pending.

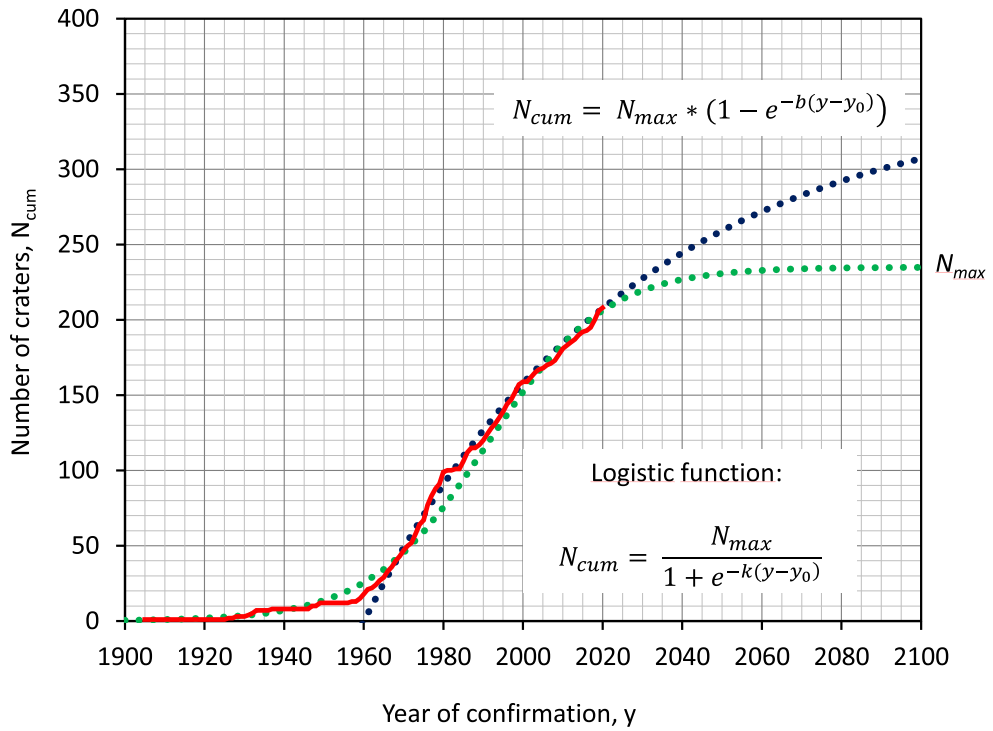

Fig. 3. Cumulative impact crater confirmations with time. The discovery history can be fitted with a logistic function (green dotted line) or an exponential function (blue dotted line). (Color figure can be viewed at wileyonlinelibrary.com.)

population of larger craters is almost complete. The diameter below which craters are strongly underrepresented coincides roughly with the simple-to-complex transitional diameter of terrestrial craters. Small craters have a shorter lifetime with respect to erosion, due to the limited depth to which they can be recognized and the relatively small volume of shocked material. In addition to that they are simply more difficult to discover. Relatively small, circular depressions can be formed by a multitude of endogenic and exogenic processes, and include maars, calderas, sinkholes in carbonate rocks or salts, dead ice holes, etc.

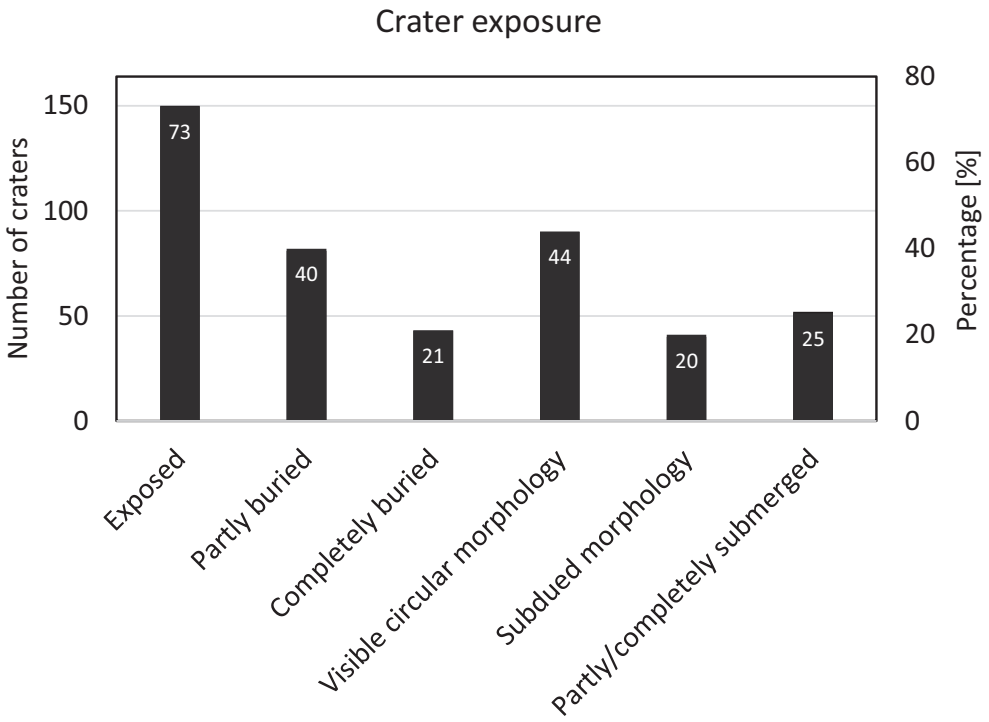

Fig. 4. Appearance of the terrestrial craters. Black columns give the absolute number of a certain crater feature (left axis), the numbers in the columns show percentages (right axis). Note that several characteristics can apply to a single crater. For example, Lockne crater is exposed, partly buried, has a subdued morphology, and is partly submerged. In contrast, Des Plaines is completely buried while none of the other features apply.

It is particularly difficult to identify small simple impact craters in periglacial regions, where the landscape is sculptured by glacier retreat and contains abundant dead ice holes. The prognosis presented here is in conflict with estimates of 845 yet-to-be discovered impact craters, measured from the year 2010 onward, by Stewart (2011).

To conclude after about 100 yr of impact crater research, the terrestrial impact crater record is still incomplete, particularly for small simple and buried craters. Antarctica and Greenland, which have a combined area of almost 16.5 million km^2 (about 10% of the land mass of the Earth), currently elude evidence of impact craters, but potential crater structures such as Hiawatha in Greenland (Kjær et al. 2018), however, suggest that these landmasses may contain many structures, in particular as they represent old cratonic continents.

EXPOSURE, BURIAL, AND POSTIMPACT DEFORMATION

Erosion and burial are the main geologic mechanisms that most severely affect the appearance of terrestrial impact craters. Of the 150 (73%) impact craters exposed at the Earth's surface, 90 (44% of all terrestrial impact craters) have a clear and easy-to-recognize circular morphology (Gottwald et al. 2020) (Figs. 4 and 5). Their circular topography, however, does not always reflect the pristine crater morphology. More often, the circularity results from selective erosion of rocks that have been involved in the cratering process (Fig. 1c). Tilting of strata toward the crater center, or away from it, leads to a concentric strike direction in the target rocks, which is then reflected in the morphology. Examples of easy-to-recognize impact structures are the more or less pristine, simple craters Barringer, Wolfe Creek, Twaing, or less well-preserved Xiuyan (Fig. 5a), to name a few simple craters. The circular topographies of large complex crater such as Serra da Cangalha (Fig. 5d), Siljan (Fig. 5e), or Vredefort (Fig. 5f) are in contrast to the results of selective erosion (Table 1). Forty impact craters (20%) (Fig. 4) have subdued morphologies, but the transition with the easily recognizable structures is not sharp and subject to bias by the observer. The recognition of subdued morphologies usually presupposes knowledge of the impact structure and requires remote sensing resources and high-resolution digital elevation models. Examples of this morphological class of craters are Strangways and Shoemaker in Australia. In addition, not all craters with a subdued morphology are exposed.

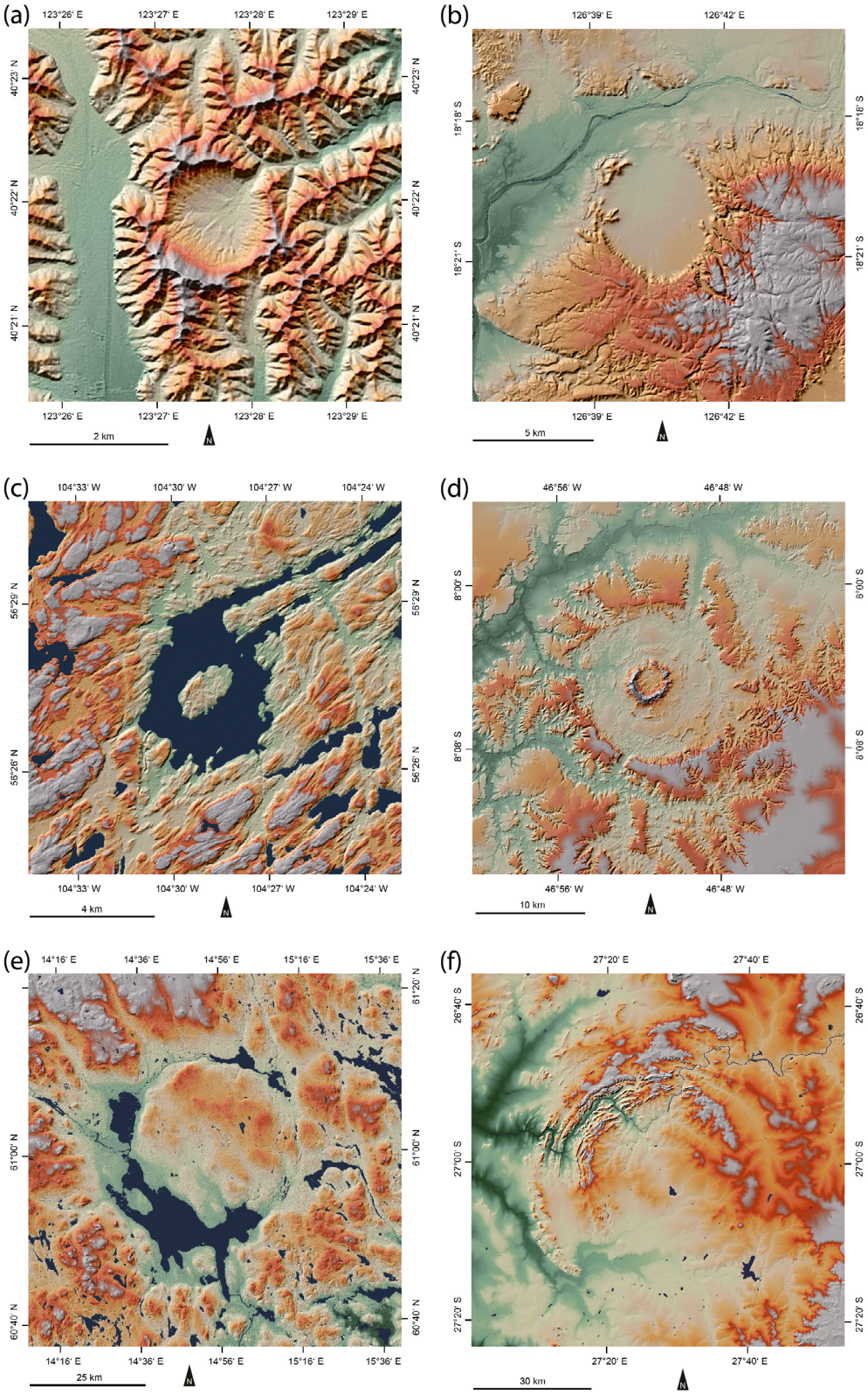

Fig. 5. TanDEM-X images of impact structures of different size and state of preservation: (A) Xiuyan, China, 1.8 km diameter; (B) Goat Paddock, WA, Australia, 5 km diameter; (C) Gow, Saskatchewan, Canada, 5 km diameter; (D) Serra da Cangalha, 13.7 km diameter; (E) Siljan, Sweden, 65 km diameter; (F) Vredefort, South Africa, 250 km diameter.

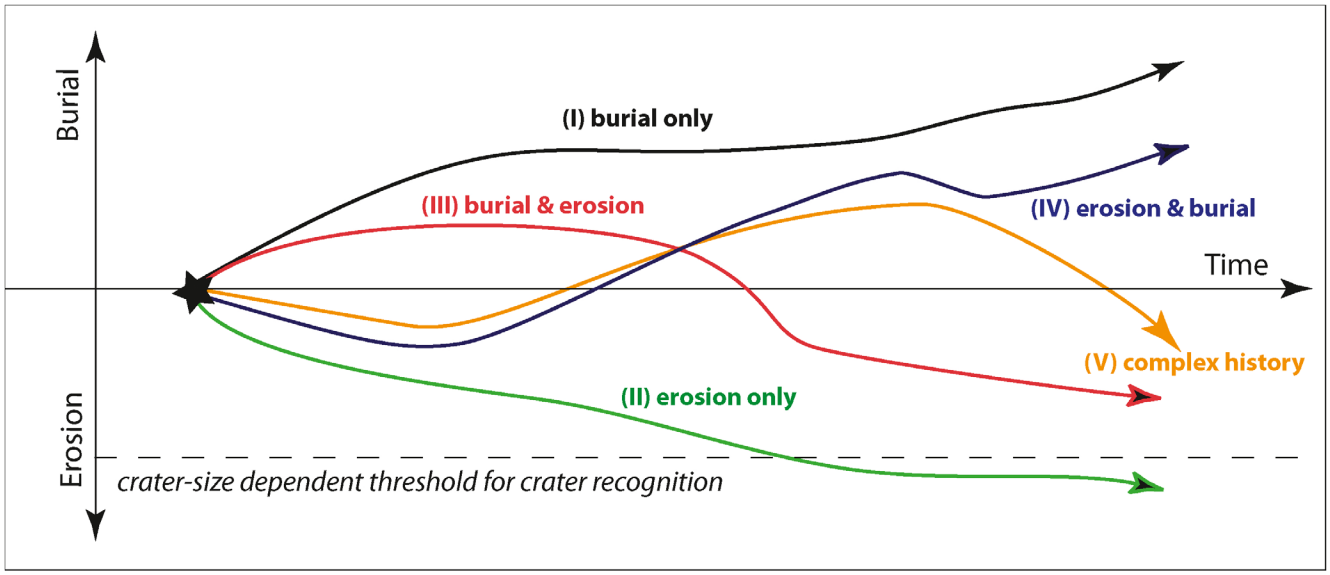

Fig. 6. Scenarios of possible postimpact histories.

Some craters of this class are buried or almost completely buried, but the structure still affects the surface and influences the course of drainage pattern (e.g., Saqqar) or forms a gentle circular depression due to differences in compaction of impact lithologies and the variable thickness of postimpact sediments (e.g., Yallalie, Holleford). Even the Chicxulub structure, which is buried by ~1 km of postimpact sediments, is expressed at the surface by a concentric array of cenotes (sinkholes) that trace one of the concentrically striking rim faults at depth. In contrast, several of the exposed craters have no morphological expression. Examples for this category are, for example, the Santa Fe, Beaverhead, or Yarrabubba impact structures.

Forty-three (21%) impact craters are buried (Fig. 4). I counted a crater as buried if more than 95% of its surface is covered by younger deposits of significant thickness. In Table 3, the category of "almost completely buried" structures is introduced to identify craters with a few percentages of exposure (e.g., Saqqar, Decorah, Yallalie, Ilyinets, Ragozinka, Karla, Kärdla). With 3 km of overburden, the 3 km diameter Newporte structure (Koeberl and Reimold 1995) appears to be the most deeply buried known structure.

Many craters, now exposed at the surface, however, have experienced significant burial in their postimpact history. Indeed, the postimpact history is often very complex and may lead to alternating phases of erosion and burial. I distinguish five general scenarios (I)–(V) (Fig. 6).

Scenario I is a crater that never underwent a phase of erosion but has been, and still is, completely buried. The submerged Mjølnir or Montagnais craters are examples for scenario I. Scenario II is a crater that has experienced continuous erosion, without any documented phases of burial. Deeply eroded craters, such as Upheaval Dome, may fall in this category. Scenario III is a crater that has undergone burial followed by exhumation and erosion. A good example for such a postimpact history is the Ordovician Lockne crater. It formed under submarine conditions in 200–500 m deep water. The event caused a forceful sediment-laden resurge into the crater that eventually graded into the normal ongoing shelf sedimentation and this burial continued until the Silurian. Then, this basin, that represented a foredeep of the Caledonian orogeny, narrowed and the crater eventually became overthrust by a several kilometer thick pile of tectonic nappes. Uplift, exhumation, and partial erosion happened only in the Quaternary. Relics of the nappes still exist as inliers within the crater depressions. This crater along with others (e.g., Ritland) belongs to the large group of partly covered craters (Table 3). Another example of this group is the Permian Douglas crater strewn field. Shortly after their formation, the small crater pits were covered by lagoonal muds and this prevented the destruction of the craters. An extended period of burial lasted until the Laramide orogeny that resulted in uplift and final exhumation. Scenario IV is the opposite and starts with an initial phase of erosion followed by a period of sedimentation. Some of the buried craters of the Ukrainian Shield belong to this group. Craters such as Kursk were peneplained prior to burial; as a result, the postimpact sediments that cover the crater are horizontal in dips. Even more complex postimpact scenarios are possible, for example, a phase of erosion

and subsequent burial, followed by exhumation and erosion. The Saqqar impact structure, for example, experienced severe denudation before burial took place. Nowadays the structure's southern margin has reappeared at the surface. More complexities of the postimpact history also arise from the fact that crater relief causes simultaneous erosion and sedimentation. That is, combinations of the above are possible. For example, the crater rim and the ejecta of Meteor Crater, Wolfe Creek, Roter Kamm, and Tabun Kara-Obo have experienced erosion since the formation of the crater (scenario I) while their crater depression has experienced more or less continued sedimentation (scenario II).

The absolute amount of sediment load above a buried impact structure is a relevant quantity in impact crater studies, because the petrophysical properties of target rocks and impactites change as a function of the overburden pressure and affect the geophysical signature of a crater. Such properties include, for example, porosity, degree of compaction, mineral reactions and mineralization, and the mobilization of hydrocarbons (oil/gas). Hydrothermal alteration of the target rocks and impact lithologies may also belong to postimpact processes and are often initiated by the thermal pulse of the impact event itself. Forty-two craters exhibit clear signs of hydrothermal alterations (Table 3).

In addition to the absolute amount of overburden, the effects of postimpact burial are related to the size and depth of the crater. A crater 12 km diameter can pause through 200 m of overburden (e.g., Yallalie) by differential compaction of impactites and the postimpact sediment fill that has a variable thickness, but a crater 100 m in diameter will not be able to imprint through a sediment pile of 200 m. To make the terminology of burial more precise, we restrict the term "shallowly buried" to craters that, although buried, still affect the landscape.

Figure 7 is an attempt to illustrate the current state of erosion and burial of the terrestrial impact craters. On the one hand, the large error bars reflect our limited knowledge of the exact amount of erosion and sediment overburden; on the other hand, the craters' original relief causes variation in the amount of burial and erosion. As noted earlier, some of the craters are both eroded and buried to some degree due to their relief. The crater detection limit, H, shown in Fig. 7 is taken from Hergarten and Kenkmann (2015, equation 2 therein). It represents a threshold defined by the maximum depth, $H(D)$, down to which shock effects are recognizable for a given diameter, D. The kink in the curve reflects the simple-to-complex transition of terrestrial impact craters. Craters near this detection limit are the deeply eroded Upheaval Dome crater (Kenkmann et al. 2005), and the Douglas crater pits, the latter represented by a single dot. Picaninny may have exceeded this limit already, as ultimate proof, in the form of shocked materials has yet to be documented. The other dotted lines are parallel shifts of the crater detection limit H and are defined as follows: 1/3 H: deeply eroded, 1/10 H: moderately, and 1/30 H: weakly eroded. Burial is defined accordingly: −1/30 H: shallowly buried, −1/10 H moderately buried, −1/3 H: deeply buried.

Aside from erosion and burial, tectonic deformation may overprint a crater structure. There are 18 impact structures that have been severely affected by postimpact deformation: Lockne, Målingen, Ritland, Beaverhead, and Sudbury have been thrusted over by large-scale nappe systems within orogenic belts. Craters such as Santa Fe, Cloud Creek, and the Douglas craters have been tilted and deformed by Laramide-style Rocky Mountain orogeny. Luizi, Charlevoix, and Lappajärvi have been displaced or truncated by large-scale fault zones.

HYDROLOGY AND DRAINAGE PATTERN

Impact structures with visible circular morphology or subdued topography often show a characteristic drainage pattern that can be characterized as (1) radial-centripetal, (2) radial centrifugal, (3) concentric, or a combination of (1)–(3). Radial stream networks, often associated with central lakes, are particularly frequent in small craters with simple morphologies and occur in more than one quarter of all craters (Fig. 8). Pristine simple craters, such as Meteor crater, develop a radial-centripetal drainage system in their crater interior, while the rim crest defines the catchment (see also Fig. 5a). The ejecta blanket is characterized by a radial centrifugal drainage system. If the ejecta blanket contains ramparts, the radial-centrifugal system can be combined locally with concentric elements, for example, Bosumtwi (Wulf et al. 2019). Landscape evolution modeling shows that the drainage pattern behaves conservatively and is capable of keeping its channel pattern even if the cause of the original pattern has been removed (Wulf et al. 2019). This may allow us to better estimate the original crater size of degraded craters. Radial drainage patterns in complex craters are relatively rare (e.g., Yallalie, Conolly Basin, Söderfjärden). Eroded craters dominated by a central peak may have a dominant radial centrifugal drainage system (e.g., Sierra Madera). Twelve impact craters show dominant concentric stream networks, all of them belong to the group of complex craters formed in a layered target with dominantly siliciclastic lithologies. These are Vargeão, Sao Miguel do Tapuio, Tunnunik,

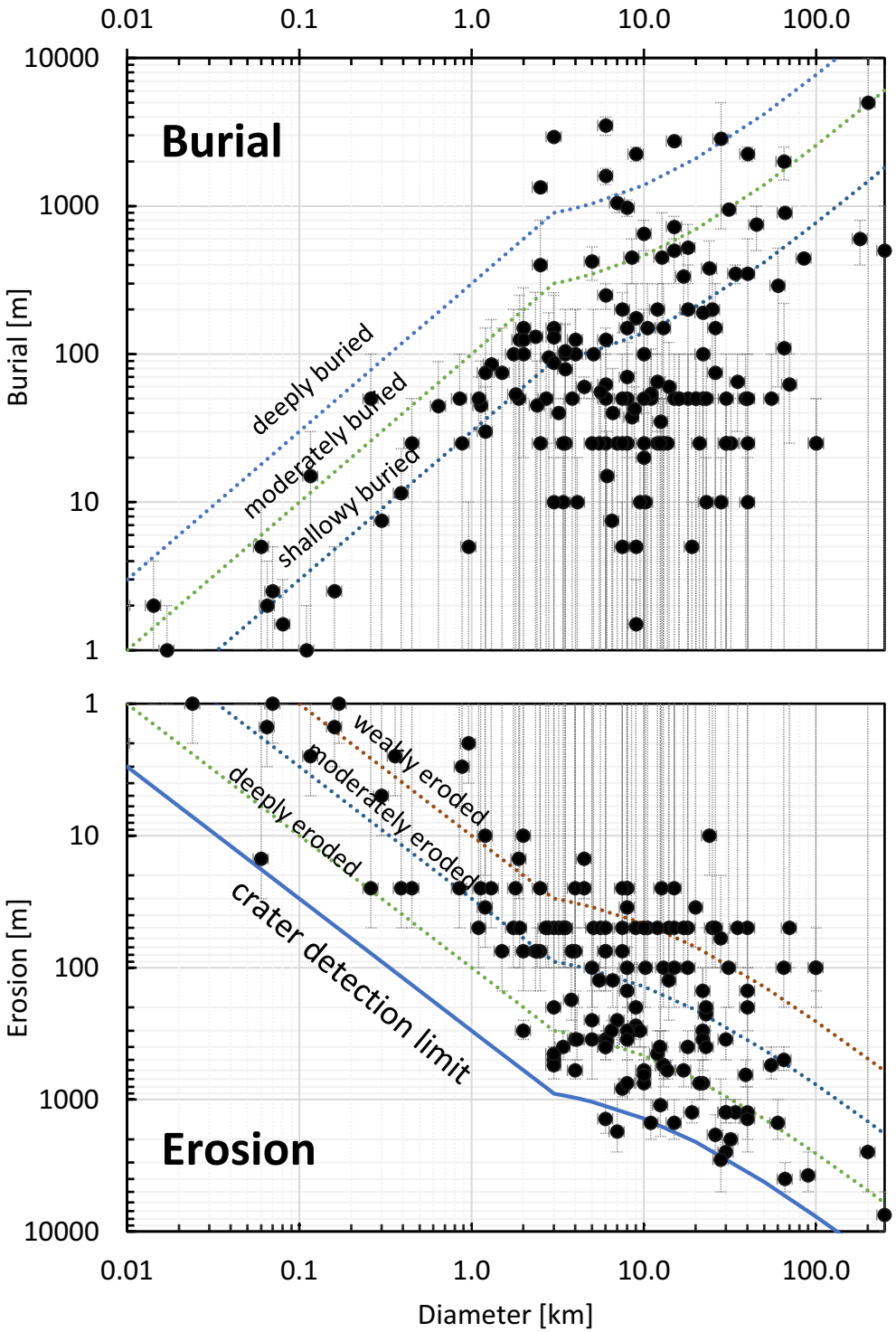

Fig. 7. Estimation of present-day erosion and burial of impact craters. (Color figure can be viewed at wileyonlinelibrary.com.)

Upheaval Dome, Strangways, Spider, Goyder, Foelsche, Chiyli, Tin Bider, B.P., and Aorounga. If selective erosion of the central uplift forms ring-like topographic highs, called collars, alternating with a central depression and an annular moat (e.g., Serra da Cangalha [Fig. 5d], Gosses Bluff, Ramgarh, Jebel Waqf as Suwwan), then those collars are acting as local divides and cause a combination of radial-centripetal,

radial-centrifugal, and concentric drainage. Such combinations are typical for many of the complex impact craters (15%) (Fig. 8).

In humid climate zones, the centripetal drainage and the morphological depression of the crater lead to the formation of lakes. These lakes are often circular and deep. More than a quarter of all known terrestrial impact craters are covered to a significant degree by a lake, 15 of them are completely submerged (Fig. 8). Of those Suvasvesi North and South, Clearwater East, Summanen, Karikkoselkä, Wanapitei, Couture, Pilot, Bloody Creek, and West Hawk are submerged in freshwater lakes; Tvären, Lumparn, and Neugrund in the brackish to marine water of the Baltic Sea; and only two, Mjølnir and Montagnais, occur in a shelf environment of the Atlantic Ocean. As mentioned earlier, Eltanin is the only currently known cratering-induced disturbance at the deep floor of the Pacific Ocean.

Lakes are particularly frequent in regions that have been glaciated throughout the Pleistocene. Most of the craters in Scandinavia and in Canada contain a lake. Both regions were denudated by several cycles of Pleistocene glaciation. The resulting morphology is a hummocky terrain sculptured by the deposits of ground moraines, esker, etc. Regional tectonic joint systems and easy-to-erode lithologies are preferentially scoured. Ancient impact craters of those regions, which contain strongly fractured and brecciated bedrock and friable crater fill breccia are sites of intense glacial scouring and, consequently, form deep circular depressions filled with till and subsurface water. These rather deep lakes deviate in shape and depth from typical glacially formed lakes that are commonly strongly elongated, of a preferred orientation, and irregular in shape (Grieve 2006). The drainage pattern of craters in terrains with glacial and periglacial landforms is less significant for impact craters and is often a mixture of the regional pattern with some deflections by the circular crater anomaly.

With increasing exposure age and crater denudation, the influence of the crater landform usually diminishes. The catchment area then deviates more and more from the crater shape. Eventually, superordinate catchments dominate the crater region and rivers may cross the crater. Consequently, a large number of the exposed or partly exposed and buried craters have stream networks that are entirely unrelated to the presence of the impact crater (Fig. 8).

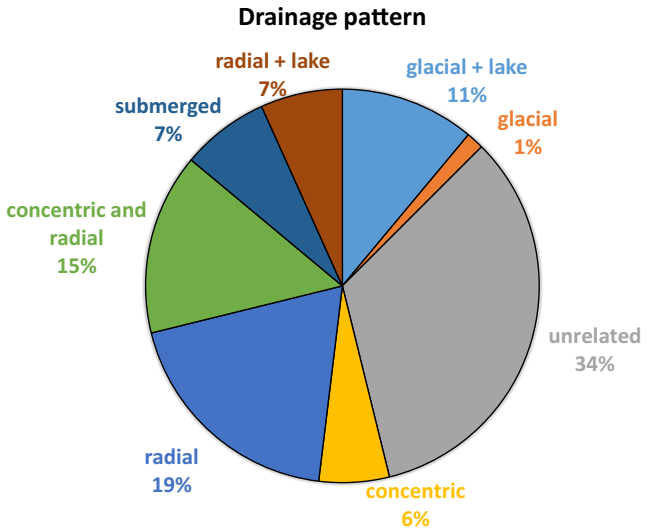

Fig. 8. Hydrology/drainage pattern of terrestrial impact craters. (Color figure can be viewed at wileyonlinelibrary.com.)

CRATER OUTLINES

Although terrestrial craters are degraded to variable degrees, the majority of them have circular outlines. Thirty-four craters have an uneven or somewhat elliptical outline with an aspect ratio (ratio of long diameter axis to short diameter axis) of larger than 1.05 and 11 have values of 1.2 or higher. Elliptical outlines of terrestrial impact structures and other deviations from circular planforms may have different origins (1) strongly oblique impact of less than about 20°, measured from the surface; (2) target anisotropy/heterogeneity; (3) uneven erosion of a crater structure/topographic effects; or (4) postimpact deformation of the crater.

1. An elliptical outline due to a very oblique impact trajectory is known for Goat Paddock (Milton and MacDonald 2005) (Fig. 5b), Matt Wilson (Kenkmann and Poelchau 2009), and for some of the Douglas crater pits (Kenkmann et al. 2018b). The highly elliptical depressions of the Rio Cuarto crater field most likely formed as windblown deflation depressions.
2. Target heterogeneity can cause deviations from circular planforms and may lead to polygonal outlines. Impact craters with a polygonal outline are well known from other planetary bodies, such as Mars or the Moon (Öhman et al. 2006). Fourteen of the terrestrial impact craters have polygonal outlines. The most prominent example is Meteor (Barringer) crater that is almost quadrangular (Kring 2017). The most important reasons for the polygonality of craters are regional joint sets, fissures, and large-scale shear zones delimiting parts of the craters. While in simple craters tectonic joint sets are oriented diagonal to the straight segments of a crater outline (Poelchau et al. 2009) and allow a more efficient crater excavation, joint sets usually

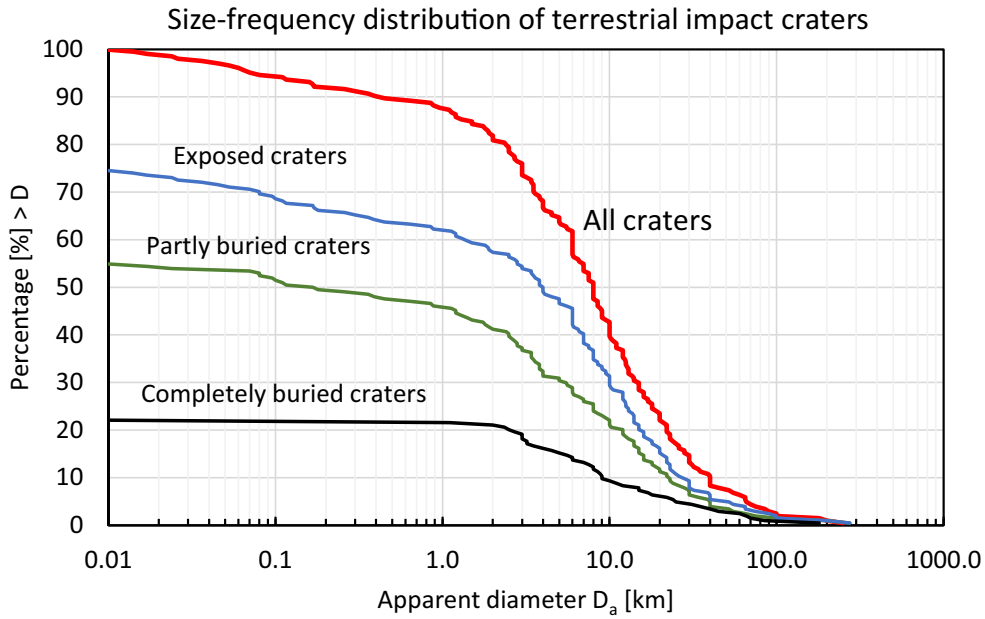

Fig. 9. Cumulative crater size–frequency distribution of terrestrial craters, normalized to 100%.

trend parallel to the straight rim segments in complex craters. Examples for the latter are Jebel Waqf as Suwwan crater in Jordan (Kenkmann et al. 2017) or Serra da Cangalha in Brazil (Kenkmann et al. 2011).

3. Craters affected by uneven erosion occur in high relief regions and may deviate from circular planforms. Gardnos (French et al. 1997), for example, is exposed at the slope of a glacial valley in Norway and, due to this, the preservation ranges from completely eroded to partly buried, with an influence on the apparent circularity of the structure. Moreover, small craters such as Whitecourt (Herd et al. 2008) are strongly influenced in their morphology by the local topography (Aschauer and Kenkmann 2017).
4. The most prominent impact crater that was strongly deformed and received an elliptical outline by postimpact deformation is Sudbury (Riller 2005). However, the outline of Sudbury is a preservation bias. The entire rim area has been eroded. Due to tectonic overthrust, the southern segment represents a deeper crater section. Other examples include Luizi that is cut by a large mylonitic shear zone (Ferrière et al. 2011) or the Charlevoix crater that is cut by the St-Lawrence graben system (Trepmann and Spray 2005). Beaverhead is believed to be entirely allochthonous and transported over deca-kilometers as part of a tectonic nappe (Kellogg et al. 2003).

SIZE–FREQUENCY DISTRIBUTION OF TERRESTRIAL IMPACT STRUCTURES

The diameter of an impact crater is probably its most important characteristic feature. The crater size scales with the impact energy and it is well known that crater size and frequency of impacts of a certain size inversely correlate with each other. Analyzing the impact crater size–frequency distribution is currently the only remote method to determine ages of planetary surfaces (e.g., Hartmann 1970). Isotopically calibrated for the Moon by Apollo and Luna samples, the lunar crater production function has been successfully transferred to other planetary bodies, such as Mars (Neukum et al. 2001). Figure 9 shows the cumulative size–frequency distribution of all known terrestrial impact craters, normalized to 100%.

The slope of the size–frequency distribution begins very shallow for craters ranging between 10 m and 1 km and shows a gradual steepening between 1 and 4–6 km. This reflects the incomplete record of smaller craters and causes the strong deviation from size–frequency distributions of impact craters from the Moon or from Mars (Neukum et al. 2001). A more subtle change in slope can also be recognized at a crater diameter of about 30–40 km. The general trend in the size–frequency distribution is similar for exposed crater, partly, and completely buried crater structures. The detection, however, of buried simple craters by means of geophysical methods is particularly difficult due to

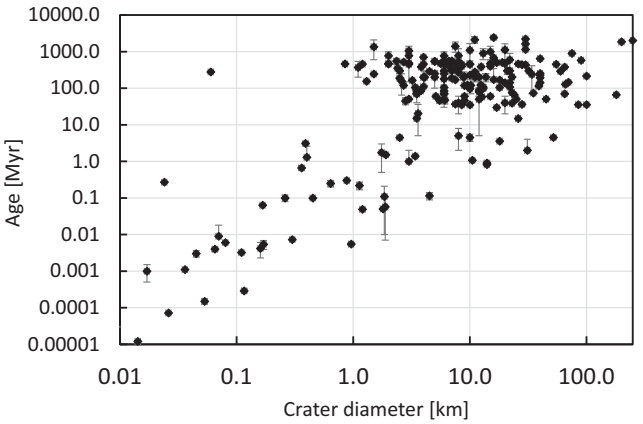

Fig. 10. Crater diameter versus crater age. There is a striking deficit of craters below 3 km size that are older than 100.000 years.

their small sizes and buried craters with diameter of less than a kilometer have yet to be identified.

The deficit of smaller impact craters also becomes obvious in Fig. 10, where the crater size is displayed against the crater's age. Craters smaller than about 3 km in diameter and older than 100,000 years are almost absent because of their shorter lifetime (Hergarten and Kenkmann 2015).

AGE–FREQUENCY DISTRIBUTION OF TERRESTRIAL IMPACT STRUCTURES

With ages of 2229–2246 Myr (Erickson et al. 2020) and 2023 ± 4 Myr (Kamo et al. 1996), the oldest impact structures currently known on Earth are the Paleoproterozoic Yarrabubba structure in Australia and the Vredefort impact structure in South Africa, respectively. Disregarding the Archean impact spherule beds in the Pilbara craton, Australia, and the Witwatersrand craton, South Africa (Byerly et al. 2002), more than two billion years of the early cratering record on Earth are currently not represented in the known terrestrial impact record. There are no Hadean or Archean impact structures presently known, although this period had an enhanced impact cratering rate (Bottke and Norman 2017).

The quality of available ages for the formation of impact craters varies considerably (Fig. 11). Stratigraphic or relative dating sometimes provides only a broad bracket for the formation age (Kelley and Sherlock 2012). Isotopic ages exist for 46% of known craters. In principle, an approximate stratigraphic age can be determined for most craters. The youngest rock units affected by the impact provide a maximum (oldest possible) age for the impact and the oldest undisturbed rocks filling the crater after its formation constrain the minimum (youngest possible) impact age (Schmieder and Kring 2020). If the target, however, is composed of igneous or metamorphic rocks and the crater is devoid of postimpact sediments, isotopic age constraints are the required only option.

Considerable progress has been made over the past decade or so in determining crater formation ages (Jourdan et al. 2009, 2012; Kelley and Sherlock 2012). A comprehensive review of crater ages has been presented by Schmieder and Kring (2020). With the exception of a few cases, the data used here match with the compilation by Schmieder and Kring (2020). As described in the Methods section, stratigraphic ages were recalculated to mean values with a stratigraphic error, even if only a minimum and/or maximum age is provided in the literature (Equations 1–3). It is still, however, a minority of the craters that are precisely dated by means of isotopic methods (Fig. 11). Only two craters have ages with standard deviations of 0.1% or less, Manicouagan and Sudbury, and only 23 craters with standard deviations <1% with respect to the mean age (Table 3). All other craters are less well defined. The majority of medium-sized impact craters have standard deviations that range between 1 and 10% of their given age (Fig. 11). Some craters have stratigraphic uncertainties, *Es*, that are of the same order as the mean age, *Ts*, itself. Considering this, it is clear why the links among impact events, stratigraphic event layers, and mass extinctions are elusive and a challenge for future research. Currently, only the Chicxulub impact event is, beyond doubt, linked with a major mass extinction event, namely the Cretaceous–Paleogene boundary (Schulte et al. 2010). Likewise, the unambiguous identification of crater doublets is hampered by often imprecise age determinations. Currently, it is even queried by some researchers if the well-known Ries–Steinheim pair is a crater doublet (Schmieder et al. 2014). Only the Kamensk–Gusev and Lockne–Målingen crater pairs can be considered as doublets formed in one impact event (Schmieder et al. 2014).

Figure 12a illustrates the cumulative age–frequency distribution of all currently known impact craters. Kinks in the curve occur at around 35 Ma, 450–470 Myr, and 550 Myr. The most remarkable kink is at 35 Myr and corresponds to the putative Late Eocene impact shower (Farley et al. 1998). The cluster of large craters comprises Popigai, Chesapeake Bay, Mistastin, and Wanapitei impact structures. The kink is also caused by an apparent deficit of craters younger than 28 Myr and older than 8 Myr. The second change in slope at 450–470 Myr is an accumulation of mainly shallow marine craters in the late Ordovician. With improved dating techniques, it became apparent that

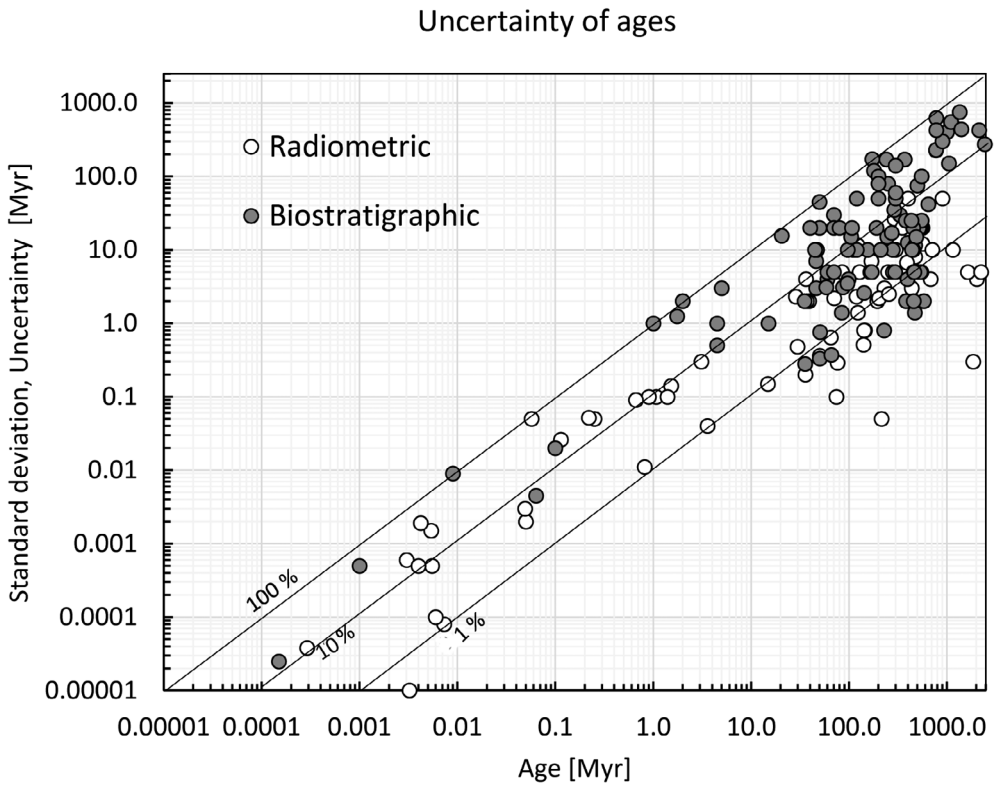

Fig. 11. Relative and absolute ages of terrestrial impact craters and their errors. The 100% line represents an uncertainty equal to the estimated age of a particular crater. Data on the 1% line mean that the uncertainty is 1% of the given age estimate.

about 35 impact structures fall in this age range. While this accumulation could be the result of a preservation bias, it has been interpreted as a spike in the production rate caused by a major disruption event in the asteroid belt (Table 3) (Alwmark and Schmitz 2007). Figure 12b shows the impact event in a linear, noncumulative way. For each isotopic age, the probability density function, $Pr(x)$, of the Gaussian normal distribution was calculated according to Equation 4, for stratigraphic ages, a triangular probability density, $Ps(x)$, was determined according to Equations 3a and 3b. The obtained data were stacked as a frequency density plot of the events through time (Eq. 5). The diagram shows a depletion of craters in all time periods owing to erosion. The record is particularly scarce for the Proterozoic. The frequency density distribution increases to younger periods. The large scatter of the frequency density distribution and the overall low values illustrate the limited preservation of terrestrial impact craters. The data are not suitable to infer changes in the production rate. Mazrouei et al. (2019) proposed a deficit of large terrestrial craters between 300 and 650 Myr relative to more recent times and proposed a lower impact flux rather than a preservation bias. They concluded that the impact flux has significantly increased 290 Myr ago. This is not substantiated by the data shown here. In reply to Mazrouei et al. (2019), Hergarten et al. (2019) showed that the age–frequency distribution can be reproduced by a constant crater production in combination with constant over time, but spatially variable, erosion.

The third kink at 550 Myr roughly overlaps with the transition from the Precambrian to the Phanerozoic era and indicates a relatively low number of preserved Precambrian craters with respect to the Phanerozoic crater record. Precambrian craters are often very imprecisely dated. Mazrouei et al. (2019) suggested a massive global-scale erosion event at the end of the Precambrian era that erased the Precambrian record and suggested a causal connection to the snowball Earth scenario. While this interesting approach remains to be critically discussed further, the apparently reduced number of Precambrian craters discovered, so far, may also reflect our limited understanding and recognition of very deeply eroded craters in crystalline targets. For example, the oldest known crater Yarrabubba in Western Australia shows neither imprints in the morphology and drainage nor any sort of easy-to-interpret structural features, such as a central dome or a ring-like syncline.

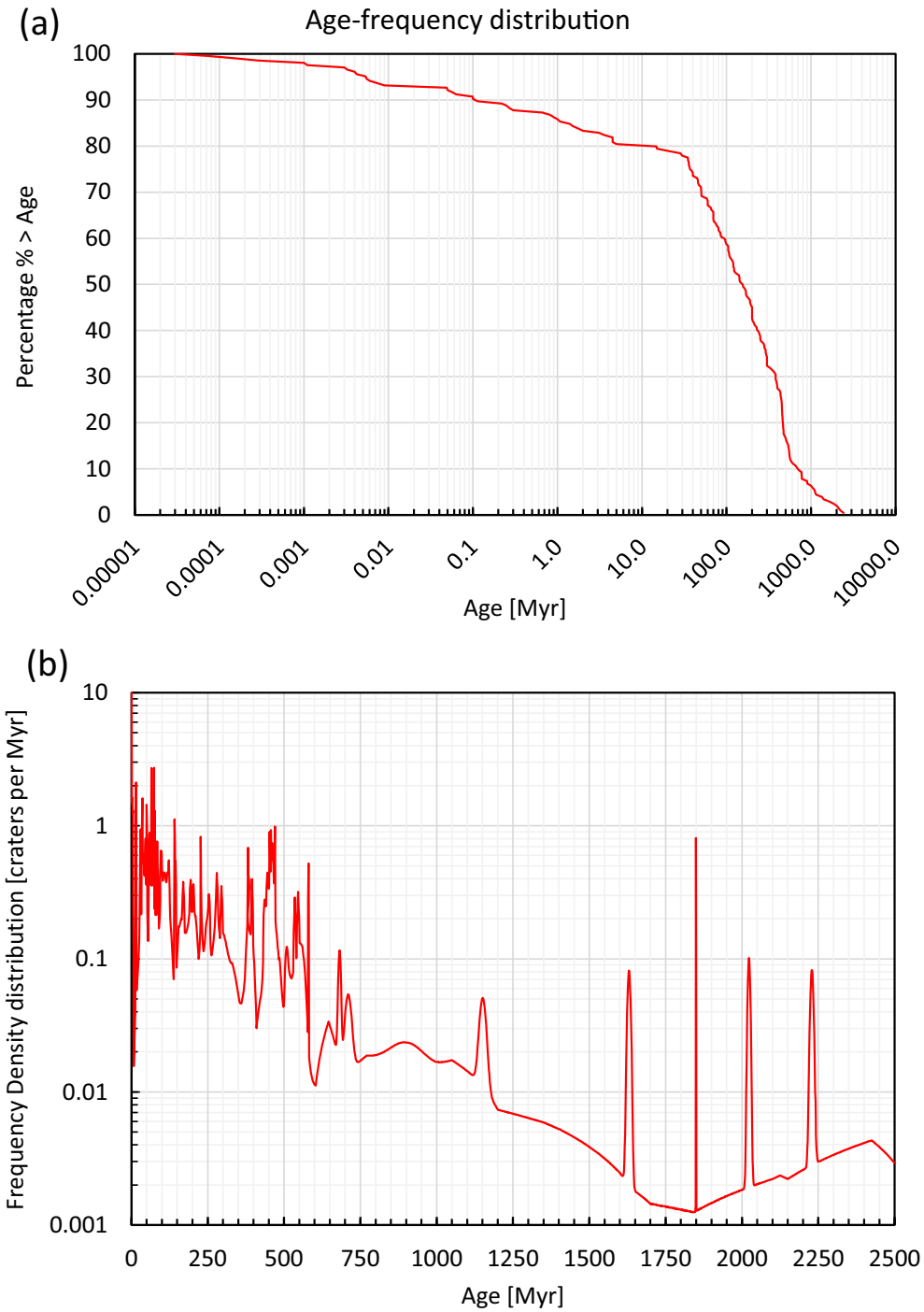

Fig. 12. a) Cumulative age frequency distribution of the currently known terrestrial impact structures. b) Frequency density function of the Gaussian normal distribution of radiometric ages and triangular normal distribution of stratigraphic ages of the terrestrial impact structures. (Color figure can be viewed at wileyonlinelibrary.com.)

STRUCTURE OF TERRESTRIAL IMPACT CRATERS

Impact craters are subdivided into simple and complex impact structures (Melosh 1989; Grieve 1991; Kenkmann et al. 2014). The former has a bowl-shaped cavity with a raised rim and a brim of ejecta. Modification from the transient cavity is mainly restricted to mass movements along the steep transient cavity rim and the presence of brecciated material that

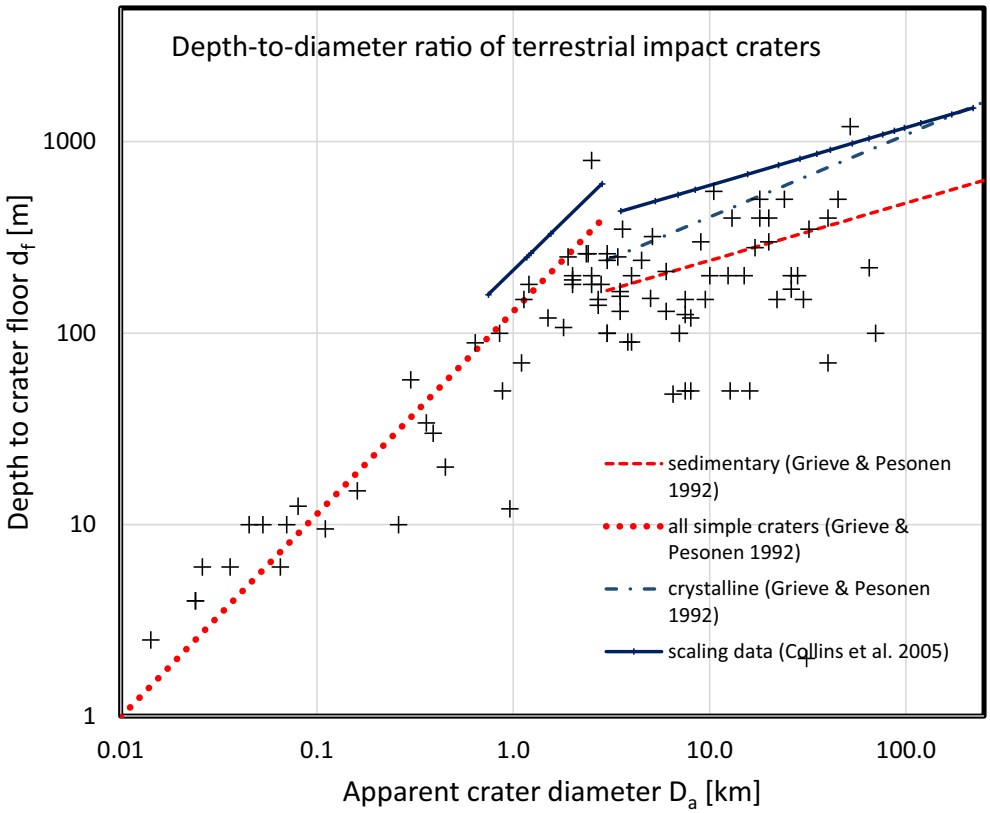

Fig. 13. The simple to complex transition of terrestrial crater morphologies. (Color figure can be viewed at wileyonlinelibrary.com.)

fills the cavity. This lowers the depth-to-diameter ratio of simple craters to a value of about 0.2, with respect to that of the initial transient cavity of 0.35, which formed at the end of the excavation stage. The lower part of the autochthonous crater wall is usually covered by talus deposits.

"Complex crater" is generic term that encompasses central peak craters, central pit craters, peak-ring, and multi-ring structures. All of them are larger than simple craters. They have in common the much more extensive modification of the transient cavity with an uplift of the central crater floor and are, consequently, relatively shallower than simple craters. The size-dependent surface representation of the centrally uplifted area as a single peak, a peak ring, or multi-ring is unfortunately often obscured by erosion. Complex craters typically have a rather flat crater floor surrounding the central uplift, a terraced rim zone consisting of slump blocks bounded by concentrically striking normal faults (Kenkmann et al. 2014). The strong modification is the result of extensive gravity-driven collapse. The collapse starts at the deepest point of the transient cavity that begins to rise upward. The uplift of the central crater floor causes the steeper crater walls and the deeper subsurface to move inward. This eventually leads to down-faulting of the steep rim zone of the transient cavity and causes an enlargement of the crater (Kenkmann et al. 2012). The classification of crater morphology into simple and complex applies for all planetary bodies in the solar system. The simple-to-complex transition diameter has shown to vary inversely with the surface gravity of a given planetary body (Pike 1985) and this circumstance suggests that gravity is the main driving force for crater modification. Of secondary importance is the target strength.

The database presented here (Table 3), shows 56 (28%) simple craters and 140 complex craters (69%). Seven craters (3%) are tentatively listed here as transitional craters (Fig. 13). From their diameter alone, transitional craters may be considered complex craters. A central uplift, however, has yet to be detected in craters of this group. A recent statistical analysis of the depth-to-diameter ratio of lunar craters has substantiated the presence of transitional craters (Krüger et al. 2018; Osinski et al. 2019) as a separate group. The largest terrestrial simple crater formed in sedimentary strata has a diameter of 3 km (Gusev), in a mixed target also 3 km (Iso-Naakkima, Newporte), and in a crystalline target 4 km (New Quebec, Suvasvesi North and South). The smallest complex crater in a

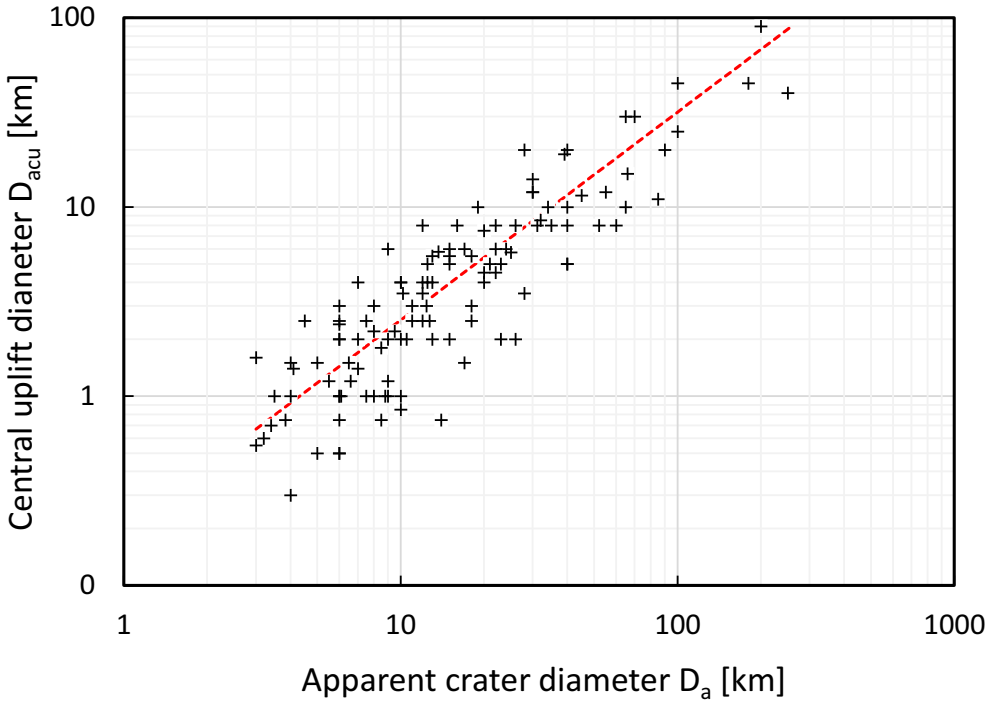

Fig. 14. Apparent crater diameter versus the apparent central uplift diameter. (Color figure can be viewed at wileyonlinelibrary.com.)

purely sedimentary target has a diameter of 3 km (Goyder) and in a crystalline target <4 km (Zapadnaya, 3.2 km; Zeleny Gai 3.5 km). For sedimentary targets, a simple-to-complex transition at 3 km is generally accepted. For crystalline targets, the transition diameter is slightly higher at 3–4 km diameter (Grieve 1991). Craters that are listed as transitional are Kgagodi (3.5 km), Ouarkziz (3.5 km), Colonia (3.6 km), Goat Paddock (5.1 km), Decorah (5.6 km), Lumparn (7 km), and Passelkä (10 km).

The depth-to-diameter ratios of simple and complex craters on other planetary bodies can be precisely determined, due to the limited degradation of many craters (e.g., Krüger et al. 2018). For the Earth, a relationship of $d_f = 0.13\ D^{1.06}$ was determined by Grieve and Pesonen (1992) for simple craters based on the measurement of seven craters (Fig. 13). The term d_f refers to the apparent depth to the bottom of the topographic crater, measured from the target surface, and corresponds to d_a in the older literature. For complex craters, Grieve and Pesonen (1992) found the relationship $d_f = 0.12\ D^{0.30}$ and $d_f = 0.15\ D^{0.43}$ for sedimentary and crystalline targets, respectively (Fig. 13). For comparison, the blue dotted data points in Fig. 13 show the results for impacts of variously sized projectiles with a density of 3000 kg/m^3 impacting onto a target with a density of 2500 kg/m^3 at 20 km/s and 45° using the scaling relationships applied in Collins et al. (2005). The large scatter of data in Fig. 13 reflects the various degrees of erosion of terrestrial craters. The relationship derived by Grieve and Pesonen (1992) fits reasonably well to the enhanced data set and is, therefore, not recalculated here.

The majority of the known complex craters on Earth are central peak craters. Systematic relationships exist between the apparent crater diameter, D_a, and some first-order structural properties of complex craters. A nearly linear trend is found between the apparent crater diameter and the apparent central uplift diameter (Fig. 14), with the relationship

$$D_{acu} = 0.2 D_a^{1.1} \quad (8)$$

The scatter, however, is large. This is primarily due to the different levels of erosion of the craters. It is well known that the apparent diameter of a central uplift increases with the amount of erosion, while the apparent crater diameter shrinks with erosion. This circumstance leads to a shift of the ratio D_{acu}/D_a from about 0.25 for pristine craters to ratios of up to 0.8 for very deeply eroded craters (Kurta et al. 2009). Further parameters that cause data scattering are variations in the impact angle, the different mechanical behavior of crystalline and sedimentary target rocks, and differences in the definition of the outline of a central uplift.

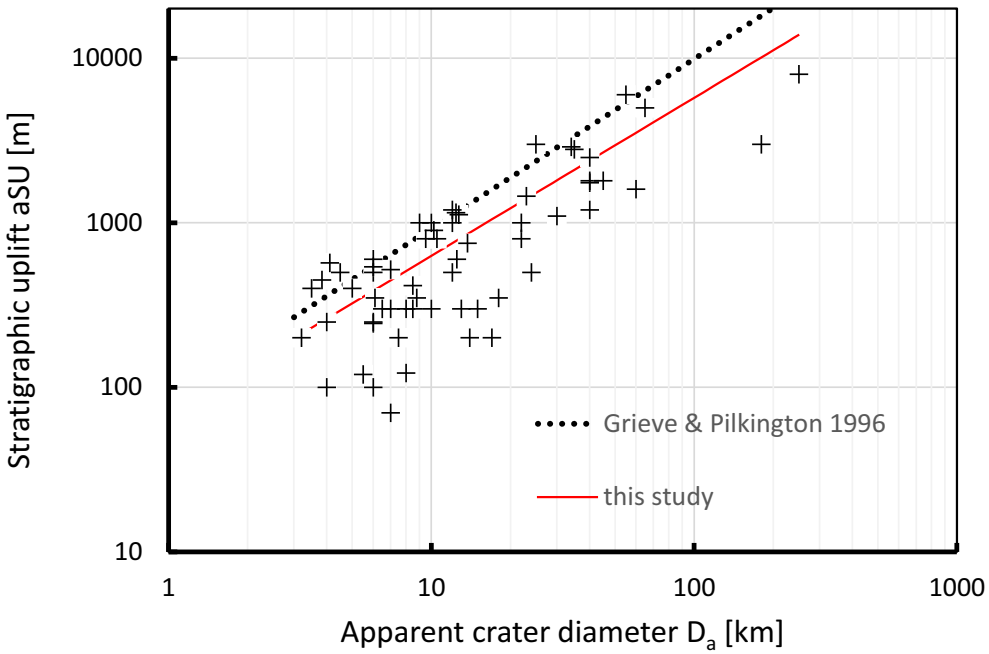

Fig. 15. Apparent crater diameter versus the stratigraphic uplift. (Color figure can be viewed at wileyonlinelibrary.com.)

Based on 24 craters, Grieve and Pilkington (1996) derived a relationship between crater diameter D and stratigraphic uplift, SU, of SU = 0.086 $D^{1.03}$, measured in kilometers (Fig. 15). The current database lists the stratigraphic uplift for 62 craters and yields a similar though somewhat lower relationship of

$$\mathrm{aSU} = 0.069 D_{\mathrm{a}}^{0.96} \tag{9}$$

The quality of this data set, however, suffers partly from imprecise measurements of the stratigraphic uplift.

The allocation of craters to the peak-ring category is difficult and depends on the crater's state of preservation. An obvious peak-ring structure is Chicxulub (Morgan et al. 2016). A proper structural classification of Vredefort and Sudbury is difficult due to the deep level of erosion and the strong postimpact deformation overprint, respectively. Popigai also has a peak-ring structure. Craters that show some indications of a peak-ring structure include Siljan, Morokweng, Strangways, Clearwater West, and Araguainha. Some terrestrial craters additionally show indications for a pit structure in the middle of their massive central uplift, for example, Puchezh-Katunki (4 km diameter crater pit), and the Ries (11 km crater pit), but whether or not these structural features can be compared to the central pits of planetary craters is a subject on its own and will not further discussed here. The ring syncline surrounds the centrally uplifted zone of a complex crater (Figs. 1 and 16). The ring syncline axis, D_{syn} marks the deepest point of the ring depression and could be determined in 98 complex craters. It has the following relationship to the apparent crater diameter, D_{a}:

$$D_{\mathrm{syn}} = 0.65 D_{\mathrm{a}}^{0.92} \tag{10}$$

The crater rim is an important structural and morphological feature of both simple and complex craters. The rim height depends on crater size, target rheology, and the emplacement mechanism of the ejecta (Pike 1988). It is, however, among the first features that undergoes degradation by erosion, and, therefore, it is not possible to derive a relationship between the crater diameter and the rim height for terrestrial craters. Only the young and pristine craters show elevated crater rims. In simple craters, the rim height is believed to be equally formed by the uplift of the target and by the ejecta resting on top of the rim (Melosh 1989). In contrast, complex craters on the Moon and on Mars show that the structural rim uplift amounts to about 70% and 80% of the rim height, while the ejecta thickness only contributes ~30% and 20%, for lunar (Krüger et al. 2017) and Martian craters (Sturm et al. 2016), respectively.

The crater rim of some of the terrestrial impact craters can be classified with respect to its structure. Thirty-two craters show relics of an overturned ejecta flap. The overturned ejecta flap represents the most proximal part of the continuous ejecta blanket that rests on top of the rim crest. Craters whose ejecta blanket is removed often display circumferential normal faults that delineate the crater. Fifty-seven craters show such

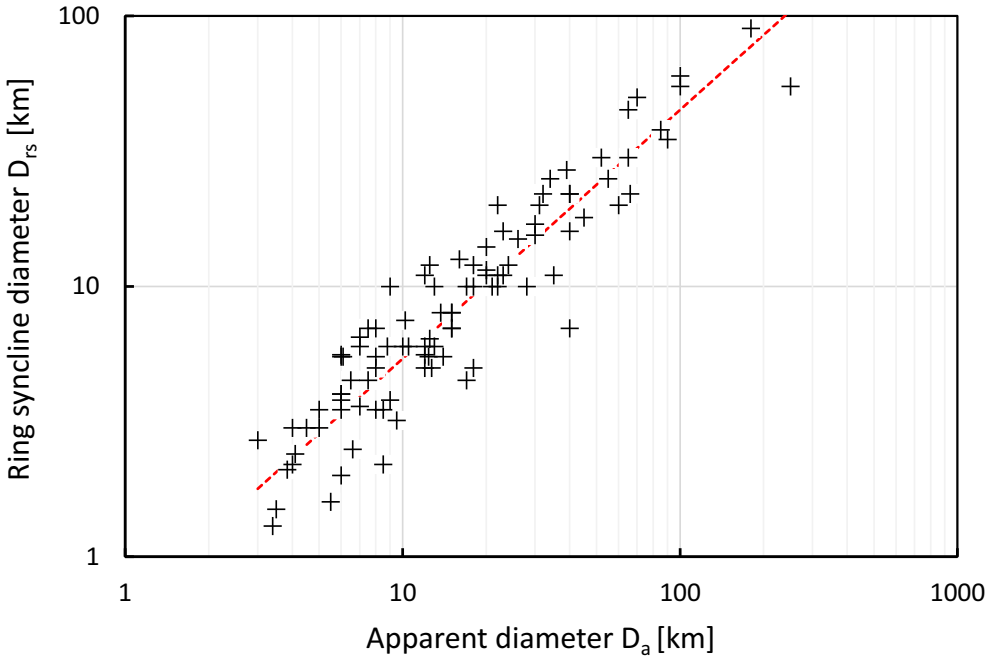

Fig. 16. Apparent diameter versus the diameter of the ring syncline axis. (Color figure can be viewed at wileyonlinelibrary.com.)

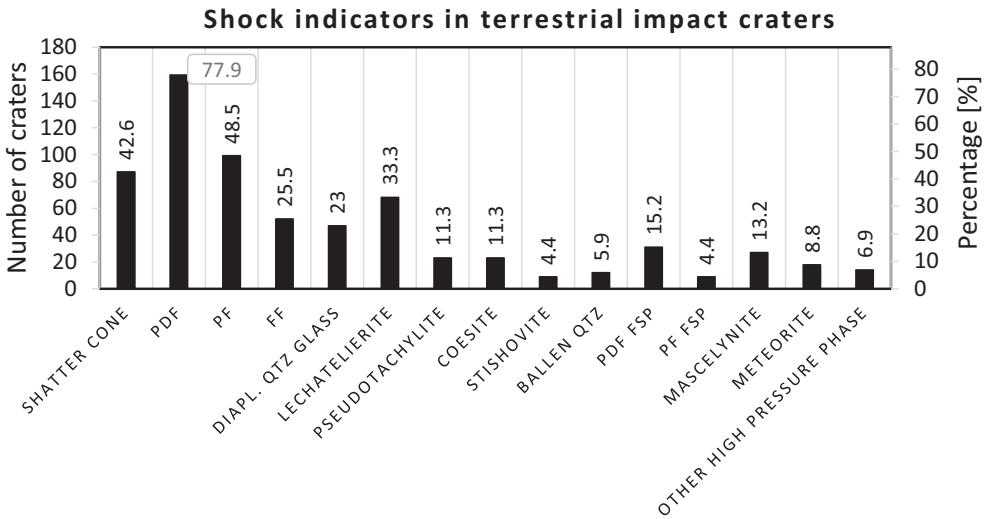

Fig. 17. Shock features recorded in terrestrial impact structures and their frequency.

normal faults. In even more deeply eroded crater structures, the crater rim is defined by crater inward dipping monoclines or circumferential folds (Kenkmann et al. 2014).

SHOCK EFFECTS

"Shock metamorphism is the physical consequence of hypervelocity impacts of planetary projectiles (e.g., asteroids and comets) into solid target rocks exposed on planetary bodies" (Stöffler et al. 2017). Hypervelocity impact is the only natural process where strong shock waves can develop. The documentation of unequivocal shock features or the presence of meteoritic relics is a prerequisite for a crater structure to become a confirmed impact structure. The occurrence of PDFs in quartz is the most important and reliable shock feature. According to the present compilation, PDFs are reported from about 78% of all crater structures, followed by PFs in quartz that have been documented

in almost 50% of all craters (Fig. 17). Shatter cones are the only diagnostic shock feature that can be recognized with the naked eye (French and Koeberl 2010; Ferriére and Osinski 2012; Baratoux and Reimold 2016) and are, therefore, of utmost importance for the recognition of impact structures. Shatter cones are known from 87 impact craters or 42% of all crater structures. Feather features (FFs) in quartz have recently become another important diagnostic microstructural tool. They have been recorded in about one quarter of all impact structures (Poelchau and Kenkmann 2011) (Fig. 17). Diaplectic glasses and lechatelierite, and high pressure polymorphs are predominantly known from craters with preserved allochthonous polymict breccia layers. Pseudotachylites, although not uniquely formed in impact craters, are related to large impact structures within crystalline basement. Shock features in feldspar are also reported from craters with either allochthonous impact breccia and/or crystalline, preferentially granitic target lithologies. The preservation of meteoritic material is commonly related to simple craters.

TARGET LITHOLOGIES

Target lithologies have a strong influence on the crater structure. As a hypervelocity impact is a near-surface event, often layered sedimentary target lithologies are the most frequent type (43%) (Fig. 18a, Table 3). This stratification commonly correlates with an anisotropy of the target strength. Bedding surfaces may act as zones for a mechanical decoupling during crater modification. Crystalline targets (26%) (Fig. 18a) usually have a higher strength than sedimentary targets. Mixed targets (31%) (Fig. 18a) are commonly composed of a denudated crystalline basement that is superposed by sedimentary strata. The unconformity between the basement and the sediments is an important first-order rheological discontinuity that influences both the excavation flow field as well as the movements during crater modification and may lead to a nested crater structure as can be seen, for example, at the Chesapeake Bay impact structure (Poag et al. 2004).

Among the crystalline target rocks, metamorphic rocks are more frequent than plutonic or volcanic rocks (Fig. 18b). The plutonic target rocks are dominated by granite, followed by granodiorite and gabbro (Fig. 18c). Volcanic target rocks are predominantly basalt, dolerite, or rhyolite (Fig. 18d). Among the metamorphic target rocks, gneisses are most frequent, followed by schists and amphibolites (Fig. 18e). The dominating sedimentary lithologies are sandstones, followed by carbonates, mudstones, and siltstones (Fig. 18f). Some 10% of the sedimentary target rocks are unconsolidated.

IMPACT LITHOLOGIES

The subcommission on the classification of metamorphic rocks of the International Union of Geological Sciences (IUGS) dealt also with "impactites" (Stöffler and Grieve 2007). This classification scheme was further improved by Stöffler et al. (2017). On Earth, impactites generally formed in a single impact event. This is in contrast to all other planetary bodies, where, due to a near lack of erosion, the effects of multiple impact events have to be taken into account and result in the formation of a thick regolith covering the surface of the planetary body. To date, only the Wanapitei and East Clearwater Lake impacts are known to have occurred in a target of pre-shocked rocks formed by another impact event, namely the Sudbury and West Clearwater Lake impacts, respectively. The lack of multiple impactite formation means that the occurrence of specific impact lithologies can be related to specific locations within the crater structure.

In terrestrial impact structures, lithic breccia is the dominant impact lithology with respect to the volume they occupy and the frequency at which they are reported (Fig. 19). Monomict lithic breccias, crystalline breccias, and fault breccias are particularly frequent in deeply eroded craters, where only the parautochthonous crater subsurface is preserved. Such breccias may or may not show a shock metamorphic overprint. Polymict lithic breccia and suevitic breccia form during the excavation process and are abundant if either the allochthonous breccia infill of the crater depression, the annular moat, or parts of the ejecta blanket have been preserved. This is the case for about 130 terrestrial impact structures. Thus, polymict lithic breccia and suevitic breccia preferentially occur in weakly eroded craters. Impact melt rock and pseudotachylitic breccia are particularly frequent in large impact structures, where the volume of melt rock unproportionally increases with respect to the crater dimensions (Grieve and Cintala 1992). Reworked breccias, with rounded to subrounded clasts, are frequently found in buried impact craters, where the basal postimpact sedimentation is preserved and shows reworking of various breccia types. Craters formed in an aquatic environment are commonly associated with forceful resurge flows that typically contain reworked impact breccia (Ormö and Lindström 2000).

PROJECTILES AND EJECTA

Relics of projectile material are commonly found in small simple crater pits formed as part of larger crater strewn fields and in some of the larger simple craters.

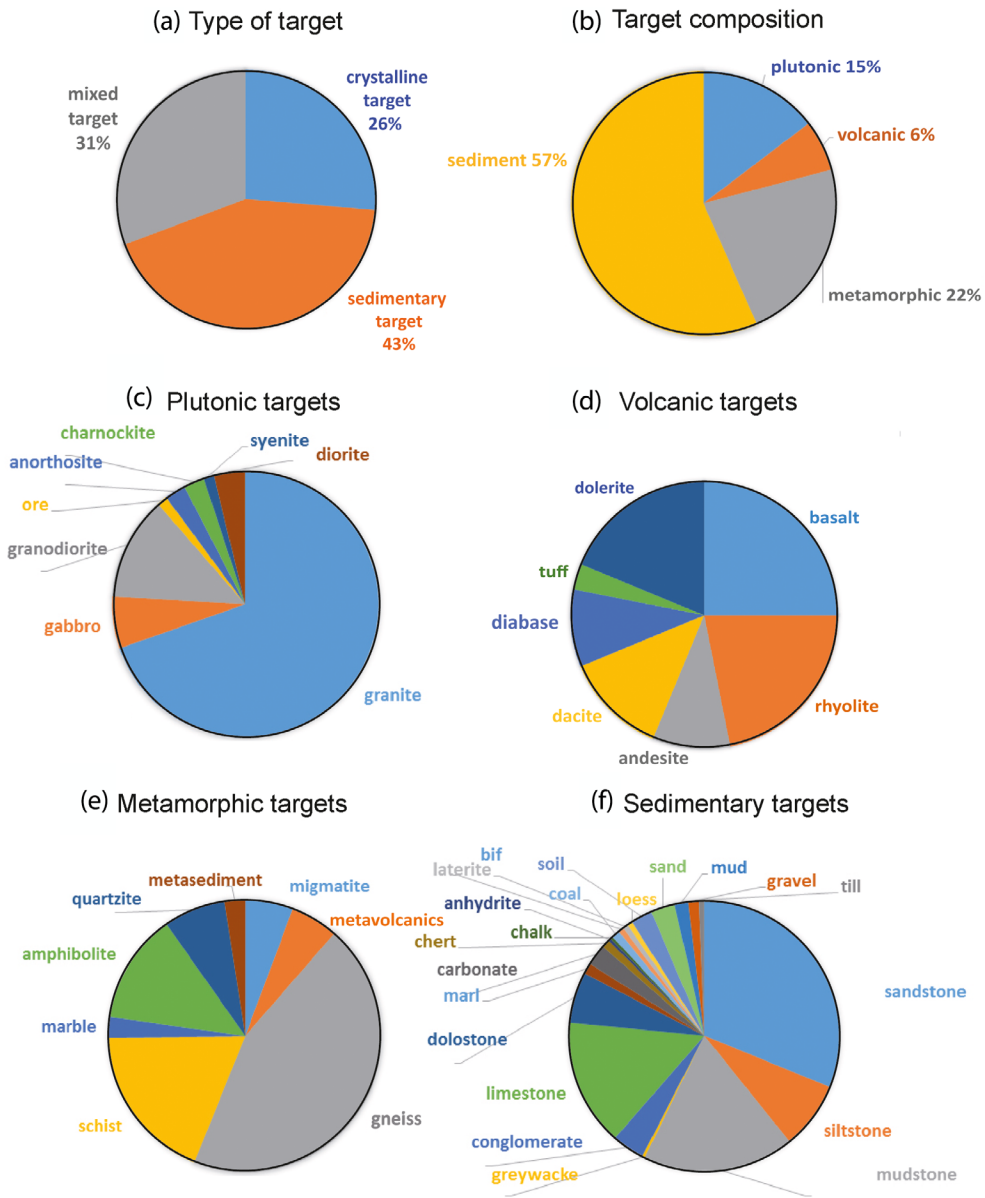

Fig. 18. Target lithologies of terrestrial impact structures.

Of the known eight terrestrial crater strewn fields: Douglas, Campo del Cielo, Henbury, Odessa, Wabar, Sikhote-Alin, Kaalijärv, and Morasko, all except Douglas are associated with iron meteorites, for which the projectile could not yet be identified. In total, 21 impact craters are associated with meteoritic material, which is commonly spreading along the crater rim, the inner crater slope, and the proximal ejecta blanket as shrapnel or small meteorite pieces. Except for Carancas, unmelted meteorites are commonly iron meteorites. The probability that the meteoritic material will remain unmelted decreases with increasing impact energy and crater size, as the shock level within the projectile increases and exceeds 60 GPa (Pierazzo and Melosh 2000). Only in very oblique impacts, minor parts at the rear side of the projectile may remain unmelted. The identification of the impacting bolide of larger impact structures is based on trace geochemical techniques. Projectile identification has been possible in about 40 craters by the analysis of siderophile and platinum group elements, and the specific isotopic systems of osmium and chromium (Koeberl 1998; Tagle and Hecht 2006).

The ejecta blanket surrounding a terrestrial crater composed of polymict lithic breccia, suevitic breccia, and impact melt rock lenses is among the first features

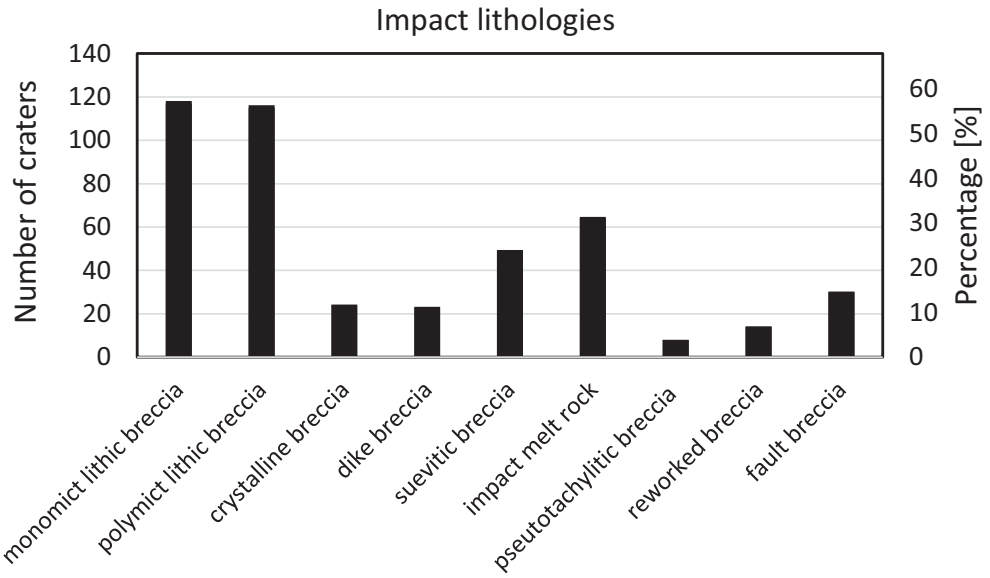

Fig. 19. The frequency of various impactites in terrestrial impact craters.

that disappear during denudation. According to the database about one quarter of the terrestrial craters have parts of their ejecta blanket preserved. Relics of the proximal ejecta blanket are commonly more frequently preserved than distal ejecta. Thirty-two craters show relics of the overturned ejecta flap along the crater rim of simple craters. Thirty-one craters show relics of distal ejecta that is discontinuous, most likely right from its formation. A few of the large craters have no proximal ejecta preserved but show distal ejecta containing accretionary lapilli and spherules, for example, Sudbury (Addison et al. 2005) and Chicxulub (Ocampo et al 1996). Recently, it could be demonstrated in a few cases that several of the preserved ejecta blankets of terrestrial craters contain ramparts, similar to double-layer ejecta craters on Mars. Among them are the Ries (Sturm et al. 2013) and Bosumtwi (Wulf et al. 2019) craters, and potentially five more (Wulf and Kenkmann 2021).

IMPACT INTO WATER

There are large-scale examples of impact events into shallow marine shelf environments such as Chicxulub (Morgan et al. 2016) and Chesapeake Bay (Poag et al. 2004). These crater structures are still partly submerged and are buried beneath younger marine sediments. Montagnais and Mjølnir are fully submerged and buried craters, with currently 115 and 350 m average water depth, respectively. Other craters, once formed in a shallow marine environment, are now exposed on land. One of the best studied marine impact structures is the Lockne crater in Sweden (Ormö and Lindström 2000). For 33 craters, evidence for formation under marine or aquatic conditions is obvious through the presence of reworked breccia and resurge deposits filling the crater depression (Fig. 19, Table 3). Characteristic features of craters formed under submarine conditions are: (1) a nested crater morphology, with an upper crater formed in unconsolidated sediments that is enlarged by the water excavation and resurge, and a smaller sized central crater formed in consolidated target rocks, (2) the replacement of a clear crater rim by a broad brim zone that may be radially dissected by resurge gullies, and (3) a thick sequence of resurge deposits within the crater depression, with indications of soft sediment deformation, and a continuous postimpact sediment sequence. Craters showing a significant amount of erosion may have also formed under submarine conditions. However, their marine origin cannot be determined unequivocally and is obscured once resurge deposits have been eroded.

GEOPHYSICAL SURVEYING OF IMPACT CRATERS

Impact craters produce distinctive magnetic, electromagnetic, and gravity anomalies (e.g., Pilkington and Grieve 1992; Ugalde et al. 2005; Gilder et al. 2018) that have helped to discover degraded or buried impact structures, though such anomalies alone are insufficient to prove an impact. The geophysical anomalies of impact craters are commonly circular in outline and their diameters relate to the size of the crater structures.

Figure 20 displays the number of terrestrial impact structures that have been studied with respect to their

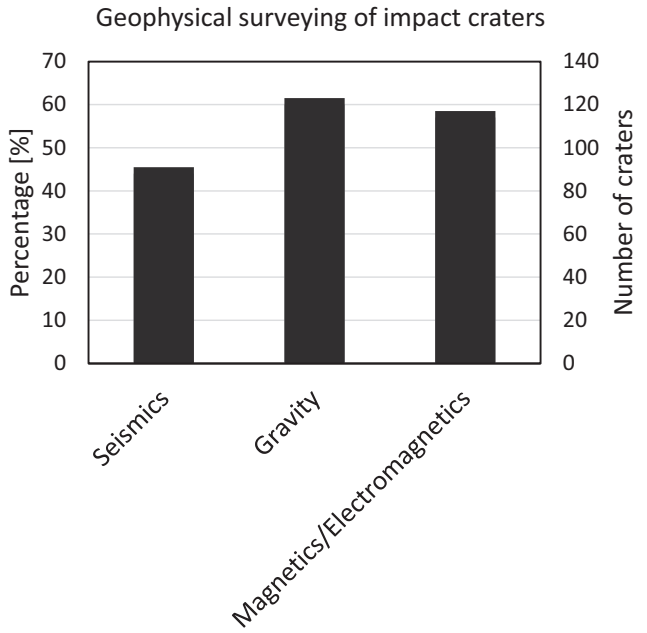

Fig. 20. Geophysical exploration of terrestrial impact craters.

gravity, magnetic, or electromagnetic signatures. Such geophysical explorations are available for about 50–60% of all craters but with different spatial resolution and quality (Fig. 20).

After removal of the regional gravity field, impact craters usually have negative Bouguer gravity anomalies. The negative gravity signature of simple craters is usually caused by the presence of breccia infill in the crater depression. The shattered crater subsurface is of subordinate importance (Pilkington and Grieve 1992). In complex craters, the overall negative gravity anomaly is the result of the breccia fill of the annular moat plus the displaced and fractured crater subsurface. Due to uplift of deeper seated, denser material, the central uplift of complex craters is often associated with a positive gravity excursion within the larger negative crater anomaly. The size of the gravity anomaly generally increases with increasing crater diameter and reaches a maximum of 20–30 mGal at crater diameters of 20–30 km (Pilkington and Grieve 1992).

Magnetic and electromagnetic anomalies of impact craters are more difficult to interpret and strongly depend on the nature of the target rocks, including their remanent magnetization and polarities, their electrical conductivity, and the presence of postimpact sediments. The signatures also depend on the latitude and longitude position of the crater. It has been shown that shock waves can permanently modify the magnetic properties of the target rocks, but it is difficult to assess the relative influence between thermal and pressure effects on their remanent magnetizations (Gilder et al. 2018). In crystalline targets with strong remanent magnetization, smaller crater structures often possess a weak relief magnetic signature with a circular shape, in contrast to the unaffected country rocks. Such low-relief magnetic zones have resulted in the identification of several smaller ancient impact structures, such as Summanen in Fennoscandia (Plado et al. 2018). The weak relief is related to a variety of possible causes including shock-induced demagnetization of rocks in the crater, the random distribution of magnetic vectors due to chaotic displacements related to the cratering process, oxidization of magnetite, and the deposition of postimpact sediments with a weak magnetization. In larger craters, the volume of melt-bearing breccia such as suevite and coherent impact melt rock masses increases unproportionally. As melt passed through the Curie temperature after deposition, these melt-bearing breccias and impact melt rocks are associated with strong remanent magnetizations of constant polarity.

Reflection seismic studies, onshore or offshore, are the most powerful tool to analyze the hidden subsurface structure of any type of crater, for example, Morgan et al. (2016). They can be applied to simple craters as well as to the largest craters on Earth, such as Sudbury and Chicxulub. Seismic impedance contrasts between postimpact sediments, various impact lithologies, the target rocks and major fault zones often allow the mapping of first-order structural features, such as the size and geometry of the central uplift, the presence of a peak ring and annular moat, and the size of slump blocks and terraces. Owing to intense deformation and the limited size of blocks with homogeneous reflectors, the central portions of craters commonly remain unresolved and fuzzy in reflection seismic studies. Less than 50% of the known terrestrial craters have available reflection or refraction seismic data (Fig. 20).

ECONOMIC USE

The natural economic resources of impact structures have been classified according to their time of formation relative to the impact event (Grieve 2005) as progenetic, syngenetic, and epigenetic. Progenetic resources are those that existed prior to the impact event. They were displaced by the cratering event and brought close to the surface, where they could be exploited. Syngenetic economic deposits formed by the impact event by shock-induced mineral transformation and melting or by subsequent hydrothermal activity. Epigenetic resources formed after the impact either within the crater depression or in the crater subsurface, most often by fluid flow and migration of hydrocarbons.

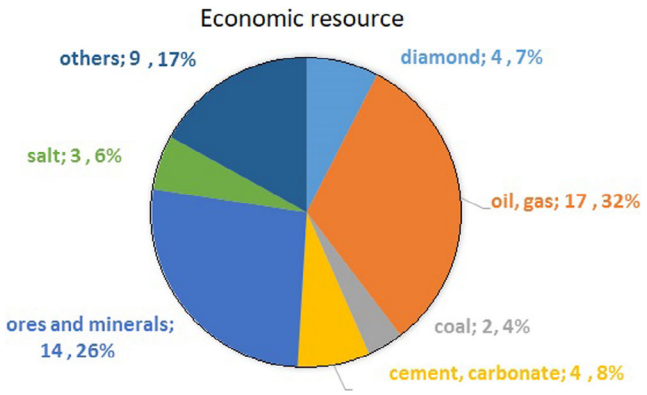

Fig. 21. Economic use of impact craters. (Color figure can be viewed at wileyonlinelibrary.com.)

More than a quarter (53; 26%) of all known impact craters are exploited for natural resources (Fig. 21). Several crater target rocks are quarried for building stones, gravel, or cement production. Here, the fact that the rock is fractured by the impact, and thus, more easily degradable is exploited. Such rock resources are progenetic. Some of the ores exploited in impact structures are also progenetic. Examples are the uranium ores of Carswell; the iron ores of Ternovka; the zinc, lead, and silver ores of Lawn Hill; or the gold deposits at Vredefort (Table 3). These craters, however, also show a secondary, syngenetic hydrothermal ore mobilization by the thermal imprint of the impact. World class sites of syngenetic ore formation are the copper, nickel, and platinum group element concentrations related to the impact melt rock (the so-called Sudbury Igneous Complex) at the Sudbury structure. The Russian craters Popigai, Puchezh-Katunki, and Kara are well known for their occurrences of shock-induced diamonds. Other syngenetic ores of hydrothermal origin include the lead and zinc sulfides of small complex craters, such as Crooked Creek, Decaturville, or Serpent Mound. About one-third of the craters with economic potential contain oil and gas that migrated into traps formed by the displaced rocks (Fig. 21). Craters exploited for hydrocarbons are exclusively located in Canada or the United States. These are typical epigenetic resources. Other epigenetic resources include the deposition of a variety of salt mineralizations within the crater depressions or the extraction of ground water from the crater subsurface.

CONCLUSIONS

Impact cratering is a fundamental geological process on planet Earth like on other planetary bodies in the solar system. This article provides an update of the characteristics of the currently known 208 terrestrial impact structures and is complementary to the atlas of the terrestrial impact structures (Gottwald et al. 2020). The crater structures have been investigated statistically by means of their size, morphology, structure, petrography, age, and other properties. Key results are:

1. The discovery history of the terrestrial impact structures can be described by either a logistic function or an exponential function (starting in the year 1960) and allows projections to the future. Among the 100+ missing craters, there are, in particular, many small simple craters that await discovery. Such craters, however, are the most difficult to detect.
2. The size– and age–frequency distributions of terrestrial impact structures are mainly controlled by preservation.
3. About 20% of the known impact craters are buried and 44% of the craters have a clear morphological expression and show either a preferred radial, a preferred concentric, or a combination of radial and concentric drainage pattern.
4. Among the known craters are 28% classified as simple craters and 69% as complex craters, and 3% are tentatively classified as transitional craters. This relationship is also preservation bias.
5. New scaling relationships are derived between the apparent crater diameter and the central uplift diameter, stratigraphic uplift, and the ring syncline diameter.
6. Among the diagnostic shock effects, PDFs in quartz are the most important shock feature and have been found in about 78% of all known crater structures, followed by PFs in quartz and shatter cones. The latter have been documented in more than 42% of all craters. Monomict and polymict lithic breccia are the most frequently occurring impact lithologies in terrestrial craters.
7. The most common target lithologies are sedimentary rocks.
8. Of all craters 50–60% have been studied by means of gravity, magnetic, and electromagnetic surveying, and 43% by seismic investigations. More than a quarter of all known impact craters are exploited for natural resources.

Acknowledgments—The compilation of the data is to a certain extent a by-product of my contribution to the creation of the atlas of the terrestrial impact structures (Gottwald et al. 2020). In this context, I would like to express my gratitude to M. Gottwald and W.U. Reimold for the multiple exchanges and excellent

cooperation over the past years. I would like to thank M. Gottwald for creating Figures 2 and 5 of this publication. Fruitful discussions with my colleagues M. H. Poelchau and G. Wulf helped to improve the database. I am very grateful to the reviewers R. A. F. Grieve and B. A. Ivanov for their extremely useful comments and to N. A. Artemieva for the editorial handling.

Data Availability Statement—The data that support the findings of this study are available on request from the corresponding author.

Editorial Handling—Dr. Natalia Artemieva

REFERENCES

Aaloe A. O. 1963. *New data on the structure of Ilumetsa craters*. Trudy: Akademii Nauk Estonskoy, SSR, Institiut Geologii.

Addison W. D., Brumpton G. R., Vallini D. A., McNaughton N. J., Davis D. W., Kissin S. A., Fralick P. W., and Hammond A. L. 2005. Discovery of distal ejecta from the 1850 Ma Sudbury impact event. *Geology* 33:193–196.

Alderman A. R. 1931. The meteorite craters at Henbury, Central Australia, with an addendum by L. J. Spencer. *Mineralogical Magazine* 23:19–32.

Alwmark C. 2009. Shocked quartz grains in the polymict breccia of the Granby structure, Sweden—Verification of an impact. *Meteoritics & Planetary Science* 44:1107–1113.

Alwmark C. and Schmitz B. 2007. Extraterrestrial chromite in the resurge deposits of the early Late Ordovician Lockne crater, central Sweden. *Earth and Planetary Science Letters* 253:291–303.

Alwmark C., Ferrière L., Holm-Alwmark S., Ormö J., Leroux H., and Sturkell E. 2015. Impact origin for the Hummeln structure (Sweden) and its link to the Ordovician disruption of the L chondrite parent body. *Geology* 43:279–282.

Amgaa T. and Koeberl C. 2009. Impact origin of Tabun Khara Obo Crater, Mongolia, confirmed by drill core studies (abstract). *Geological Society of America* 41:533.

Andreoli M. A. G., Ashwal L. D., Hart R. J., Smith C. B., Webb S. J., Tredoux M., Gabrielli F., Cox R. M., and Hambleton-Jones B. B. 1995. The impact origin of the Morokweng Ring Structure, Southern Kalahari, South Africa (abstract). Centennial Geocongress of the Geological Society of South Africa, Johannesburg, South Africa. pp. 541–554.

Aschauer J. and Kenkmann T. 2017. Impact cratering on slope. *Icarus* 290:89–95.

Baratoux D. and Reimold W. U. 2016. The current state of knowledge about shatter cones: Introduction to the special issue. *Meteoritics & Planetary Science* 51:1389–1434.

Barringer D. M. 1910. Meteor Crater in northern central Arizona. Paper presented at the National Academy of Sciences, Princeton University, 16 November 1909, 24 pp. (plus 18 plates and 3 maps).

Beals C. S. 1960. A probable meteorite crater of Precambrian age at Holleford, Ontario. *Publication of the Dominion Observatory Ottawa* 24:117–142.

Becq-Giraudon J. F., Rouzeau O., Goachet E., and Solages S. 1992. Impact hyperveloce d'une météorite géante a l'origine de la dépression circulaire d'Aorounga au Tchad (Afrique). *Comptes Rendus de l'Académie des Sciences, Paris* 315:83–88.

Bibbins A. B. 1926. A small meteor crater in Texas. *Engineering and Mining Journal Press* 121:932.

Bland P. A. and Artemieva N. A. 2006. The rate of small impacts on Earth. *Meteoritics & Planetary Science* 41:607–631.

Bottke W. F. and Norman M. D. 2017. The late heavy bombardment. *Annual Review of Earth and Planetary Sciences* 45:619–647.

Brandt D., Holmes H., Reimold W. U., Paya B. K., Koeberl C., and Hancox P. J. 2002. Kgagodi Basin: The first impact structure recognized in Botswana. *Meteoritics & Planetary Science* 37:1765–1779.

Brenan R. L., Peterson B. L., and Smith H. J. 1975. The origin of Red Wing Creek structure: McKenzie County, North Dakota. *Wyoming Geological Association Earth Science Bulletin* 8:41.

Brett R., Guppy D. J., and Milton D. J. 1970. Two circular structures of impact origin in Northern Territory, Australia (abstract). *Meteoritics* 5:184.

Bucher W. H. 1936. Cryptoexplosion structures caused from without or from within the Earth? *American Journal of Science* 261:597–649.

Buchner E. and Kenkmann T. 2008. Upheaval Dome, Utah: Impact origin confirmed. *Geology* 36:227–230.

Bunch T. E. and Cohen A. J. 1967. Natural terrestrial maskelynite. *American Mineralogist* 52:244–253.

Bunting J. A., de Laeter J. R., and Libby W. G. 1980. Evidence for the age and cryptoexplosive origin of the Teague Ring structure, Western Australia. *Western Australia Geological Survey Annual Report* 1979:125–129.

Byerly G. R., Lowe D. R., Wooden J. L., and Xie X. 2002. An Archean impact layer from the Pilbara and Kaapvaal Cratons. *Science* 297:1325–1327.

Carlton R. W., Koeberl C., Baranoski M. T., and Schumacker G. A. 1998. Discovery of microscopic evidence for shock metamorphism at the Serpent Mound structure, south–central Ohio: Confirmation of an origin by impact. *Earth and Planetary Science Letters* 162:177–185.

Carrigy M. A. and Short M. N. 1968. Evidence of shock metamorphism in rocks from the Steen River structure, Alberta. In *Shock metamorphism of natural materials*, edited by French B. M. and Short N. M. Baltimore, Maryland: Mono Book Corp. pp. 367–378.

Carter N. L. 1965. Basal quartz deformation lamellae, a criterion for recognition of impactites. *American Journal of Science* 263:786–806.

Caty J. L., Chown E. H., and Roy D. W. 1976. A new astrobleme: Île Rouleau structure, Lake Mistassini, Quebec. *Canadian Journal of Earth Sciences* 13:824–831.

Chabou M. C. 2019. Meteorite impact structures in the Arab world: An overview. In *The geology of the Arab world—An overview*, edited by Bendaoud A., Hamimi Z., Hamoudi M., Djemai S., and Zoheir B. Cham: Springer Geology. pp. 455–506.

Chao E. C. T., Shoemaker E. M., and Madsen B. M. 1960. First natural occurrence of coesite. *Science* 132:220–222.

Chen M., Xiao W., and Xie X. 2010. Coesite and quartz characteristic of crystallization from shock-produced silica melt in the Xiuyan crater. *Earth and Planetary Science Letters* 297:306–314.

Chen M., Xie X., Xiao W., and Tan D. 2019. Yilan crater, a newly identified impact structure in northeast China (in Chinese with English summary). *Chinese Science Bulletin*. https://doi.org/10.1360/TB-2019-0704.

Cognéa J. P., Humler E., and Courtillot V. 2006. Mean age of oceanic lithosphere drives eustatic sea-level changes since Pangea breakup. *Earth and Planetary Science Letters* 245:115–122.

Cohen K. M., Finney S. C., Gibbard P. L., and Fan J. X. 2013. The ICS International Chronostratigraphic Chart. *Episodes* 36:199–204.

Collins G. S., Melosh H. J., and Ivanov B. A. 2004. Modeling damage and deformation in impact simulations. *Meteoritics & Planetary Science* 39:217–231.

Collins G. S., Melosh H. J., and Marcus B. A. 2005. Earth Impact Effects Program: A Web-based computer program for calculating the regional environmental consequences of a meteoroid impact on Earth. *Meteoritics & Planetary Science* 40:817–840.

Cox M. A., Cavosie A. J., Ferrière L., Timms N. E., Bland P. A., Miljkovic K., Erickson T. M., and Hess B. 2019. Shocked quartz in polymict impact breccia from the Upper Cretaceous Yallalie impact structure in Western Australia. *Meteoritics & Planetary Science* 54:621–637.

Crósta A. P., Koeberl C., Furuie R. A., and Kazzuo-Vieira C. 2010. Vista Alegre, southern Brazil: A new impact structure in the Paraná flood basalts. *Meteoritics & Planetary Science* 45:181–194.

Crósta A. P., Kazzuo-Vieira C., Pitarello L., Koeberl C., and Kenkmann T. 2012. Geology and impact features of Vargeão Dome, southern Brazil. *Meteoritics & Planetary Science* 47:51–71.

Crósta A. P., Reimold W. U., Vasconcelos M. A. R., Hauser N., Oliveira G. J. G., Mazivieiro M. V., and Góes A. M. 2019a. Impact cratering: The South American record—Part 1. *Geochemistry—Chemie der Erde* 79:1–61.

Crósta A. P., Reimold W. U., Vasconcelos M. A. R., Hauser N., Oliveira G. J. G., Maziviero M. V., and Góes A. M. 2019b. Impact cratering: The South American record—Part 2. *Geochemistry—Chemie der Erde* 79:191–220.

Crósta A. P., Reimold W. U., and Vasconcelos M. A. R. 2019c. Cerro Do Jarau and São Miguel do Tapuio: Two newly confirmed large impact structures in Brazil (abstract #3042). 50th Lunar and Planetary Science Conference. CD-ROM.

Currie K. L. 1969. Geological notes on the Carswell circular structure, Saskatchewan. *Canadian Geological Survey of Canada Paper* 67–32:60.

Currie K. L. and Dence M. R. 1963. Rock deformation in the rim of the New Quebec crater, Canada. *Nature* 198:153.

De Oliveira G. J. G., Vasconcelos M. A. R., Crósta A. P., Reimold W. U., Góes A. M., and Kowitz A. 2014. Shatter cones and planar deformation features confirm Santa Marta in Piauí State, Brazil, as an impact structure. *Meteoritics & Planetary Science* 49:1915–1928.

Dence M. R. 1964. A comparative structural and petrographic study of probable Canadian meteorite craters. *Meteoritics* 2:249–270.

Dence M. R., Innes M. J. S., and Robertson P. B. 1968. Recent geological and geophysical studies of Canadian craters. In *Shock metamorphism of natural materials*, edited by French B. M. and Short N. M. Baltimore, Maryland: Mono Book Corp. pp. 339–362.

Dence M. R., and Popelar J. 1972. Evidence for an impact origin for Lake Wanapitei, Ontario. In *New developments in Sudbury geology*, edited by Guy-Bray J. V. Geological Association of Canada Special Paper 10:117 pp.

Dewing K., Pratt B. R., Hadlari T., Brent T., Bédard J., and Rainbird R. H. 2013. Newly identified "Tunnunik" impact structure, Prince Albert Peninsula, northwestern Victoria Island, Arctic Canada. *Meteoritics & Planetary Science* 48:211–223.

Dietz R. S. 1947. Meteorite impact suggested by the orientation of shatter cones at the Kentland, Indiana, disturbance. *Science* 105:42–43.

Dietz R. S. 1959. Shatter cones in cryptoexplosion structures (meteorite impact?). *The Journal of Geology* 67:496–505.

Dietz R. S. 1960. Meteorite impact suggested by shatter cone in rock. *Science* 131:1781–1784.

Dietz R. S. 1966. Shatter cones at the Middlesboro structure. *Kentucky*. *Meteoritics*. 3:27–29.

Dietz R. S. 1967. Shatter cone orientation at Gosses Bluff astrobleme. *Nature* 216:1082–1084.

Dietz R. S. and Butler L. W. 1964. Shatter-cone orientation at Sudbury, Canada. *Nature* 204:280–281.

Dietz R. S. and French B. M. 1973. Two probable astroblemes in Brazil. *Nature* 244:561–562.

Dietz R. S. and Lambert P. 1980. Shock metamorphism at Crooked Creek crypto-explosion structure, MO (abstract). *Meteoritics* 15:281–282.

Dons J. A. and Naterstad J. 1992. The Gardnos impact structure, Norway (Abstract). *Meteoritics* 27:215.

Dypvik H., Gudlaugsson S. T., Tsikalas F., Attrep M. Jr, Ferrell R. E. Jr, Krinsley D. H., Mork A., Faleide J. I., and Nagy J. 1996. Mjølnir structure: An impact crater in the Barents Sea. *Geology* 24:779–782.

Earth Impact Database. 2020. http://www.passc.net/EarthImpactDatabase/New website_05-2018/Index.html

Eggleton R. E. and Shoemaker E. M. 1961. Breccia at Sierra Madera, Texas. *U.S. Geological Survey Professional Paper* 424-D:D151–D153.

El Kerni H., Chennaoui-Aoudjehane H., Baratoux D., Aoudjehane M., Charrière A., Ibouh H., Rochette P., Quesnel Y., Uehara M., Kenkmann T., Wulf G., Poelchau M. H., Nguyen V. B., Aboulahris M., Makhoukhi S., Aumaître G., Bourlès D., and Keddadouche K. 2019. Geological and geophysical studies of the Agoudal impact structure (Central High Atlas, Morocco): New evidence for crater size and age. *Meteoritics & Planetary Science* 54:2483–2509.

Elo S., Kuivasaari T., Lehtinen M., Sarapää O., and Uutela A. 1993. Iso-Naakkima, a circular structure filled with neoproterozoic sediments, Pieksämäki, Southeastern Finland. *Bulletin of the Geological Society of Finland* 65:3–30.

Erickson T. M., Kirkland C. L., Timms N. E., Cavosie A. J., and Davison T. M. 2020. Precise radiometric age establishes Yarrabubba, Western Australia, as Earth's oldest recognised meteorite impact structure. *Nature Communications* 11:1–8.

Ezeji-Okoye S. 1985. The origin of the Eagle Butte structure, Eagle Butte, Alberta Canada. Unpublished Report for Pan Canadian Petroleum. 75 p.

Fabre J., Kazi-Tani N., and Megartsi M. 1970. Le rond de l'Ouarkziz (Sahara nordoccidental), un astroblème. *Comptes Rendus de l'Académie des Sciences, Paris* D270:1212–1215.

Fackelman S. P., McElvain T. H., Morrow J. R., and Koeberl C. 2007. Shatter cone exposures indicate a new bolide impact structure near Santa Fe, New Mexico (abstract #1207). 38th Lunar and Planetary Science Conference. CD-ROM.

Farley K. A., Montanari A., Shoemaker E. M., and Shoemaker C. S. 1998. Geochemical evidence for a comet shower in the Late Eocene. *Science* 280:1250–1253. https://doi.org/10.1126/science.280.5367.1250.

Fassett C. I., Kadish S. J., Head J. W., Solomon S. C., and Strom R. G. 2011. The global population of large craters on Mercury and comparison with the Moon. *Geophysical Research Letters* 38:L10202. https://doi.org/10.1029/2011GL047294.

Fel'dman V. I., Granovsky L. B., and Lomonosov M. V. 1978. Meteoritic crater Shunak, the central Kazakhstan, U.S.S.R. (abstract). 9th Lunar and Planetary Science Conference. p. 312.

Ferrière L. and Osinski G. R. 2012. Shock metamorphism. In *Impact cratering: Processes and products*, edited by Osinski G. R. and Pierazzo E. Chichester: John Wiley & Sons. pp. 106–124.

Ferrière L., Lubala F. R. T., Osinski G. R., and Kaseti P. K. 2011. The newly confirmed Luizi impact structure, Democratic Republic of Congo—Insights into central uplift formation and post-impact erosion. *Geology* 39:851–854.

Firsov L. and Kieffer S. W. 1973. Concerning the meteoritic origin of the Puchezh-Katunki Crater. *Meteoritics* 8:223–244.

Florenskiy P. V., Short N., Winzer S. R., and Fredriksson K. 1977. The Zhamanshin structure: Geology and petrography (abstract). *Meteoritics* 12:227–228.

Folco L., Di Martino M., El Barkooky A., D'Orazio M., Lethy A., Urbini S., Nicolosi I., Hafez M., Cordier C., van Ginneken M., Zeoli A., Radwan A. M., El Khrepy S., El Gabry M., Gomaa M., Barakat A. A., Serra R., and El Sharkawi M. 2010. The Kamil Crater in Egypt. *Science* 329:804.

French B. M. 1998. *Traces of catastrophe: A handbook of shock-metamorphic effects in terrestrial meteorite impact structures*. LPI Contribution 954. Houston, Texas: Lunar and Planetary Institute. 120 p.

French B. M. and Koeberl C. 2010. The convincing identification of terrestrial meteorite impact structures: What works, what doesn't, and why. *Earth-Science Reviews* 98:123–170.

French B. M., Hartung J. B., Short N. M., and Dietz R. S. 1970. Tenoumer crater, Mauritania: Age and petrologic evidence for origin by meteorite impact. *Journal of Geophysical Research* 75:4396–4406.

French B. M., Underwood J. R., and Fisk E. P. 1974. Shock metamorphic features in two meteorite impact structures, south-eastern Libya. *Geological Society of America Bulletin* 85:1425–1428.

French B. M., Koeberl C., Gilmour I., Shirley S. B., Dons J. A., and Naterstad J. 1997. The Gardnos impact structure, Norway: Petrology and geochemistry of target rocks and impactites. *Geochimica et Cosmochimica Acta* 61:873–904.

French B. M., Cordua W. S., and Plescia J. B. 2004. The Rock Elm meteorite impact structure, Wisconsin; Geology and shock-metamorphic effects in quartz. *Geological Society of America Bulletin* 116:200–218.

French B. M., McKay R. M., Liu H. P., Briggs D. E. G., and Witzke B. J. 2018. The Decorah structure, northeastern Iowa: Geology and evidence for formation by meteorite impact. *Geological Society of America Bulletin* 130:2062–2086.

Gallagher B. 2011. Peak oil analyzed with a logistic function and idealized Hubbert curve. *Energy Policy* 39:790–802.

Gault D. E., Quaide W. L., and Oberbeck V. R. 1974. Impact cratering mechanics and structures. In *A primer in lunar geology*, edited by Greeley, R. and Schultz, P. Washington, D.C.: NASA, pp. 177–189.

Gerlach T. R., Forsman N. F., and Anderson N. L. 1994. *Evidence for an impact origin of the Newporte structure, Renville County, North Dakota (abstract)*. Seattle, Washington: Geological Society of America.

Gersonde R., Kyte F. T., Bleil U., Diekmann B., Flores J. A., Gohl K., Grahl G., Hagen R., Kuhn G., Sierro F. J., Völker D., Abelmann A., and Bostwick J. A. 1997. Geological record and reconstruction of the late Pliocene impact of the Eltanin asteroid in the Southern Ocean. *Nature* 390:357–363.

Gilder S. A., Pohl J., and Eitel M. 2018. Magnetic signatures of terrestrial meteorite impact craters: A summary. In *Magnetic fields in the solar system*, edited by Lühr H., Wicht J., Gilder S. A., and Holschneider M. Cham: Springer. Astrophysics and Space Science Library. Vol. 448, p., 357–382.

Glikson A., Hickman A., and Crossley R. 2016. Evidence for a shock metamorphic breccia within a buried impact crater, Lake Raeside, Yilgarn Craton, Western Australia. *Australian Journal of Earth Sciences* 63:99–109.

Gold D. P., Tanner J. G., and Halliday D. W. 1978. The Lac La Moinerie crater: A probable impact site in New Quebec. *Geological Society of America* 10:44.

Gostin V. A. and Therriault A. M. 1997. Tookoonooka, a large buried Early Cretaceous impact structure in the Eromanga Basin of southwestern Queensland, Australia. *Meteoritics & Planetary Science* 32:593–599.

Gottwald M., Kenkmann T., and Reimold W. U. 2020. *Terrestrial impact structures. The TanDEM-X atlas*. Munich: Verlag Dr. Friedrich Pfeil. 608 p.

Grieve R. A. F. 1982. The record of impact on Earth: Implications for a major Cretaceous/Tertiary impact event. *Geological Society of America Special Paper* 190:25–37.

Grieve R. A. F. 1991. Terrestrial impact: The record in the rocks. *Meteoritics* 26:175–194.

Grieve R. A. F. 2005. Economic natural resource deposits at terrestrial impact structures. In *Mineral deposits and Earth evolution*, edited by McDonald I., Boyce A. J., Butler I. B., Herrington R. J., and Polya D. A. London: Geological Society. Special Publications. Vol 248, p. 1–29.

Grieve R. A. F. 2006. Impact structures in Canada. *GeoText* 5:210.

Grieve R. A. F. and Cintala M. J. 1992. An analysis of differential impact melt-crater scaling and implications for the terrestrial impact record. *Meteoritics* 27:526–538.

Grieve R. A. F. and Garvin J. B. 1984. A geometric model for excavation and modification at terrestrial simple impact craters. *Journal of Geophysical Research* 89:11,561–11,572.

Grieve R. A. F. and Pesonen L. J. 1992. The terrestrial impact cratering record. *Tectonophysics* 216:1–30.

Grieve R. A. F. and Pilkington M. 1996. The signature of terrestrial impacts. *AGSO. Journal of Australian Geology and Geophysics* 16:399–420.

Grieve R. A. F., Langenhorst F., and Stöffler D. 1996. Shock metamorphism of quartz in nature and experiment: II. Significance in geoscience. *Meteoritics & Planetary Science* 31:6–35.

Grieve R. A. F., Kreis K., Therriault A. M., and Robertson P. B. 1998. Impact structures in the Williston Basin. *Meteoritics & Planetary Science* 33:A63–A64.

Guppy D. J., Brett R., and Milton D. J. 1971. Liverpoool and Strangways craters, Northern Territory: Two structures of probable impact origin. *Journal of Geophysical Research* 76:5387–5393.

Gurov E. P., Val'ter A. A., Gurova E. P., and Serebrennikov A. I. 1978. The El'gygytgyn meteorite explosion crater in Chukotka (in Russian). *Doklady Academii Nauk SSSR*. 240:1407–1410.

Gurov E. P., Gurova H. P., and Kovalyukh N. N. 1987. The Macha meteorite-crater group, western Yakutia (in Russian). *Doklady Akademii Nauk SSSR* 296:185–188.

Gurov E. P., Gurova H. P., Rakitskaya R. B., and Yamnichenko A. Y. 1993. The Karakul depression in the Pamirs—The first impact structure in central Asia (abstract). 24th Lunar and Planetary Science Conference. p. 591.

Gurov E. P., Kelley S. P., Koeberl C., and Dykan N. I. 2006. Sediments and impact rocks filling the Boltysh impact crater. In *Biological processes associated with impact events*, edited by Cockell C. S., Koeberl C., and Gilmour I. Berlin: Springer. pp. 335–358.

Gurov E. P., Nikolaenko N., Shevchuk H., and Yamnichenko A. 2017. Kamenetsk—A new impact structure in the Ukrainian Shield. *Meteoritics & Planetary Science* 52:2461–2469.

Haines P. W. 1996. Goyder impact structure, Arnhem Land, Northern Territory. *AGSO Journal of Australian Geology and Geophysics* 16:561–566.

Haines P. W. 2005. Impact cratering and distal ejecta: The Australian record. *Australian Journal of Earth Sciences* 52:481–507.

Haines P. W. 2017. Drilling to basement at Hickman Crater, Western Australia. In *International workshop on shock metamorphism in terrestrial and extra-terrestrial rocks*. June 26–29, 2017, Curtin University, Perth.

Haines P. W. and Rawlings D. J. 2002. The Foelsche structure, Northern Territory, Australia: An impact crater of probable Neoproterozoic age. *Meteoritics & Planetary Science* 37:269–280.

Haines P. W., Therriault A. M., and Kelly S. P. 1999. Evidence for mid-Cenozoic (?) low-angle multiple impacts in South Australia. *Meteoritics & Planetary Science* 34: A49–A50.

Haines P. W., Sweet I. P., and Mitchell K. 2012. Cleanskin structure, Northern Territory and Queensland, Australia: Evidence for an impact origin (abstract #5176). *Meteoritics & Planetary Science* 47

Halliday I. and Griffin A. A. 1963. Evidence in support of a meteoritic origin for West Hawk Lake, Manitoba, Canada. *Journal of Geophysical Research* 68:5297–5305.

Halls H. C. and Grieve R. A. F. 1976. The Slate Islands: A probable complex meteorite impact structure in Lake Superior. *Canadian Journal of Earth Sciences* 13:1301–1309.

Hargraves R. B. 1961. Shatter cones in the rocks of the Vredefort ring. *Geological Society South Africa Transactions* 64:147–154.

Hargraves R. B., Christiansen P. P., Cullicott C. E., Deffeyes K. S., Fiske P. S., and Hougen S. 1990. Shatter cones and shocked rocks in southwestern Montana: The Beaverhead impact structure. *Geology* 18:832–834.

Harms J. E., Milton D. J., Ferguson J., Gilbert D. J., Harris W. K., and Goleby B. 1980. Goat Paddock cryptoexplosion crater, Western Australia. *Nature* 286:704–706.

Hartmann W. K. 1970. Lunar cratering chronology. *Icarus* 13:299–301.

Herd C. D. K., Froese D. G., Walton E. L., Kofman R. S., Herd E. P. K., and Duke M. J. M. 2008. Anatomy of a young impact event in central Alberta, Canada: Prospects for the missing Holocene impact record. *Geology* 36:955–958.

Hergarten S. and Kenkmann T. 2015. The number of impact craters on Earth: Any room for further discoveries? *Earth and Planetary Science Letters* 425:187–192.

Hergarten S. and Kenkmann T. 2019. Long-term erosion rates as a function of climate derived from the impact crater inventory. *Earth Surface Dynamics* 7:459–473.

Hergarten S., Wulf G., and Kenkmann T. 2019. Comment on "Earth and Moon impact flux increased at the end of the Paleozoic." *Science* 23. Science10.1126/science. aaw7471.

Herrick R. R., Sharpton V. L., Malin M. C., Lyons S. N., and Freely K. 1997. Morphology and morphometry of impact craters. In *Venus II*, edited by Bougher S. W., Hunten D. M., and Phillips R. J. Tucson, Arizona: The University of Arizona Press. pp. 1015–1046.

Higgins M. and Tait L. 1990. A possible new impact structure near Lac de la Presqu'île, Quebec, Canada. *Meteoritics* 25:235–236.

Hildebrand A. R., Penfield G. T., Kring D. A., Pilkington M., Camargo Z. A., Jacobsen S. B., and Boynton W. V. 1991. Chicxulub Crater: A possible Cretaceous/Tertiary boundary impact crater on the Yucatan Peninsula, Mexico. *Geology* 19:867–871.

Innes M. J. S. 1957. A possible impact crater at Deep Bay, Saskatchewan, Canada. *Journal of the Royal Astronomical Society of Canada* 51:235–240.

Innes M. J. S. 1964. Recent advances in meteorite crater research at the Dominion Observatory, Ottawa, Canada. *Meteoritics & Planetary Science* 2:219–241.

Ivanov B. A. and Artemieva N. A. 2002. Numerical modelling of the formation of large impact craters. In *Catastrophic events and mass extinctions: Impact and beyond*, edited by Koeberl, C. and MacLeod, K. G. Special Paper 356. Washington, D.C.: Geological Society of America. pp. 619–630.

Jansa L. F. and Pe-Piper G. 1987. Identification of an underwater extraterrestrial impact crater. *Nature* 327:612–614.

Johnson B. C. and Bowling T. J. 2014. Where have all the craters gone? Earth's bombardment history and the expected terrestrial cratering record. *Geology* 42:587–590.

Jourdan F., Renne P. R., and Reimold W. U. 2009. An appraisal of the ages of terrestrial impact structures. *Earth and Planetary Science Letters* 286:1–13.

Jourdan F., Reimold W. U., and Deutsch A. 2012. Dating terrestrial impact structures. *Elements* 8:49–53.

Kamo S. L., Reimold W. U., Krogh T. E., and Colliston P. W. 1996. A 2.023 Ga age for the Vredefort impact event and a first report of shock metamorphosed zircons in

pseudotachylitic breccias and Granophyre. *Earth and Planetary Science Letters* 144:369–387.
Karaszewski W. 1974. Geological studies of "meteorite" craters in Noerdlingen Ries (West Germany) and at Morasko (Poland). *Przeglad Geologiczny* 22:626–627.
Kelley S. P. and Sherlock S. C. 2012. The geochronology of impact craters. In *Impact cratering: Processes and products*, edited by Osinski G. R. and Pierazzo E. Chichester: John Wiley & Sons. pp. 240–253.
Kellogg K. S., Snee L. W., and Unruh D. M. 2003. The Mesoproterozoic Beaverhead impact structure and its tectonic setting, Montana-Idaho: ^{40}Ar-^{39}Ar and U-Pb isotopic constraints. *The Journal of Geology* 111:639–652.
Kenkmann T. and Poelchau M. H. 2009. Low-angle collision with Earth: The elliptical impact crater Matt Wilson, Northern Territory, Australia. *Geology* 37:459–462.
Kenkmann T., Jahn D., Ivanov B.A. 2005. *Structure and formation of a central uplift: A case study at the Upheaval Dome impact crater, Utah. In Large Meteorite Impacts III*, edited by Kenkmann T., Hörz F., and Deutsch A. Geological Society of America Special Paper 384, Boulder, Colorado: Geological Society of America. pp. 85–116.
Kenkmann T., Vasconcelos M. A. R., Crósta A. P., and Reimold W. U. 2011. The complex impact structure Serra da Cangalha, Tocantins State, Brazil. *Meteoritics & Planetary Science* 46:875–889.
Kenkmann T., Collins G. S., and Wünnemann K. 2012. The modification stage of crater formation. In *Impact cratering: Processes and products*, edited by Osinski G. R. and Pierazzo E. Chichester: John Wiley & Sons. pp. 60–75.
Kenkmann T., Poelchau M. H., and Wulf G. 2014. Structural geology of impact craters. *Journal of Structural Geology* 62:156–182.
Kenkmann T., Afifi A. M., Stewart S. A., Poelchau M. H., Cook D. J., and Neville A. S. 2015. Saqqar: A new 34 km diameter impact crater in Saudi Arabia. *Meteoritics & Planetary Science* 50:1925–1940.
Kenkmann T., Sturm S., Krüger T., Salameh E., Al-Raggad M., and Konsul K. 2017. The structural inventory of a small complex impact crater: Jebel Waqf as Suwwan, Jordan. *Meteoritics & Planetary Science* 52:1351–1370.
Kenkmann T., Deutsch A., Thoma K., Ebert M., Poelchau M., Buhl E., Carl E. R., Danilewsky A., Dresen G., Dufresne A., Durr N., Ehm L., Grosse C., Gulde M., Güldemeister N., Hecht L., Hiermeier S., Hoerth T., Hamann C., Kowitz A., Langenhorst F., Lexow B., Liermann H.-P., Luther R., Mansfeld U., Moser D., Raith M., Reimold W. U., Sauer M., Schäfer F., Schmitt R. T., Sommer F., Wilk J., Winkler R., and Wünnemann K. 2018a. Experimental impact cratering: A summary of the major results of the MEMIN research unit. *Meteoritics & Planetary Science* 53:1543–1568.
Kenkmann T., Sundell K. A., and Cook D. 2018b. Evidence for a large Paleozoic impact crater strewn field in the Rocky Mountains. *Scientific Reports* 8:246.
Kenkmann T., Haines P. W., Sweet I. P., and Mitchell K. 2019. Shock deformation and faulting in the Cleanskin impact structure, Northern Territory, Australia (abstract #5014). Large Meteorite Impact Conference VI, Brasilia.
Kenkmann T., Wulf G., and Agarwal A. 2020. Ramgarh, Rajasthan, India: A 10 km diameter complex impact crater. *Meteoritics & Planetary Science* 55:936–961.
Khryanina L. P. 1981. Sobolevskiy meteorite crater (Sikhote-Alin' Range). *International Geology Review* 23:1–10.
King D. T. Jr, Neathery T. L., Petruny L. W., Koeberl C., and Hames W. E. 1999. Evidence confirming meteoritic impact at Wetumpka crater, Alabama, USA. *Meteoritics & Planetary Science* 34:63–64.
Kirschner C. E., Grantz A., and Mullen M. W. 1992. Impact origin of the Avak Structure, Arctic Alaska, and genesis of the Barrow gas fields. *The American Association of Petroleum Geologists Bulletin*. 76:651–679.
Kiselev N. P. and Korotuschenko Y. G. 1986. The Bigach astrobleme, Eastern Kazkhstan (in Russian). *Meteoritika* 45:119–121.
Kjær K. H., Larsen N. K., Binder T., Bjørk A. A., Eisen O., Fahnestock M. A., Funder S., Garde A. A., Haack H., Helm V., Houmark-Nielsen M., Kjeldsen K. K., Khan S. A., Machguth H., McDonald I., Morlighem M., Mouginot J., Paden J. D., Waight T. E., Weikusat C., Willerslev E., and MacGregor J. A. 2018. A large impact crater beneath Hiawatha Glacier in northwest Greenland. *Science Advances* 4:eaar8173.
Koeberl C. 1998. Identification of meteoritic component in impactites. In *Meteorites: Flux with time and impact effects*, edited by Grady M. M., Hutchinson R., McCall G. J. H., and Rothery R. A. London: The Geological Society. pp. 133–153.
Koeberl C. and Ferrière L. 2019. Libyan Desert Glass area in western Egypt: Shocked quartz in bedrock points to a possible deeply eroded impact structure in the region. *Meteoritics & Planetary Science* 54:2398–2408.
Koeberl C. and Reimold W. U. 1995. The Newporte impact structure, North Dakota, USA. *Geochimica et Cosmochimica Acta* 59:4747–4767.
Koeberl C., Reimold W. U., Shirey S. B., and Le Roux F. G. 1994a. Kalkkop crater, Cape Province, South Africa: Confirmation of impact origin using osmium isotope systematics. *Geochimica et Cosmochimica Acta*. 58:1229–1234.
Koeberl C., Reimold W. U., and Powell R. A. 1994b. Shocked quartz and impact melt rock at the Ames structure, Oklahoma (abstract). *Meteoritics* 29:483.
Koeberl C., Poag C. W., Reimold W. U., and Brandt D. 1996. Impact origin of Chesapeake Bay structure and the source for the North American tektites. *Science* 271:1263–1266.
Koeberl C., Reimold W. U., and Shirey S. B. 1998. The Aouelloul crater, Mauritania: On the problem of confirming the impact origin of a small crater. *Meteoritics & Planetary Science*. 33:513–517.
Kring D. A. 2017. *Guidebook to the geology of Barringer Meteorite Crater, Arizona (a.k.a. Meteor Crater)*, 2nd ed. LPI Contribution 2040. Houston, Texas: Lunar and Planetary Institute. p. 270.
Krinov E. L. 1959. The main conditions of the fall of a meteoritic shower (in Russian). In *The Sikhote-Alin iron meteorite shower*, edited by Fesenkov V. G. and Krinov E. L. Moscow: Publishing House of the USSR Academy of Sciences. Vol. 1, p. 99–156.
Krüger T., Kenkmann T., and Hergarten S. 2017. Structural uplift and ejecta thickness of lunar mare craters: New insights into the formation of complex crater rims. *Meteoritics & Planetary Science* 52:2220–2240.
Krüger T., Hergarten S., and Kenkmann T. 2018. Deriving morphometric parameters and the simple-to-complex transition diameter from a high resolution, global database

of fresh lunar impact craters (D ≥ ~ 3 km). *Journal of Geophysical Research—Planets* 123:2667–2690.
Kurta A. T., Wünnemann K., and Kenkmann T. 2009. Morphometry and structure of eroded complex impact craters: A parameter study using hydrocode modeling (abstract #1948). 40th Lunar and Planetary Science Conference. CD-ROM.
Lambert P. 1977. The Rochechouart Crater: Shock zoning study. *Earth and Planetary Science Letters* 35:258–268.
Lambert P., McHone J. F., Dietz R. S., and Houfani M. 1980. Impact and impact-like structures in Algeria: Part 1, four bowl-shaped depressions. *Meteoritics* 15:157–179.
Lambert P., McHone J. F., Dietz R. S., Briedj M., and Djender M. 1981. Impact and impact-like structures in Algeria, Part 2. Multi-ringed structures. *Meteoritics* 16:203–227.
Le Feuvre M. and Wieczorek M. A. 2008. Nonuniform cratering of the terrestrial planets. *Icarus* 197:291–306.
Lehtinen M. 1976. Lake Lappajarvi, a meteorite impact site in western Finland. *Geological Survey of Finland Bulletin* 282:92.
Lehtinen M., Pesonen L. J., Puranen R., and Deutsch A. 1996. Karikkoselkä—A new impact structure in Finland (abstract). 27th Lunar and Planetary Science Conference. p. 739.
Lehtinen M., Pesonen L. J., Stehlik H., and Kuulusa M. 2002. The Suvasvesi South structure, Central Finland: New evidence for impact (abstract #1188). 33rd Lunar and Planetary Science Conference. CD-ROM.
Lehtovaara J. J. 1985. 40K–40Ar dating of the Söderfjärden crater, Vaasa, western Finland. *Geologiska Föreningen i Stockholm Förhandlingar* 107:1–6.
Lindström M., Ekvall J., Hagenfeldt S. E., Säwe B., and Sturkell E. F. F. 1991. A well-preserved Cambrian impact exposed in Central Sweden. *Geologische Rundschau* 80:201–204.
Lindström M., Flodén T., Grahn Y., and Kathol B. 1994. Post-impact deposits in Tvären, a marine Middle Ordovician crater south of Stockholm, Sweden. *Geological Magazine* 131:91–103.
Littler J., Fahey J. J., Dietz R. S., and Chao E. C. T. 1962. Coesite from the Lake Bosumtwi crater, Ashanti, Ghana (abstract). *Geological Society of America Special Paper* 68:218.
Macdonald F. A., Bunting J. A., and Cina S. E. 2003. Yarrabubba—A large, deeply eroded impact structure in the Yilgarn Craton, Western Australia. *Earth and Planetary Science Letters* 213:235–247.
MacDonald F. A. and Mitchel K. A. 2003. Amelia Creek, Northern Territory, Australia: A 20 x 12 km oblique impact structure with no central uplift. Workshop on Impact Cratering.
Macedo L. and Macharé J. 2007. The Carancas meteorite fall, 15 September 2007. Official INGEMMET initial report. http:// www.ingemmet.gob.pe/
Madigan C. T. 1937. The Boxhole crater and the Huckitta meteorite (central Australia). *Royal Society South Australia Transactions and Proceedings* 61:187–190.
Masaitis V. L. 1973. *Geological consequences of the falls of the crater forming meteorites*. Leningrad, Russia: Nedra Press. p. 18. In Russian
Masaitis V. L. 1974. Some ancient meteorite craters on the USSR territory. *Meteoritika* 33:64–68. In Russian
Masaitis V. L. 1999. Impact structures of northeastern Eurasia: The territories of Russia and adjacent countries. *Meteoritics & Planetary Science* 34:691–711.
Masaitis V. L., Mikhailov M. V., and Selivanovskaia T. V. 1971. Popigai Basin—An explosion meteorite crater. *Doklady Akademii Nauk SSSR* 197:39–46. In Russian
Masaitis V. L., Sindeev A. S., and Staritsky Y. G. 1976. The impactites of the Jänisjärvi astrobleme. *Meteoritika* 35:103–110. In Russian
Masaitis V. L., Danilin V. N., Mashchak M. S., Raikhlin A. I., Selivanovskaty A. V., and Shadenkov E. M. 1980. *The geology of astroblemes*. Leningrad, Russia: Nedra Press. p. 231.
Mashchak M. S. and Orlova J. V. 1986. Shock deformations in lower Proterozoic breccias of the Lake Suav'yarvi region (central Karelia). *Meteoritika* 45:137–141. In Russian
Maziviero M. V., Vasconcelos M. A. R., Crósta A. P., Góes A. M., Reimold W. U., and Carneiro C. C. 2013. Geology and impact features of Riachão structure, northern Brazil. *Meteoritics & Planetary Science* 48:2044–2058.
Mazrouei S., Ghent R. R., Bottke W. F., Parker A. H., and Gernon T. M. 2019. Earth and Moon impact flux increased at the end of the Paleozoic. *Science* 363:253–257.
McCabe H. R. and Bannatyne B. B. 1970. Lake St. Martin crypto-explosion crater and geology of the surrounding area. Manitoba Department of Mines and Natural Resources, Mines Branch, Geological Paper. 3/70:79 p.
McCall G. J. H. 2009. Half a century of progress in research on terrestrial impact structures: A review. *Earth-Science Reviews* 92:99–116.
McHone J. F., Sargent M. L., and Nelson W. J. 1986. Shatter cones in Illinois: Evidence for meteoritic impacts at Glasford and Des Plaines (abstract). *Meteoritics* 21:446.
McIntyre D. B. 1962. Impact metamorphism at Clearwater Lake, Quebec. *Journal of Geophysical Research* 67:1647–1653.
McKinnon W. B. and Schenk P. M. 1985. Ejecta blanket scaling on the Moon and Mercury—Inferences for projectile populations (abstract). 16th Lunar and Planetary Science Conference. p. 544
Melosh H. J. 1989. *Impact cratering: A geologic process*. Oxford: Clarendon Press. 245 p.
Mikhailov M. V., Shurygin A. G., and Khariusovl S. 1979. Beenchime-Salaaty meteoritic crater (in Russian). *Doklady AN SSSR* 245:911–914.
Millman P. M., Liberty B. A., Clark J. F., Willmore P., and Innes M. J. S. 1960. The Brent Crater. *Ottawa Dominion Observatory Publications* 24:43 pp.
Milstein R. L. 1994. The Calvin impact crater, Cass County, Michigan: Identification and analysis of a subsurface Ordovician astrobleme. Ph.D. thesis, Corvallis, Oregon: Oregon State University. 114 p.
Milton D. J. and MacDonald F. A. 2005. Goat Paddock, Western Australia: An impact crater near the simple-complex transition. *Australian Journal of Earth Sciences* 52:691–698.
Morgan J. V., Gulick S. P. S., Bralower T., Chenot E., Christeson G., Claeys P., Cockell C., Collins G. S., Coolen M. J. L., Ferrière L., Gebhardt C., Goto K., Jones H., Kring D. A., Le Ber E., Lofi J., Long X., Lowery C., Mellet C., Ocampo-Torres R., Osinski G. R., Perez-Cruz L., Pickersgill A., Poelchau M. H., Rae A., Rasmussen C., Rebolledo-Vieyra M., Riller U., Sato H., Schmitt D. R., Smit J., Tikoo S., Tomioka N., Urrutia-Fucugauchi J.,

Whalen M., Wittmann A., Yamaguchi K. E., and Zylberman W. 2016. The formation of peak rings in large impact craters. *Science* 354:878–882.

Mory A. J., Iasky R. P., Glikson A. Y., and Pirajno F. 2000. Woodleigh, Carnarvon Basin, Western Australia: A new 120 km diameter impact structure. *Earth and Planetary Science Letters* 177:119–128.

Motuza G. B. and Gailius P. 1978. On the supposed astroblemes in Lithuania. In *Local structures in Belarus and the Baltic region*, edited by Press M. and Suveizdis P. I. Vilnius, Lithuania: Geological Research Institute. pp. 91–94. In Russian

Movshoviceh V. and Milayvskay E. 1975. The problem of the origin of agglomerate of northern Donetsk area (in Russian). *Geotectonika* 2:114–124.

Nayak V. K. 1972. Glassy objects (impactite glasses?): A possible new evidence for meteoritic origin of the Lonar Crater, Maharashtra State, India. *Earth and Planetary Science Letters* 14:1–6.

Neukum G., Ivanov B. A., and Hartmann W. K. 2001. Cratering records in the inner solar system in relation to the lunar reference system. In *Chronology and evolution of Mars*, edited by Kallenbach R., Geiss J., and Hartmann W. K. Dordrecht: Springer. pp. 55–86.

Nininger H. H. and Figgins J. D. 1933. The excavation of a meteorite crater near Haviland, Kiowa County, Kansas. *American Journal of Science* 28:312–313.

Nininger H. H. and Huss G. I. 1960. The unique meteorite crater at Dalgaranga, Western Australia. *Mineralogical Magazine* 32:619–639.

Oberbeck V. R. 1968. Application of high explosion cratering data to planetary problems. In *Impact and explosion cratering*, edited by Roddy D. J., Pepin R. O., and Merrill R. B. New York: Pergamon Press. pp. 45–65.

Ocampo A. R., Pope K. O., and Fischer A. G. 1996. Ejecta blanket deposits of the Chicxulub crater from Albion Island, Belize. In *The Cretaceous-Tertiary event and other catastrophes in Earth history*, edited by Ryder G., Fastovsky D., and Gartner S. Boulder, Colorado: Geological Society of America. pp. 75–88.

Offield T. W. and Pohn H. A. 1979. Geology of the Decaturville impact structure, Missouri. *U.S. Geological Survey Professional Paper* 1042:48.

Öhman T., Aittola M., Kostama V. P., Hyvärinen M., and Raitala J. 2006. Polygonal impact craters in the Argyre region, Mars: Evidence for influence of target structure on the final crater morphology. *Meteoritics & Planetary Science* 41:1163–1173.

Ormö J. and Lindström M. 2000. When a cosmic impact strikes the sea bed. *Geological Magazine* 137:67–80.

Ormö J., Sturkell E., Olvak J. N., Melero-Asensio I., Frisk A., and Wikström T. 2014. The geology of the Målingen structure: A probable doublet to the Lockne marine-target impact crater, central Sweden. *Meteoritics & Planetary Science* 49:313–327.

Osinski G. R. and Pierazzo E., eds. 2012. *Impact cratering—Processes and products*. Hoboken, New Jersey: Wiley-Blackwell. 316 p.

Osinski G. R., Silber E. A., Clayton J., Grieve R. A. F., Hansen K., Kalynn J., and Tornabene L. L. 2019. Transitional impact craters on the Moon: Insight into the effect of target lithology on the impact cratering process. *Meteoritics & Planetary Science* 54:573–591.

Papunen H. 1969. Possible impact metamorphic textures in the erratics of the Lake Saaksjärvi area in southwestern Finland. *Bulletin of the Geological Society of Finland* 41:151–155.

Pati J. K. 2005. The Dhala structure, Bundelkhand Craton, Central India—A new large Paleoproterozoic impact structure (abstract #5092). *Meteoritics & Planetary Science Supplement*, 40(s1), 5092

Pesonen L. J. 1998. The Lake Saarijarvi—A new meteorite impact structure in northern Finland (abstract #1262). 29th Lunar and Planetary Science Conference. CD-ROM.

Pesonen L. J., Järvelä J., Sarapää O., and Pietarinen H. 1996. The Iso-Naakkima meteorite impact structure: Physical properties and paleomagnetism of a drill core (abstract). *Meteoritics & Planetary Science* 31:A105–A106.

Pesonen L. J., Elo S., Lehtinen M., Jokinen T., Puranen R., and Kivekäs L. 1999. Lake Karikkoselkä impact structure, central Finland: New geophysical and petrographic results. In *Large meteorite impacts and planetary evolution II*, edited by Dressler B. O. and Sharpton V. L. Boulder, Colorado: Geological Society of America. Special Paper. Vol. 339, p. 131–147.

Petaev M. I., Kisarev Y. L., Mustafin S. A., Shakurov R. K., Pavlov A. V., and Ivanov B. A. 1991. Meteorite Sterlitamak—A new crater forming fall (abstract). 22nd Lunar and Planetary Science Conference. p. 1059.

Philby H. S. J. 1933. *The empty quarter*. London: Constable and Company Ltd. 433 p.

Pierazzo E. and Melosh H. J. 2000. Understanding oblique impacts from experiments, observations, and modeling. *Earth and Planetary Science Letters* 28:141–167.

Pike R. J. 1977. Size-dependence in the shape of fresh impact craters on the Moon. In *Impact and explosion cratering*, edited by Roddy D. J., Pepin R. O., and Merrill R. B. New York: Pergamon Press. pp. 489–509.

Pike R. J. 1985. Some morphologic systematics of complex impact structures. *Meteoritics* 20:49–68.

Pike R. J. 1988. Geomorphology of impact craters on Mercury. In *Mercury*, edited by Vilas, F., Chapman, C. R. and Shapley-Matthews, M. Tucson, Arizona: The University of Arizona Press. pp. 165–273.

Pilkington M. and Grieve R. A. F. 1992. The geophysical signature of terrestrial impact craters. *Review of Geophysics* 30:161–181.

Plado J., Hietala S., Kreitsmann T., Lerssi J., Nenonen J., and Pesonen L. 2018. Summanen, a new meteorite impact structure in Central Finland. *Meteoritics & Planetary Science* 53:2413–2426.

Poag C. W., Koeberl C., and Reimold W. U. 2004. *The Chesapeake Bay crater. Geology and geophysics of a late Eocene submarine impact structure*. Berlin: Springer. 522 p.

Poelchau M. H. and Kenkmann T. 2011. Feather features: A low-shock-pressure indicator in quartz. *Journal of Geophysical Research* 116:B02201.

Poelchau M. H., Kenkmann T., and Kring D. A. 2009. Rim uplift and crater shape in Meteor Crater: Effects of target heterogeneities and trajectory obliquity. *Journal of Geophysical Research* 114:E01006.

Read W. F. 1983. Shatter cones at Glover Bluff, Wisconsin. *Meteoritics* 18:241–243.

Reeves F. and Chalmers R. O. 1949. The Wolfe Creek crater. *The Australian Journal of Science* 11:154–156.

Reimold W. U. and Koeberl C. 2014. Impact structures in Africa: A review. *Journal of African Earth Sciences* 93:57–175.

Reimold W. U. and Miller R. M. G. 1989. The Roter Kamm impact crater, SWA/Namibia. Proceedings, 19th Lunar and Planetary Science Conference. pp. 711–732.

Reimold W. U., Koeberl C., Kerr S. J., and Partridge T. C. 1991. The Pretoria Saltpan—The first firm evidence for an origin by impact (abstract). 22nd Lunar and Planetary Science Conference. p. 1117.

Reimold W. U., Crósta A. P., Hasch M., Kowitz A., Hauser N., Sanchez J. P., Amarante Simões L. S., de Oliveira G. J., and Zaag P. T. 2018. Shock deformation confirms the impact origin for the Cerro do Jarau, Rio Grande do Sul, Brazil, structure. *Meteoritics & Planetary Science* 54:2384–2397.

Reimold W. U., Vasconcelos M. A. R., Jessell M., Crósta A. P., Ferrière L., Hauser N., Gottwald M., and Baratoux D. 2020. Nova Colinas—A new complex impact structure in Maranhão State, Brazil. Contribution to 50th *Congress of the Sociedade Brasileira de Geologia* (SBG), Brasilia, October 2020.

Reinwald I. 1928. Bericht über geologische Untersuchungen am Kaalijärv (Krater von Sall) auf Ösel. *Loodusuurijate Seltsi Aruanded* 35:30–70.

Riis F., Kalleson E., Dypvik H., Krøgly S. O., and Nilsen O. 2011. The Ritland impact structure, southwestern Norway. *Meteoritics & Planetary Science* 46:748–761.

Riller U. 2005. Structural characteristics of the Sudbury impact structure, Canada: Impact-induced versus orogenic deformation—A review. *Meteoritics & Planetary Science* 40:1723–1740.

Robertson, P. B. 1968. Meteoritics. *La Malbaie structure, Quebec: A Paleozoic impact site* 4:511–518.

Robertson P. B. and Mason G. D. 1975. Shatter cones from Haughton Dome, Devon Island, Canada. *Nature* 255:393–394.

Rochette P., Alac R., Beck P., Brocard G., Cavosie A. J., Debaille V., Devouard B., Jourdan F., Mougel B., Moustard F., Moynier F., Nomade S., Osinski G. R., Reynard B., and Cornec J. 2019. Pantasma: Evidence for a Pleistocene circa 14 km diameter impact crater in Nicaragua. *Meteoritics & Planetary Science* 54:880–901.

Roddy D. J. 1977. Pre-impact conditions and cratering processes at the Flynn Creek crater, Tennessee. In *Impact and explosion cratering*, edited by Roddy D. J., Pepin R. A., and Merrill R. B. New York: Pergamon Press. pp. 277–308.

Rondot J. 1966. Geology of La Malbaie area. Charlevoix County. Department of Natural Resources, Quebec. Preliminary report. 544, 18 p.

Salameh E., Khoury H., Reimold W. U., and Schneider W. 2008. The first large meteorite impact structure discovered in the Middle East: Jebel Waqf as Suwwan. *Meteoritics & Planetary Science* 43:1681–1690.

Sanchez J. and Cassidy W. 1966. A previously undescribed meteorite crater in Chile. *Journal of Geophysical Research* 71:4891–4895.

Schmidt R. M. and Housen K. R. 1987. Some recent advances in the scaling of impact and explosion cratering. *International Journal of Impact Engineering* 5:543–560.

Schmieder M. and Kring D. A. 2020. Earth's impact events through geologic time: A list of recommended ages for terrestrial impact structures and deposits. *Astrobiology* 20:1–51.

Schmieder M., Trieloff M., Schwarz W. H., Buchner E., and Jourdan F. 2014. Supportive comment on: "Morphology and population of binary asteroid impact craters", by K. Miljkovi´c, G.S. Collins, S. Mannick and P.A. Bland [Earth Planet. Sci. Lett. 363 2013) 121–132]—An updated assessment. *Earth and Planetary Science Letters* 405:281–284.

Schulte P., Alegret L., Arenillas I., Arz J. A., Barton P. J., Bown P. R., Bralower T. J., Christeson G. L., Claeys P., Cockell C. S., Collins G. S., Deutsch A., Goldin T. J., Goto K., Grajales-Nishimura J. M., Grieve R. A. F., Gulick S. P. S., Johnson K. R., Kiessling W., Koeberl C., Kring D. A., MacLeod K. G., Matsui T., Melosh J., Montanari A., Morgan J. V., Neal C. R., Nichols D. J., Norris R. D., Pierazzo E., Ravizza G., Rebolledo-Vieyra M., Reimold W. U., Robin E., Salge T., Speijer R. P., Sweet A. R., Urrutia-Fucugauchi J., Vajda V., Whalen M. T., and Willumsen P. S. 2010. The Chicxulub asteroid impact and mass extinction at the Cretaceous-Paleogene boundary. *Science* 327:1214–1218.

Schultz P. H. and Lianza R. E. 1992. Recent grazing impacts on the Earth recorded in the Rio Cuarto crater field, Argentina. *Nature* 355:234–237.

Sharpton V. L. and Gibson J. W. Jr. 1990. The Marquez Dome impact structure, Leon County, Texas (abstract). 21st Lunar and Planetary Science Conference. p. 1136.

Shoemaker E. M. 1977. Why study impact craters? In *Impact and explosion cratering*, edited by Roddy D. J., Pepin R. O., and Merill R. B. New York: Pergamon Press. pp. 1–10.

Shoemaker E. M. and Chao E. C. T. 1961. New evidence for the impact origin of the Ries basin, Bavaria, Germany. *Journal of Geophysical Research* 66:3371–3378.

Shoemaker E. M. and Shoemaker C. S. 1985. Impact structures of Western Australia. *Meteoritics* 20:754–756.

Shoemaker E. M. and Shoemaker C. S. 1997. Glikson, a probable impact structure, Western Australia (abstract #1669). 28th Lunar and Planetary Science Conference. CD-ROM.

Short N. M. 1966. Shock processes in geology. *Journal of Geological Education* 14:149–166.

Spencer L. J. 1933. Meteorite craters as topographic features of the Earth's surface. *Geographic Journal* 81:227–248.

Spooner I., Stevens G., Morrow J., Pufahl P., Grieve R. A. F., Raeside R., Pilon J., Stanley C., Barr S., and McMullin D. 2009. Identification of the Bloody Creek structure, a possible impact crater in southwestern Nova Scotia, Canada. *Meteoritics & Planetary Science* 44:1193–1202.

Stewart A. and Mitchell K. 1987. Shatter cones at the Lawn Hill circular structure, northwestern Queensland: Presumed astrobleme. *Australian Journal of Earth Sciences* 34:477–485.

Stewart S. A. 2011. Estimates of yet-to-find impact crater population on Earth. *Journal of the Geological Society* 168:1–14.

Stöffler D. and Langenhorst F. 1994. Shock metamorphism of quartz in nature and experiment: 1. Basic observation and theory. *Meteoritics* 29:155–181.

Stöffler D. and Grieve R. A. F. 2007. Impactites. In *Metamorphic rocks: A classification and glossary of terms, recommendations of the International Union of Geological Sciences*, edited by Fettes D. and Desmons J. Cambridge:

Cambridge University Press. pp. 82–91, 111–125, and 126–242.
Stöffler D., Hamann C., and Metzler K. 2017. Shock metamorphism of planetary silicate rocks and sediments: Proposal for an updated classification system. *Meteoritics & Planetary Science*. 53:5–49.
Stone D. S. and Therriault A. M. 2003. The Cloud Creek structure, central Wyoming, U.S.A.—Impact origin confirmed. *Meteoritics & Planetary Science* 38:445–455.
Sturm S., Wulf G., Jung D., and Kenkmann T. 2013. The Ries impact, a double-layer rampart crater on Earth. *Geology* 41:531–534.
Sturm S., Kenkmann T., and Hergarten S. 2016. Ejecta thickness and structural rim uplift measurements of Martian impact craters: Implications for the rim formation of complex impact craters. *Journal of Geophysical Research Planets* 121:1026–1053.
Suuroja K. and Suuroja S. 2000. Neugrund structure—The newly discovered submarine Early Cambrian impact crater. In *Impacts and the early Earth*, vol. 91, edited by Gilmour I. and Koeberl C. Berlin: Springer. pp. 389–416.
Svensson N. B. 1968. The Dellen lakes: A probable meteorite impact in central Sweden. *Geologiska Föreningen i Stockholm Förhandlingar* 90:14–316.
Svensson N. B. 1971. Probable meteorite impact crater in central Sweden. *Nature* 229:90–92.
Svensson N. B. 1993. Lumparn Bay: A meteorite impact crater in the Åland archipelago, southwest Finland. *Meteoritics* 28:245.
Svensson N. B. and Wickman F. E. 1965. Coesite from Lake Mien, southern Sweden. *Nature* 205:1202–1203.
Tagle R. and Hecht L. 2006. Geochemical identification of projectiles in impact rocks. *Meteoritics & Planetary Science* 41:1721–1735.
Taylor E. C. and Dence M. R. 1969. A probable meteorite origin for Mistastin Lake, Labrador. *Canadian Journal of Earth Sciences* 6:39–45.
Thomas M. D. and Innes M. J. S. 1977. The Gow Lake impact structure, northern Saskatchewan. *Canadian Journal of Earth Sciences* 14:1788–1795.
Tonkin P. E. 1973. Discovery of shatter cones at Kelly West near Tennant Creek, Northern Territory, Australia. *Geological Society of Australia Journal* 20:99–102.
Trepmann C. A. and Spray J. G. 2005. Planar microstructure and Dauphiné twins in shocked quartz of the Charlevoix impact structure, Canada. In *Large meteorite impacts III*, edited by Kenkmann T., Hörz F., and Deutsch A. Boulder, Colorado: Geological Society of America, p. 315–328.
Turtle E. P., Pierazzo E., Collins G. S., Osinski G. R., Melosh H. J., Morgan J. V., and Reimold W. U. 2005. Impact structures: What does crater diameter mean? In *Large meteorite impacts III*, edited by Kenkmann T., Hörz F., and Deutsch A. Boulder, Colorado: Geological Society of America, p. 1–24.
Ugalde H., Artemieva N., and Milkereit B. 2005. Magnetization on impact structures—Constraints from numerical modelling and petrophysics. In *Large meteorite impacts III*, edited by Kenkmann T., Hörz F., and Deutsch A. Boulder, Colorado: Geological Society of America, p. 24–42.
Val'ter A. A. and Ryabenko V. A. 1977. *Explosion craters of the Ukrainian*. Kiev, Ukraine: Naukova Dumka Press. 154 p. In Russian
Val'ter A. A., Bryansky V. P., Ryabenko V. A., and Lazarenkeo E. 1976. On the explosion (meteoritic) origin of Zeleny Gai structure on the Ukrainian Shield. *Doklady ANSSSR* 229:160–162. In Russian
Veretennikov N. V., Ilkevich G., and Makhnacha S. 1979. Logoisk buried depression—An ancient meteorite crater (in Russian). *Doklady Acad Nauk BSSR* 23:156–160.
Vincent P. M. and Beauvilain A. 1996. Découverte d'un nouveau cratère Sahara de Tchad. *Comptes Rendus de l'Académie des Sciences, Paris* 323:987–997.
Vishnevsky S. A. 1995. The Chykcha impact crater, Taymyr peninsula: Heavily eroded astrobleme of Cretaceous-Paleogene age (abstract). *Meteoritics* 30:591.
Vishnevsky S. A. and Korobkov V. F. 1989. Chiyli Dome, an eroded impact structure in western Primugodzharye. *Akademiya Nauk SSSR* 1–51. In Russian
Vishnevsky S. A. and Lagutenko V. N. 1986. The Ragozinka Astrobleme: An Eocene crater in the central Urals. *Doklady Akademii Nauk SSSR* 14:42. In Russian
Wang J., Cheng W., and Zhou C. 2015. A Chang'E-1 global catalog of lunar impact craters. *Planetary and Space Science* 112:42–45.
Williams G. E. 1986. The Acraman impact structure: Source of ejecta in Late Precambrian shales, South Australia. *Science* 233:200–203.
Wulf G. and Kenkmann T. 2021. Rampart craters on Earth. In *Large Meteorite Impacts and Planetary Evolution VI*. Geological Society of America Special Paper 550. (in press).
Wulf G., Hergarten S., and Kenkmann T. 2019. Combined remote sensing analyses and landform evolution modeling reveal the terrestrial Bosumtwi impact structure as a Mars-like rampart crater. *Earth and Planetary Science Letters* 506:209–220.
Yarmolyuk, V. A. 1951. The Sobolevka crater (in Russian). *Priroda* 6:40–42.
Yeates A. N., Crowe R. W. A., and Towner R. R. 1976. The Veevers crater: A possible meteoritic feature. *BMR Journal of Australian Geology and Geophysics* 1:77–78.
Youles I. P. 1976. Mount Toondina impact structure. *Quarterly Geological Notes, The Geological Survey of South Australia* 60:10–11.